# ABSTRACT

MAULSTBY, JR., GREGORY ALLAN. Comparison of COBRA-EN and COBRA-CTF Simulation Predictions to Benchmark Data for Representative Boiling Water Reactor Conditions. (Under the direction of Dr. Joseph Michael Doster).

The purpose of this study is to compare predictions of two subchannel thermal-hydraulic codes, COBRA-EN and COBRA-CTF, under representative boiling water reactor (BWR) operating conditions with the steady-state, two-phase pressure drop benchmark data from the Nuclear Power Engineering Corporation of Japan BWR Full-size Fine-mesh Bundle Test database. Chapter two contains a brief description of the test facility used to conduct the experiments along with the test assembly, grid spacers, and operating conditions and measured pressure drop data for the test cases. Both COBRA-CTF and COBRA-EN sections include explanations of input deck entries, methods to determine axial geometry, and unique differences and challenges encountered. A mesh convergence study revealed that pressure predictions in both thermal hydraulic codes were insensitive to the axial node length for a uniform node length of 0.1545m (0.50689ft) based on the given power profile. An additional study in COBRA-EN determined two optimum combination of correlations based on pressure drop alone and another that considers vapor fraction. The comparison of both codes to the benchmark data concluded that COBRA-CTF requires further investigation of vapor fraction near the grid spacers, and that both codes slightly under predict total pressure drop. In addition, COBRA-EN and COBRA-CTF match the benchmark database well at most pressure drop identifiers but measured vapor fraction is required to definitively claim which code predictions better represent physical behavior along the length of the test bundle.

Comparison of COBRA-EN and COBRA-CTF Simulation Predictions to Benchmark Data
for Representative Boiling Water Reactor Conditions

by
Gregory Allan Maultsby Jr.

A thesis submitted to the Graduate Faculty of
North Carolina State University
in partial fulfillment of the
requirements for the degree of
Master of Science

Nuclear Engineering

Raleigh, North Carolina

2018

APPROVED BY:

_____          _____
Dr. Maria Nikolova Avramova                          Dr. Stephen D Terry


_____
Dr. Joseph Michael Doster
Chair of Advisory Committee

**BIOGRAPHY**

Gregory Allan Maultsby, Jr. was born in Raleigh, North Carolina. He graduated high school in 1993 and returned to further his education in 2009. Received an Associate in Pre-Engineering in 2012 from Wake Technical Community College. Upon completion of the associate's degree, he transferred to North Carolina State University's Nuclear Engineering program in the fall of 2012. After obtaining a bachelor in Nuclear Engineering in 2015, he stayed to pursue a Master of Science in nuclear engineering degree under the direction of Dr. Joseph Michael Doster.

# ACKNOWLEDGMENTS

"It takes a village to raise a child."

  -Unknown

By no far measure did I accomplish this master's thesis alone. I would like to acknowledge the following people for their contributions throughout this journey. First, I would like to thank my graduate school advisor Dr. J. Michael Doster, of the Nuclear Engineering Department at North Carolina State University for offering the opportunity to continue my education after my undergraduate studies. He has continued to provide mentorship through his persistent patience and guidance during the learning process of this master's thesis. I would also like to acknowledge Dr. Maria Avramova and Dr. Stephen Terry, as committee members. Also, I would like to acknowledge Dr. Bourham, for taking time out of his schedule to attend my defense as a committee member substitute. I received invaluable assistance from Dr. Taylor Blythe for COBRA-CTF technical support, Dr. Robert Salko for general COBRA-CTF support, and Dr. Konor Frick for his guidance and intellectually spirited discussions. I would like to extend my appreciation for the funding support from CASL. Lastly, I would like to acknowledge those who have contributed in a non-academic capacity. Sherry Bailey was a consistent source of moral support throughout my experience in graduate school. We should never forget those that wait for us while we chase our dreams. Ingrid Medina was a constant source of stability in my life who always stood beside me for the full duration of my academic adventure.

**TABLE OF CONTENTS**

# LIST OF TABLES

# LIST OF FIGURES

**CHAPTER 1: Introduction**

The purpose of this study is to compare predictions of two subchannel thermal-hydraulic codes, COBRA-EN and COBRA-CTF, under representative boiling water reactor (BWR) operating conditions with benchmark data from the Nuclear Power Engineering Corporation (NUPEC) of Japan BWR Full-size Fine-mesh Bundle Test (BFBT) database. This study is a continuation of the ongoing validation and verification (V&V) process pertaining to the stand-alone component, COBRA-CTF, in the code package VERA-CS sponsored by the Consortium for Advanced Simulation of Lightwater Reactors (CASL). The primary validation metric for this study is the steady-state, two-phase pressure drop benchmark from the NUPEC BFBT database. Three of twenty-two test cases were selected to explore a variety of given parameters such as thermal output, exit quality, total pressure drop, and mass flow.

First, it is important to understand the methods involved in collecting the measured benchmark data in the NUPEC BFBT database. An electrically heated test loop was designed to simulate a range of BWR operating conditions. Pressure drop measurements were taken at selected axial positions along the heated bundle illustrated in *figure 2.4* under operating conditions listed in *table 2.9*. The BWR bundle design, axial and radial peaking factors, and grid spacer positions are provided in the NUPEC BWR Full-size Fine-mesh Bundle Test (BFBT) Benchmark, Volume I: Specifications [7]. The grid spacer local loss coefficients used in this study are the same as used in previous CASL studies as represented in the, "*CTF Validation and Verification. CASL-U-2016-1113-000.*" Technical report [2].

For evaluation purposes, COBRA-EN and COBRA-CTF, are considered in separate sections. These sections briefly describe the methods and models utilized in each code. In addition, there are explanations of input deck entries, methods to determine axial geometry, and unique differences and challenges encountered in each code. Furthermore, a mesh refinement study was performed to determine the appropriate axial node length suitable for typical BWR simulations. This supplementary study determines whether decreasing the axial mesh length contributes to significant changes in code generated values at shared axial positions. The default mesh length is based on the NUPEC BFBT database provided axial power peaking factors illustrated in *figure 2.5*. These values are given for twenty-four uniform nodes of lengths 154.5mm (0.50689ft) that sum to a total heated length of 3708mm (12.1654ft). COBRA-CTF offers limited user options for choosing empirical closure relations as compared to COBRA-EN. An additional study explores various combinations of two-phase correlations and models in COBRA-EN to determine a best choice suite for comparison to the NUPEC BFBT benchmark data. The "best choice suite" of correlations and models serves as the basis for comparing the two thermal hydraulic codes.

## CHAPTER 2: NUPEC BFBT Benchmark

The experimental data utilized for this study originates from the BFBT benchmark developed by the NUPEC of Japan as a result of the fourth OECD/NRC BWR TT Benchmark Workshop held on the sixth of October 2002 in Seoul, Korea [7]. The NUPEC BFBT database addresses concerns for nuclear applications to refine models for best estimate calculations based on good quality experimental data [7]. Refer to NUPEC BWR Full-size Fine-mesh Bundle Test (BFBT) Benchmark, Volume I: Specifications for the complete collection of the benchmark details and exercises conducted. The primary focus for this study is the two-phase pressure drop, P6 series, experiments located in the Phase II, *"Critical Power Benchmark"*, Exercise 0, *"Steady State Pressure Drop Benchmark*. These experiments were conducted at the NUPEC BFBT facility that can operate at the high pressure, and high fluid temperature conditions for typical reactor power levels observed in BWRs [7].

## 2.1    NUPEC Rod Bundle Test Loop

*Figure 2.1* illustrates the test loop used to conduct the NUPEC BFBT experiments. The structural components are made of stainless steel (SUS304), and the cooling fluid is demineralized water [7]. Electrically heated rod bundles are used to simulate a full scale BWR fuel assembly [7]. The cladding, insulator, and heater were made of Inconel, boron nitride and nichrome, respectively [7]. Mechanical properties listed in the *appendix A* are based on the MATPRO model used in the TRAC code [7]. An adiabatic condition is suggested for the benchmark considering no information on heat loss is available in the NUPEC BFBT database [7]. The test loop can simulate a large range of steady-state BWR operating conditions. *Table 2.1* contains the maximum operating conditions for the BFBT test facility [7].

| Table 2.1:   Maximum Operating Conditions | | | |
|:---:|:---:|:---:|:---:|
| **Pressure** | **Temperature** | **Power** | **Flow Rate** |
| **Metric** | | | |
| 10.3 MPa | 315 °C | 12 MW | 75 t/h |
| **Standard** | | | |
| $8.97 \times 10^{13} \ \dfrac{lb_m}{ft \ hr^2}$ | 599 °F | $4.09 \times 10^7 \ \dfrac{BTU}{hr}$ | $1.653 \times 10^5 \ \dfrac{lb_m}{hr}$ |

A system diagram for the NUPEC rod bundle test series is illustrated in *figure 2.1*. A circulation pump moves the coolant through three parallel control valves of different sizes to match the desired flow rate for each case [7]. The fluid temperature entering the test section is controlled by a direct-heating tubular pre-heater [7]. Sub-cooled coolant flows upward into the test section where it is heated by the electrically heated rods to simulate the BWR operating conditions [7]. The coolant exiting the bundle is a mixture of steam and water that enters a separator where the steam is separated and condensed using a sub-cooled water spray from two air-cooled heat exchangers [7]. The condensed water is return to the circulation pump to complete the loop [7].
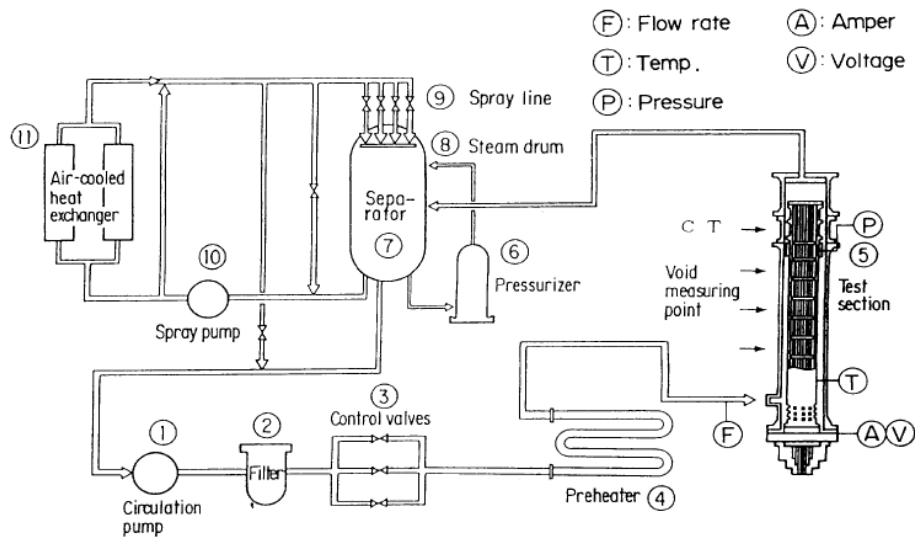


**Figure 2.1: System diagram of test facility for NUPEC rod bundle test series**

**2.2 NUPEC BFBT High Burn-Up Assembly**

The 8X8 High Burn-Up assembly is the chosen full-scale test bundle for this study. In addition, the high burn-up assembly, classified as C2A, simulates beginning of operation radial peaking conditions illustrated in *figure 2.6* [7]. *Table 2.2* list the number and dimensions of the heated rods and water channels, the number of grid spacers, and the dimensions of the BWR channel box [7].

| Table 2.2: High Burn-up 8x8 Assembly | | |
|---|---|---|
| **Electric Heated Rods** | | |
| Number of Heated Rods | 60 | |
| Heated Rod Outer Diameter | 12.3 mm | 0.484 in |
| Heated Rod Pitch | 16.3 mm | 0.642 in |
| Axial Heated Length | 3708 mm | 12.165 ft |
| **Water Channel** | | |
| Number of Water Rods | 1 | |
| Water Rod Outer Diameter | 34.0 mm | 1.339 in |
| **Channel Box** | | |
| Channel Box Inner Width | 132.5 mm | 5.217 in |
| Channel Box Corner Radius | 8.0 mm | 0.315 in |
| In Channel Flow Area | 9463 mm$^2$ | 14.668 in$^2$ |
| **Spacer Grid** | | |
| Spacer Type | Ferrule | |
| Number of Spacers | 7 | |
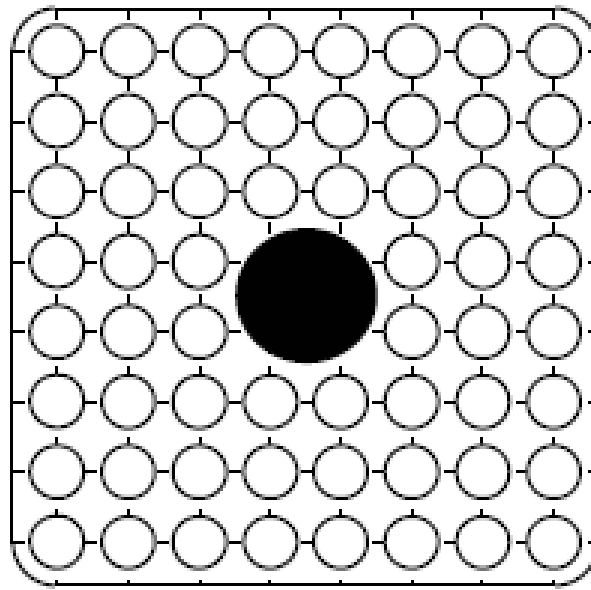
**Figure 2.2: Top-down view of the 8X8 high burn-up test bundle**

*Figure 2.3* is a diagram of the top left corner with dimensions given in *table 2.2*.
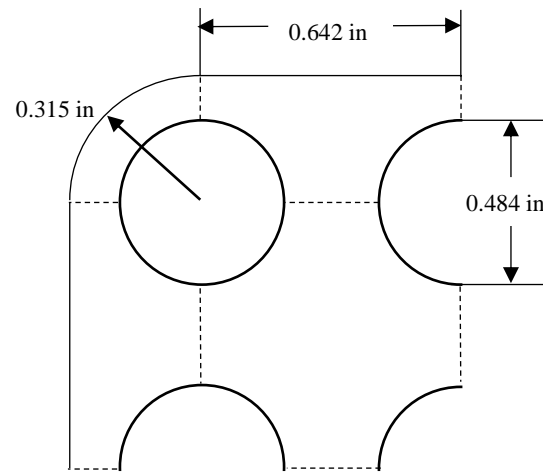


**Figure 2.3: Top left corner of 8X8 high burn-up test bundle**

## 2.3 Bundle Pressure Drop Locations

The bundle pressure drop was monitored at the locations indicated in *Figure 2.4* [7].
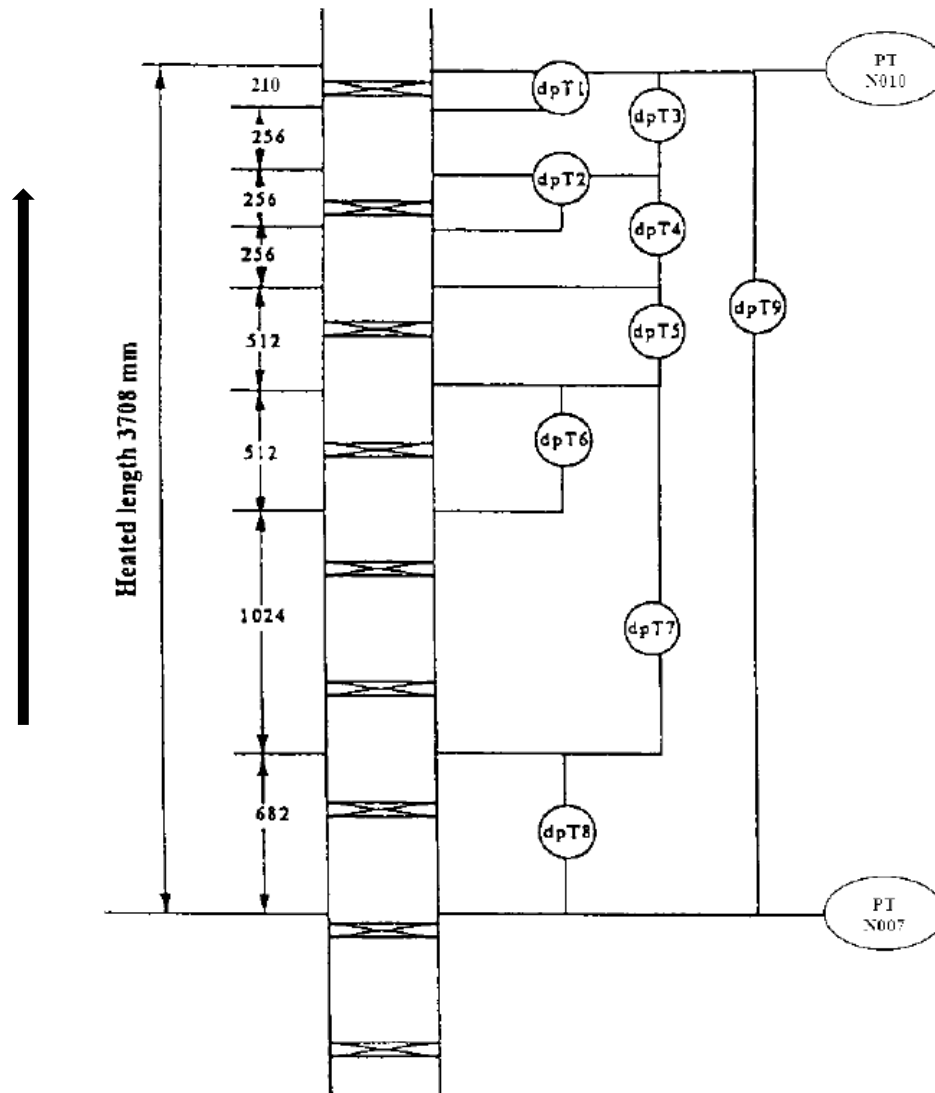


**Figure 2.4: Locations for pressure tap positions and pressure drop identifiers**

*Table 2.3* list seven pressure tap locations along the axial length of the test bundle where pressure measurements were recorded. Both codes predict pressure at these positions that will be used to determine the pressure drop at the nine pressure drop identifiers shown in *figure 2.4*.

| Table 2.3: Pressure Tap Axial Positions | | |
|---|---|---|
| **Pressure Tap Position Identifier** | **Axial Position (ft)** | **Axial Position (mm)** |
| pt1 | 2.2375 | 682 |
| pt2 | 5.5971 | 1706 |
| pt3 | 7.2769 | 2218 |
| pt4 | 8.9567 | 2730 |
| pt5 | 9.7966 | 2986 |
| pt6 | 10.6365 | 3242 |
| pt7 | 11.4764 | 3498 |

*Table 2.4* contains the nine pressure drop identifiers along with their associated lower and upper axial positions, and spacing.

| Table 2.4: Length Between Pressure Tap Positions | | | | |
|---|---|---|---|---|
| **Pressure Drop Identifier** | **Lower Axial Position (ft)** | **Upper Axial Position (ft)** | **ΔZ (ft)** | **ΔZ (mm)** |
| dpt9 | 0.0 | 12.1654 | 12.1654 | 3708 |
| dpt8 | 0.0 | 2.2375 | 2.2375 | 682 |
| dpt7 | 2.2375 | 7.2769 | 5.0394 | 1536 |
| dpt6 | 5.5971 | 7.2769 | 1.6798 | 512 |
| dpt5 | 7.2769 | 8.9567 | 1.6798 | 512 |
| dpt4 | 8.9567 | 10.6365 | 1.6798 | 512 |
| dpt3 | 10.6365 | 12.1654 | 1.5289 | 466 |
| dpt2 | 9.7966 | 10.6365 | 0.8399 | 256 |
| dpt1 | 11.4764 | 12.1654 | 0.6890 | 210 |

## 2.4 NUPEC BFBT C2A Power Profiles

The axial power peaking factors are a cosine shape as shown in *figure 2.5* [7].
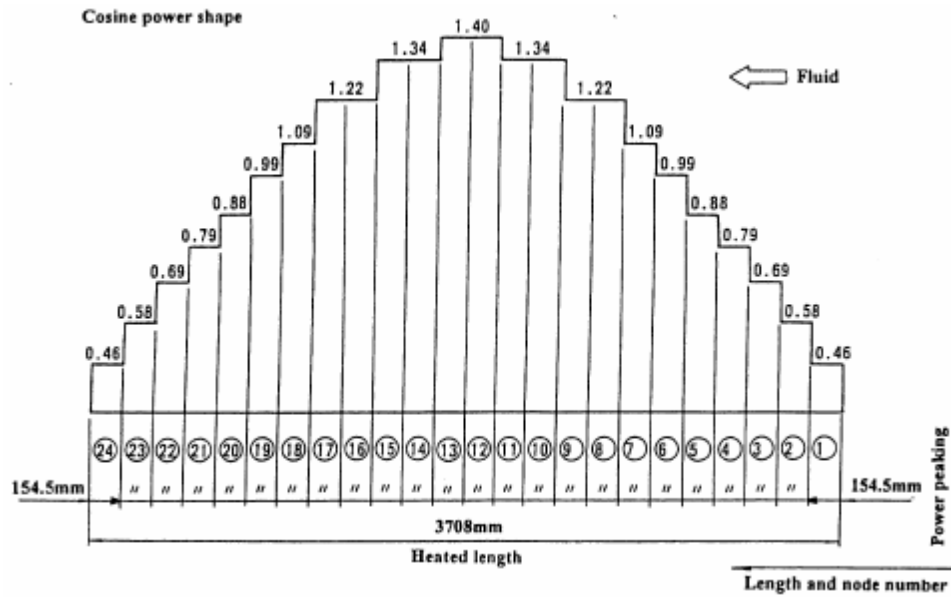


**Figure 2.5: Axial peaking factors in NUPAC BFBT C2A thermal profile**

The radial power profile for the beginning of operation (C2A) is illustrated in *figure 2.6* [7].

| | | | | | | | |
|------|------|------|------|------|------|------|------|
| 1.15 | 1.30 | 1.15 | 1.30 | 1.30 | 1.15 | 1.30 | 1.15 |
| 1.30 | 0.45 | 0.89 | 0.89 | 0.89 | 0.45 | 1.15 | 1.30 |
| 1.15 | 0.89 | 0.89 | 0.89 | 0.89 | 0.89 | 0.45 | 1.15 |
| 1.30 | 0.89 | 0.89 |      |      | 0.89 | 0.89 | 1.15 |
| 1.30 | 0.89 | 0.89 |      |      | 0.89 | 0.89 | 1.15 |
| 1.15 | 0.45 | 0.89 | 0.89 | 0.89 | 0.89 | 0.45 | 1.15 |
| 1.30 | 1.15 | 0.45 | 0.89 | 0.89 | 0.45 | 1.15 | 1.30 |
| 1.15 | 1.30 | 1.30 | 1.15 | 1.15 | 1.15 | 1.30 | 1.15 |

**Figure 2.6: Radial peaking factors in NUPAC BFBT C2A thermal profile**

## 2.5   NUPEC BFBT Grid Spacer

Spacer grids provide structural support to the rod bundle during normal operation. Grid spacers act as a local flow obstruction by means of decreasing the cross-sectional flow area resulting in a local pressure drop. A ferrule type spacer is used in the NUPEC BFBT High Burn-Up 8X8 assembly experiments. These ferrule-type spacers contain circular tubes to guide each heated rod as well as the central water rod [7]. *Table 2.5* list the grid spacer positions along the axial length of the heated rods [7].

| Table 2.5:   Spacer Grid Locations | |
| --- | --- |
| **(mm)** | **(ft)** |
| 455 | 1.493 |
| 967 | 3.173 |
| 1479 | 4.852 |
| 1991 | 6.532 |
| 2503 | 8.212 |
| 3015 | 9.892 |
| 3527 | 11.572 |

*Figure 2.7* is an illustration of the ferrule-type grid spacer used during the NUPEC BFBT High

Burn-Up 8X8 assembly C2A experiments [7].
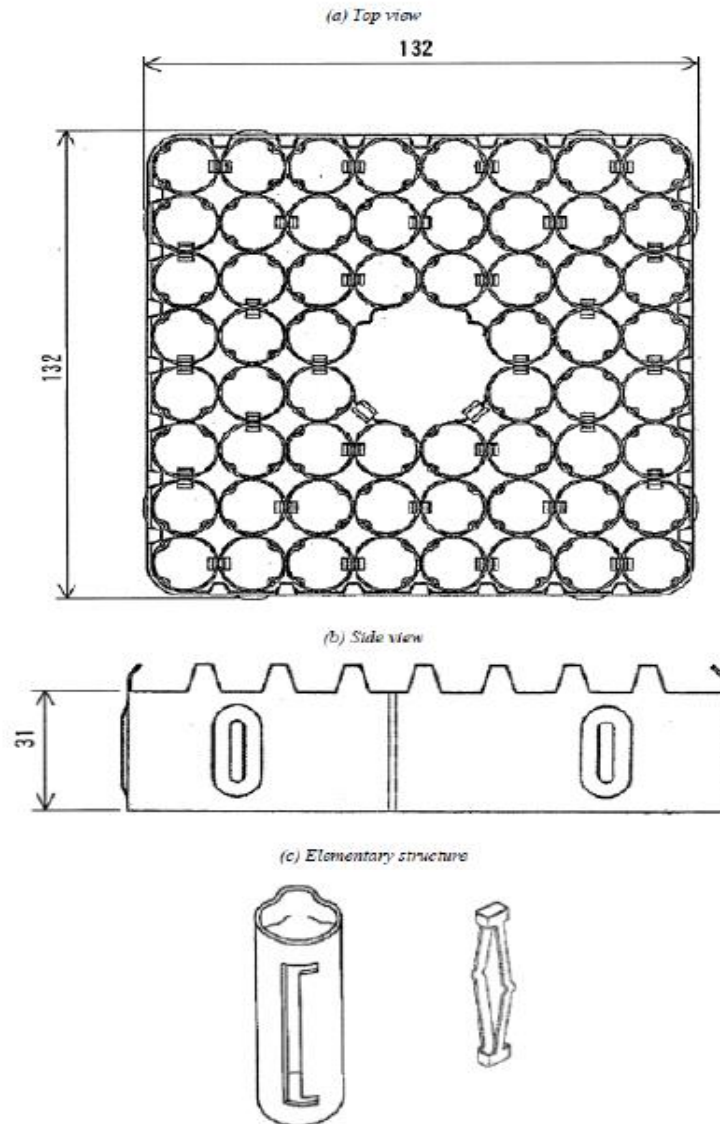


**Figure 2.7:   Dimensions of ferrule type grid spacer (mm)**

**2.6  Subchannel Grid Spacer Loss Coefficients**

For both COBRA-EN and COBRA-CTF, a local loss coefficient is supplied at user specified axial position for each subchannel to model the impact of local flow obstructions due to grid spacers. The approach in this study is to use the same loss coefficients as in CASL's prior evaluation of the NUPEC BFBT experiments illustrated in *figure 2.8* [2]. These loss coefficients were determined by B.S. Shiralkar and D.W. Radcliffe and reported in, "*An experimental and analytical study of the synthesis of grid spacer loss coefficients*. Tech. rep. NEDE-13181. General Electric, 1971" [2]. The loss coefficients identified in *figure 2.8* have not been independently verified in this study.

| 1.348 | 1.278 | 1.606 | 1.222 | 1.304 | 1.222 | 1.606 | 1.278 | 1.348 |
|-------|-------|-------|-------|-------|-------|-------|-------|-------|
| 1.606 | 0.748 | 0.748 | 0.748 | 0.748 | 0.748 | 0.748 | 0.748 | 1.606 |
| 1.278 | 0.748 | 0.748 | 0.748 | 0.748 | 0.748 | 0.748 | 0.748 | 1.278 |
| 1.304 | 0.748 | 0.748 | 1.475 | 0.926 | 1.475 | 0.748 | 0.748 | 1.304 |
| 1.222 | 0.748 | 0.748 | 0.856 |       | 0.856 | 0.748 | 0.748 | 1.222 |
| 1.304 | 0.748 | 0.748 | 0.778 | 0.926 | 0.778 | 0.748 | 0.748 | 1.304 |
| 1.278 | 0.748 | 0.748 | 0.748 | 0.748 | 0.748 | 0.748 | 0.748 | 1.278 |
| 1.606 | 0.748 | 0.748 | 0.748 | 0.748 | 0.748 | 0.748 | 0.748 | 1.606 |
| 1.348 | 1.278 | 1.606 | 1.222 | 1.304 | 1.222 | 1.606 | 1.278 | 1.348 |

**Figure 2.8:  Legend of subchannel grid spacer loss coefficients**

14
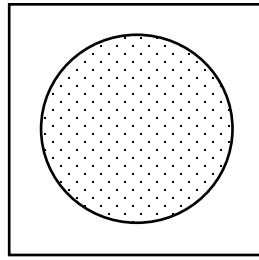


**Figure 2.9:   Typical diagram of a two-dimensional fuel channel**

*Figure 2.10* and *figure 2.11* illustrate how the local loss coefficients for subchannels at the grid spacer locations are defined as inputs to the codes. *Figure 2.10* is the top left corner of the bundle and represents a quarter of a fuel channel with a loss coefficient of 1.348, while along the wall sides the sub-channels are half a fuel channel with respective loss coefficients of 1.278 and 1.606. The subchannel with the loss coefficient of 0.748 is a typical subchannel.
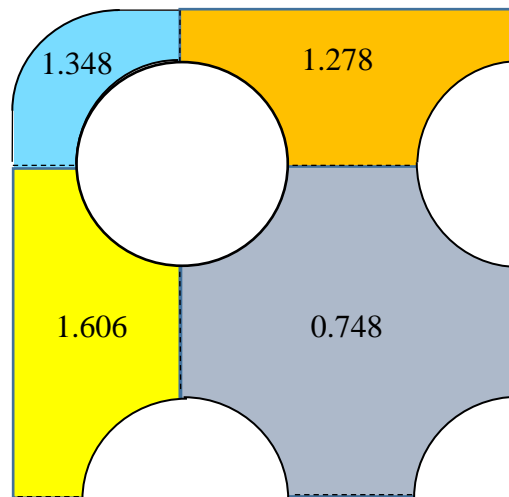


**Figure 2.10: Grid spacer loss coefficients for top left corner**

The large water channel in the center of the fuel assembly is treated as stagnant and not associated with the mass flow of the bundle. The subchannel geometry and loss coefficients surrounding the water channel are shown in *figure 2.11*.
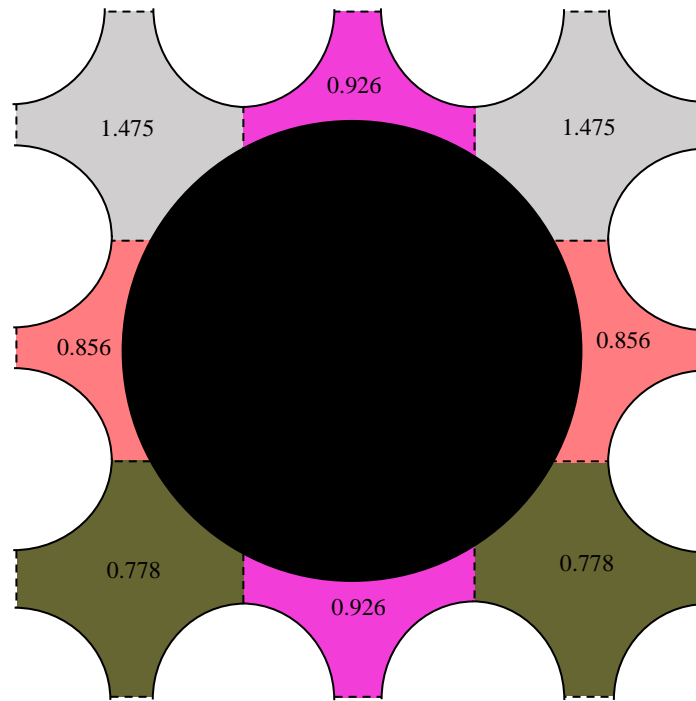


**Figure 2.11: Grid spacer loss coefficients surrounding the central water channel**

## 2.7    Representative BWR Operating Conditions

*Figure 2.12* is an operaing power/flow map comparing the natural circulation ESBWR with

typical pump-driven BWRs currently in operation [9]. *Figure 2.12* indicates that the typical

operating flow rate per bundle for currently operating BWRs is approximately 17kg/s while

the ESBWR is projected to operate near 9.0kg/s. In addition, the nominal average power per

bundle is approximately in a range between 3.8 to 5.8MWth for typical operating BWRs.
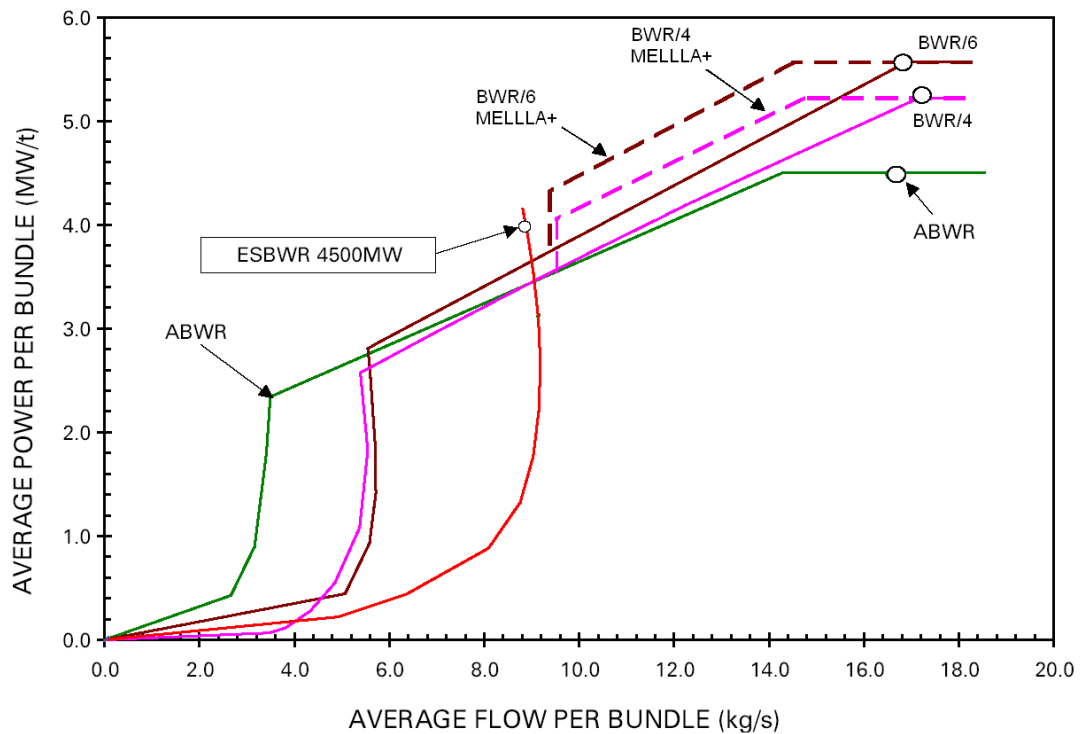


**Figure 2.12: Average power/flow per bundle map for the ESBWR and BWR**

According to the IAEA website, *https://aris.iaea.org/sites/core.html*, *table 2.6* is an additional collection of typical operating conditions for the currently operating ABWR and the licensed ESBWR [6].

| Table 2.6:   ABWR and ESBWR Operating Conditions | | | | | |
|---|---|---|---|---|---|
| Reactor Type | Thermal Output (MW) | Coolant Flow Rate (kg/s) | Operating Pressure (MPa) | Coolant inlet Temperature (°C) | Number of Assemblies |
| ABWR | 3926 | 14502 | 7.07 | 278 | 872 |
| ESBWR | 4500 | 9570 | 7.17 | 276.2 | 1132 |

Furthermore, the ABWR general design by General Electric reinforces the typical operating conditions seen in *table 2.7* [11].

| Table 2.7:   ABWR Operating Conditions | | | | | |
|---|---|---|---|---|---|
| Reactor Type | Thermal Output (MW) | Coolant Flow Rate (Mkg/hr) | Operating Pressure (MPa) | Exit Quality % | Number of Assemblies | Number of Rods per Assembly |
| ABWR | 3926 | 52.2 | 7.17 | 14.5 | 872 | 92 |

The average bundle power and mass flow have been generalized in the following calculations for comparison purposes to the test conditions in the NUPEC BFBT experiments.

ABWR average bundle power:

$$Average\ Bundle\ Power = \frac{3926MW}{872\ Bundle} = 4.502MW\ per\ Bundle$$

ABWR average bundle mass flow:

$$Average\ Bundle\ Mass\ Flow = \frac{14502\frac{kg}{s}}{872\ Bundle} = 16.63\frac{kg}{s}\ per\ Bundle$$

ESBWR average bundle power:

$$Average\ Bundle\ Power = \frac{4500MW}{1132\ Bundle} = 3.98MW\ per\ Bundle$$

ESBWR average bundle mass flow:

$$Average\ Bundle\ Mass\ Flow = \frac{9572\frac{kg}{s}}{1132\ Bundle} = 8.45\frac{kg}{s}\ per\ Bundle$$

These approximate values for the ABWR and ESBWR average bundle mass flow rates and powers are based on 10X10 assemblies and are similar to values seen in *figure 2.12*. From "*The Guide Book to Nuclear Reactors*," typical operating conditions for a pre-ABWR 8X8 are seen given in *table 2.8* [10].

| Table 2.8:   Typical 8X8 BWR Operating Conditions | | | | | |
|---|---|---|---|---|---|
| Thermal Output (MW) | Coolant Flow Rate (Mg/s) | Operating Pressure (MPa) | Exit Quality % | Number of Assemblies | Number of Rods per Assembly |
| 3579 | 13 | 7.0 | 14.7 | 748 | 62 |

BWR average bundle power:

$$Average\ Bundle\ Power = \frac{3579MW}{748\ Bundle} = 4.785MW\ per\ Bundle$$

BWR average bundle mass flow:

$$Average\ Bundle\ Mass\ Flow = \frac{13\frac{Mg}{s}}{748\ Bundle} = 17.38\frac{kg}{s}\ per\ Bundle$$

## 2.8 NUPEC BFBT Test Cases

The test cases P60001, P60007, and P60015 were selected to span a range of thermal outputs, mass flows, and exit qualities. All three test cases exhibit the typical BWR exit pressure of approximately 7.17MPa (1040psi). Test case P60015 approximates nominal BWR operating conditions.

| Table 2.9: Selected Test Case Operating Conditions and Pressure Drop Measurements | | | | | | |
|---|---|---|---|---|---|---|
| Operating Condition | Test Case | | | | | |
| | P60001 | | P60007 | | P60015 | |
| Exit Pressure | 7.16 MPa | 1038 psi | 7.17 MPa | 1040 psi | 7.17 MPa | 1040 psi |
| Inlet Fluid Temperature | 277.3°C | 531.14°F | 277.8°C | 532.04°F | 278.2°C | 532.76°F |
| Flow Rate | 20.2 t/hr | $4.44X10^4 \frac{lbm}{hr}$ | 55.0 t/hr | $1.21X10^5 \frac{lbm}{hr}$ | 70.0 t/hr | $1.54X10^5 \frac{lbm}{hr}$ |
| Power | 0.863 MW | $2.945X10^6 \frac{BTU}{hr}$ | 2.375 MW | $8.104X10^6 \frac{BTU}{hr}$ | 5.34 MW | $1.82X10^7 \frac{BTU}{hr}$ |
| Outlet Quality | 6.7 % | | 7.0 % | | 15.1 % | |
| Pressure Drop Identifier | Pressure Drop | | | | | |
| | P60001 | | P60007 | | P60015 | |
| | kPa | psi | kPa | psi | kPa | psi |
| dp01 | 1.15 | 0.167 | 5.59 | 0.811 | 14.93 | 2.165 |
| dp02 | 1.96 | 0.284 | 6.70 | 0.972 | 17.00 | 2.466 |
| dp03 | 2.53 | 0.367 | 8.11 | 1.176 | 19.33 | 2.804 |
| dp04 | 3.48 | 0.505 | 9.55 | 1.385 | 20.96 | 3.040 |
| dp05 | 3.66 | 0.531 | 9.06 | 1.314 | 20.33 | 2.949 |
| dp06 | 3.93 | 0.570 | 8.40 | 1.218 | 17.40 | 2.524 |
| dp07 | 12.27 | 1.780 | 22.84 | 3.313 | 41.22 | 5.978 |
| dp08 | 5.50 | 0.798 | 8.25 | 1.197 | 10.48 | 1.520 |
| dp09 | 27.40 | 3.974 | 57.89 | 8.396 | 113.97 | 16.530 |

The full list of test case operating conditions and pressure drop measurements for the P6 series experiments in the "*Steady State Pressure Drop Benchmark*" with the 8X8 High Burn-Up test bundle, C2A, is in *appendix B* [7]. The range of given test parameters listed for the NUPEC BFBT pressure drop experiment are given in *table 2.10*.

| Table 2.10: Range of NUPEC BFBT Test Parameters | | | |
|---|---|---|---|
| Flow Rate (t/h) | Power (MW) | Outlet Quality (%) | Total Pressure Drop (kPa) |
| 20.0 to 70.2 | 0.837 to 6.478 | 6.7 to 25.1 | 26.38 to 113.97 |

**CHAPTER 3: COBRA-CTF**

COBRA-TF was originally developed in 1980 by Pacific Northwest Laboratory under sponsorship of the Nuclear Regulatory Commission (NRC) as a thermal hydraulic rod-bundle analysis code [1]. COBRA-TF contributed toward goals set by revisions to NRC safety analysis requirements (10 CFR.50.46) in 1988 to improve plant economy and safety with the use of computational best-estimate models in plant design and operation [1]. COBRA-TF was primarily designed to perform LWR rod-bundle transient analysis and simulate pressurized water reactor (PWR) whole-vessel loss-of coolant accidents (LOCA) [1]. COBRA-CTF is an improved version of COBRA-TF developed and maintained by the Reactor Dynamics and Fuel Management Group (RDFMG) at the Pennsylvania State University (PSU) [1]. RDFMG PSU improvements include [1]:

- Transition to FORTRAN 90 source code

- Enhanced user-friendliness with improved error checking and free-form input

- Quality assurance utilizing an extensive validation & verification (V&V) matrix

- Turbulent mixing, void drift and direct heating model improvements

- Enhanced computational efficiency by implementation of new numerical solution schemes

- Better code physical model and user modeling documentation.

As of August 2015, the RDFMG has been rebranded the Reactor Dynamics and Fuel Modeling Group (RDFMG) and is located at North Carolina State University (NCSU).

COBRA-CTF uses a two-fluid modeling approach involving three separate independent flow fields which consist of a liquid film, liquid droplets, and vapor [1]. Each of the three fields is modeled with its own set of conservation equations [1]. However, the liquid and droplet flow fields are assumed to be in thermal equilibrium and share an energy equation [1]. The user may choose how the sets of conservation equations are formulated either using a Cartesian coordinate system or a subchannel approach [1]. A flow regime map based on a nodes' current time step vapor fraction determines flow topology [1]. This allows for determination of the interphase contact area, interphase heat transfer and drag, and the correct selection of closure models [1].

The sub-channel approach is used for this study where only axial and lateral flows are considered [1]. The lateral flow has no direction once it leaves a gap and applies to any orthogonal direction to the vertical axis [1]. The COBRA-CTF Theory Manual states, "This is a suitable assumption for the axially-dominated flow of a reactor fuel bundle because the relatively minuscule lateral flows transfer little momentum across sub-channel mesh cell elements [1]." The reason for choosing the simplified subchannel approach is that it utilizes one less momentum equation for each of the three flow fields and is consistent with the subchannel approach utilized in COBRA-EN [1].

The equations are solved simultaneously using the Semi-Implicit Method for Pressure-Linked Equations (SIMPLE) described in S.V. Patankar's book, "*Numerical Heat Transfer and Fluid Flow* [1]."

The steps of the SIMPLE algorithm are [1]:

1. Guess the pressure field, $p^*$.

2. Solve the momentum equations to obtain fluid velocities, $u^*$, $v^*$, and $w^*$.

3. Use the continuity equation to solve for the pressure field correction, $p'$.

4. Calculate the corrected pressure field, $p$, by adding $p'$ to $p^*$.

5. Calculate the corrected velocity field, $u$, $v$, and $w$, using the corrected pressure field.

6. Solve remaining discretized equations that influence the flow field.

7. Treat the corrected pressure, $p$, as the new guessed pressure, $p^*$ and repeat steps 1-6 until convergence is reached.

The SIMPLE method is explained in further detail in the COBRA-CTF theory manual. It is important to take notice of the first step that mentions, "…the user must provide a reference pressure... [1]." This guess for initial pressure is one of the inputs seen in *Card 1*, *PREF*, in global boundary conditions.

### 3.1 Generalized Conservation Equations

COBRA-CTF models each phase with its own set of mass, momentum, and energy equations [1]. The conservation equations for each flow field are linked by interaction terms that account for mass, energy, and momentum transfer between phases [1]. The conservation equations are discretized in space and time, and along with the appropriated closure relations, solved numerically to provide estimates of the solution variables at fixed time intervals over mesh cells representing the spatial domain [1]. There is a list of the parameters for the generalized conservation equations in *appendix C*.

Generalized Phasic Mass Conservation Equation [1]:

$$\frac{\partial}{\partial t}(\alpha_k \rho_k) + \nabla \cdot (\alpha_k \rho_k \vec{V}_k) = L_k M_e^T \qquad (1)$$

Generalized Phasic Momentum Conservation Equation [1]:

$$\frac{\partial}{\partial t}(\alpha_k \rho_k \vec{V}_k) + \frac{\partial}{\partial x}(\alpha_k \rho_k u_k \vec{V}_k) + \frac{\partial}{\partial y}(\alpha_k \rho_k v_k \vec{V}_k) + \frac{\partial}{\partial z}(\alpha_k \rho_k w_k \vec{V}_k) =$$

$$\alpha_k \rho_k \vec{g} - \alpha_k \nabla P + \nabla \cdot \left[\alpha_k (\tau_k^{ij} + T_k^{ij}) + \vec{M}_k^L + \vec{M}_k^d + \vec{M}_k^T\right] \qquad (2)$$

Generalized Phasic Energy Conservation Equation [1]:

$$\frac{\partial}{\partial t}(\alpha_k \rho_k h_k) + \nabla \cdot (\alpha_k \rho_k h_k \vec{V}_k) = -\nabla \cdot \left[\alpha_k (\vec{Q}_k + \vec{q}_k^T)\right] + \Gamma_k h_k^i + q_{wk}''' + \alpha_k \frac{\partial P}{\partial t} \qquad (3)$$

The subscript $k$ denotes the phase:

$$k = \begin{cases} v, & vapor \\ l, & liquid \\ e, & droplet \end{cases}$$

## 3.2  Normal Wall Flow Regime Map

Flow regime maps are used to characterize the flow topology in each mesh cell [1]. This allows for determination of the interphase contact area necessary for determination of interphase heat transfer and drag, as well as the correct selection of flow regime dependent closure models [1]. The normal wall flow regime map is used when the maximum wall surface temperature in the mesh cell described in *equation 4* is below the critical heat flux temperature:

$$T_W = min(705.3°F, T_{CHF}) \tag{4}$$

where the upper limit of 705.3 °F corresponds to the critical temperature of water, and the critical heat flux temperature is approximated by [1]:

$$T_{CHF} = (T_{Sat} + 75)°F \tag{5}$$

The hot wall flow regime map is used if the maximum wall temperature exceeds the value given by *equation 5*. At this point it is possible that the liquid will only partially wet the wall [1].

An initial void fraction check is made first to ensure that the mesh cell flow regime is consistent with adjacent axial mesh cells. COBRA-CTF then selects the flow regime once the appropriate void fraction is determined. *Figure 3.1* illustrates the normal wall flow regimes with associated vapor fraction ranges [1].
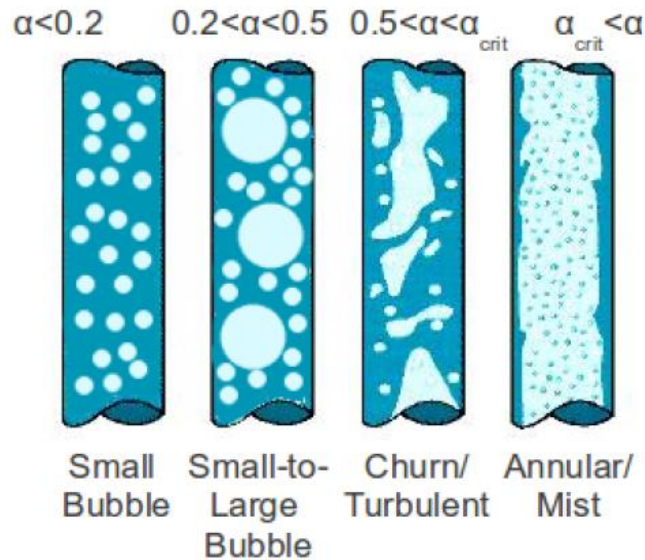


**Figure 3.1: COBRA-CTF normal wall flow regime map**

### 3.3 Pressure Drop

For more details on how pressure drop is managed in COBRA-CTF, refer to the Macro-Mesh

Cell Closure Models chapter in the COBRA-CTF theory manual [1].

#### 3.3.1 Friction Loss model

COBRA-CTF uses a two-phase pressure drop model based on the work of Wallis [1]:

$$\left.\frac{dP}{dX}\right)_{fric,k} = \frac{f_{wk}G_k^2}{2D_h\rho_k}\Phi^2 \tag{6}$$

The frictional pressure drop term is calculated for both the vapor and liquid phase fields where

the mass flux of the field of interest is, $G_k$, and $\Phi^2$, is defined as [1]:

$$\Phi^2 = \begin{cases} 1/\alpha_l & for\ normal\ wall\ conditions \\ 1/\alpha_v & for\ hot\ wall\ conditions \end{cases} \tag{7}$$

The phasic friction factor, $f_{wk}$, is defined using the phase Reynold's number [1]. The single-

phase friction factor, $f_{wk}$, selected in the frictional pressure drop term has been used with prior

CASL evaluations of NUPEC BFBT two-phase pressure drop, P6 series, experiments for the

Phase II, "*Critical Power Benchmark*", Exercise 0, "*Steady State Pressure Drop Benchmark*.

$$f_{wk} = \max\begin{cases} 64/Re_k & laminar \\ 0.204Re_k^{-0.2} & turbulent \end{cases} \tag{8}$$

Phase Reynolds number is based on phasic properties [1]:

$$Re_k = \frac{D_h|G_k|}{\mu_k} \tag{9}$$

### 3.3.2  Form (Local) Loss Model

The local pressure drop is defined as [1]:

$$\frac{dP}{dX}\bigg)_{form,k} = \alpha_k \frac{K_x}{2\Delta X} \rho_k |U_k| U_k \tag{10}$$

The phase field, $k$, can be either liquid, vapor, or entrained droplets, and $U_k$ is the field velocity [1]. The form loss coefficient, $K_x$, may be user supplied, or code-calculated [1]. The grid spacer loss coefficients labeled in *figure 2.8* are the user supplied form loss coefficient, $K_x$. COBRA-CTF provides three methods to introduce local losses which include:

1. User specified loss coefficient provided at an axial location for a specified subchannel.

2. Calculate a flow blockage coefficient with a user specified pressure loss coefficient multiplier and a user defined ratio of blocked area to flow area.

3. Grid spacer models explained in the COBRA-CTF theory manual.

This study only explored the first option as this is consistent with the method used by COBRA-EN to manage local losses due to obstructions. This approach does not explicitly consider obstruction type, geometry, or any other parameter other than its location and associated loss coefficient.

### 3.4  Water Properties

COBRA-CTF can calculate water properties such as thermal conductivity, specific heat, viscosity, surface tension, and enthalpy for subcooled liquid, superheated vapor, and saturated properties of both phases [1]. The International Association for the Properties of Water and Steam (IAPWS) correlations to calculate the properties of water and steam have been integrated into COBRA-CTF [1].

### 3.5  Global Boundary Conditions

The operating conditions are entered in *Card 1.2, Global Boundary Conditions,* for COBRA-CTF.

The total inlet mass flow rate is used to calculate subchannel mass flow rates for the user

specified subchannels flow areas [3].

| Table 3.1: Total Inlet Mass Flow Rate | | |
|---|---|---|
| **P60001** | **P60007** | **P60015** |
| **kg/s** | | |
| 5.611 | 15.278 | 19.444 |
| **lbm/s** | | |
| 12.370 | 33.682 | 42.868 |
| **t/hr** | | |
| 20.2 | 55.0 | 70.0 |

The average linear heat rate per rod is total bundle power divided by the total rod length

multiplied by the total number of rods [3]. This entry is used later to build power profiles.

*Table 3.2* consist of the test cases' value for with associated given thermal output.

$$\bar{q}' = \frac{Q}{NH_{fuel}} \tag{11}$$

where:

$N$ = Number of electrically heated rods (60)

$H_{fuel}$ = Axial length of the electrically heated rod (3708mm or 12.165ft)

$Q$ = Total bundle thermal output

| Table 3.2: Average Linear Heat Rate per Rod | | |
|---|---|---|
| **Test Case** | | |
| P60001 | P60007 | P60015 |
| **Given Thermal Output (MW)** | | |
| 0.863 | 2.375 | 5.340 |
| **Average Linear Heat Rate per Rod (kW/m)** | | |
| 3.879 | 10.675 | 24.002 |

The initial guess for pressure in the fluid domain, *PREF,* for each test cases is listed in *table 3.3*.

| Table 3.3:   Initial Guess for Pressure, PREF | | |
|---|---|---|
| **P60001** | **P60007** | **P60015** |
| bar | | |
| 71.6 | 71.7 | 71.7 |
| MPa | | |
| 7.16 | 7.17 | 7.17 |
| psi | | |
| 1038.4702 | 1039.9206 | 1039.9206 |

The user can either specify initial inlet enthalpy, *HIN*, or temperature, *TIN*, for the fluid

domain [3].

| Table 3.4:   Inlet Fluid Temperature, TIN | | |
|---|---|---|
| **P60001** | **P60007** | **P60015** |
| °C | | |
| 277.3 | 277.8 | 278.2 |
| °F | | |
| 531.14 | 532.04 | 532.76 |

### 3.4.1   Inlet and Outlet Boundary Conditions

The inlet boundary conditions are total inlet mass flow rate used to calculate subchannel mass

flow rates for the user specified subchannels flow areas, and inlet fluid temperature, *TIN*. The

outlet boundary conditions are inlet fluid temperature, *TIN*, and exit pressure, *PREF*. The

COBRA-CTF user manual does provide the following disclaimer:

*Note: The enthalpy specified at the exit is not used by COBRA-TF if flow is in the positive*

*direction (i.e. out of the model). In the case of positive flow, the user may enter any number*

*for exit enthalpy [3].*

**3.5    Convergence Study for COBRA-CTF**

A mesh refinement (convergence) study was conducted to determine the sensitivity of simulation results to axial node length. This was accomplished by establishing a uniform mesh length based on the original data provided in *figure 2.5*. It is difficult to maintain a true uniform axial mesh with COBRA-CTF as the local losses due to grid spacers require their own identifying axial positions that interrupt this uniformity. This is not the situation for COBRA-EN.

The specified uniform mesh length is propagated along the heated bundle until encountering the non-uniform nodes before and after the grid spacer positions. Adjustments are made to accommodate these varying size nodes in proximity of the grid spacer. Then, the uniform node length would continue until it encountered the next grid spacer. This "Base" technique is a viable option for a majority of the mesh refinement cases for the three test cases evaluated. Modifications were required to ensure that some test cases would converge on a solution with extra attention placed on nodes in proximity of the grid spacers. This modified technique labeled "Uniform/Variable" was required for the 7X24 and 8X24 mesh refinement cases with the P60007 and P60015 test cases. In addition, the 5X24 mesh refinement case required a node size of 0.1 mm to be absorbed into a previous node to achieve a converged solution. Lastly, there was an exploration of relative size nodes in proximity of each other conducted in the mesh refinement case 6X24 that results in accelerated run time to achieve a converged solution.

### 3.5.1 Methods for Mesh refinement

The methods chosen to conduct the mesh refinement convergence study for the three test cases follow these constraints:

- *Most importantly*, achieve a converged solution with COBRA-CTF.

- Maintain the maximum number of uniform nodes possible while still providing grid spacer identifiers.

- Attempt to maintain some uniformity between COBRA-EN and COBRA-CTF for positions along the heated bundle to acquire data at the same locations.

- Maximize the number of axial positions shared between all the mesh refinement cases to reduce the need to interpolate to determine a quantity of interest at a specific position.

This last criterion ensures that the values generated by COBRA-CTF are being evaluated at common positions instead of introducing interpolation error. The primary quantities of interest are pressure drops, considering that is the parameter being compared to in the NUPEC BFBT benchmark database. There is also an evaluation of the vapor fraction, and flow quality. These parameters influence the mixture density which is an input to MPACT in the VERA-CS package.

### 3.5.2   Base Mesh Refinement Technique

The distance before the grid spacer is determined by subtracting the upper edge of the previous uniform node from the grid spacer position. The distance after the grid spacer is determined by subtracting the grid spacer position from the lower edge of next uniform node. *Figure 3.2* illustrates the Base technique applied near the grid spacer positions. It was observed that the size of the nodes before and after the grid spacers pose issues with run time or inhibit a converged solution. Furthermore, the run would converge faster and appear to be more stable between each step if all node sizes are close to the same size as the surrounding nodes.
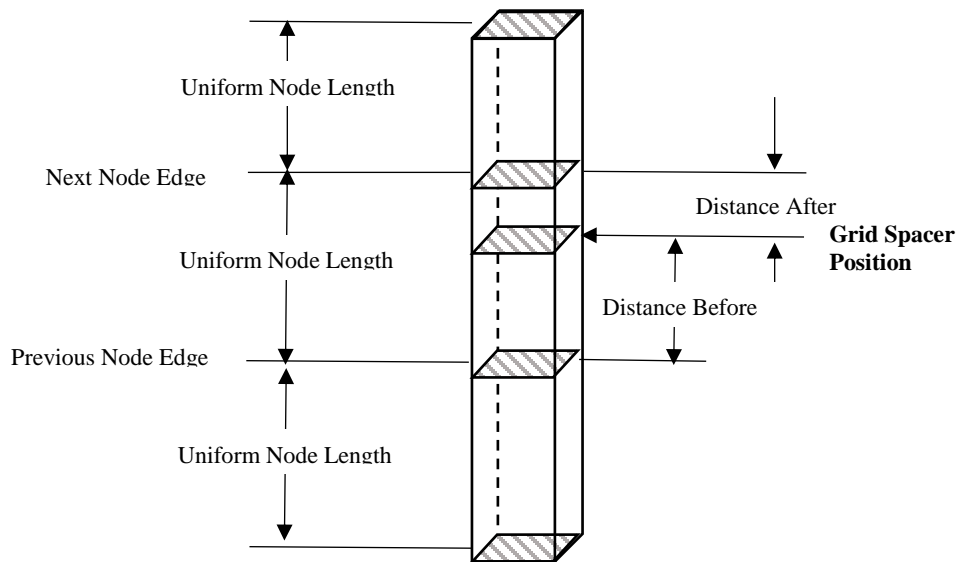


**Figure 3.2:   Diagram of the Base mesh refinement technique**

### 3.5.3  Uniform/Variable Mesh Refinement Technique

The Uniform/Variable (U/V) technique is a modified version of the Base technique built on observations that nodes of the same size in proximity to each other affect the speed and stability of reaching a converged solution. The variability introduced is due to the approximate uniform mesh lengths specified for a mesh refinement case within the distances before and after the grid spacers.

An arbitrary distance is determined by adding the previously calculated distance before the grid spacer to a collection of uniform nodes. Then, this arbitrary distance is divided to provide a node size that is approximately the same as the specified uniform node size. The same process is repeated after the grid spacer. The specified uniform mesh size is reintroduced at the end of the arbitrary distance after the grid spacer. *Figure 3.3* illustrates the U/V technique at one grid spacer. This process repeats for every grid spacer. This arbitrary distance before and after the grid spacer will be referred to as "padding." *Figure 3.4* illustrates this padding that contains a collection of equal sized nodes that are approximately of the specified uniform node length. The padding reduces the quantity of specified uniform node sizes and results in a reduction in shared axial positions for the mesh refinement cases. Furthermore, this padding will introduce error due to need for interpolation to determine the values at shared positions.

35
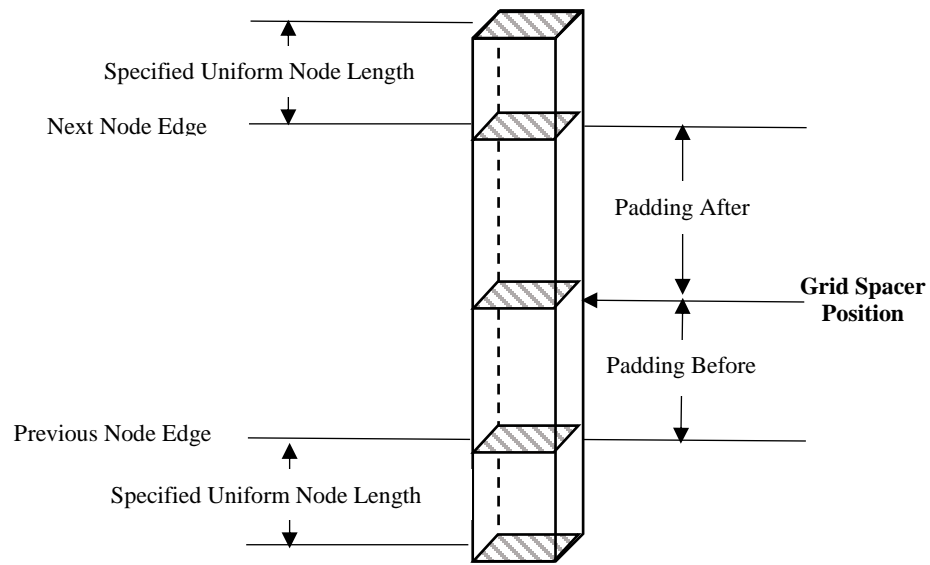


**Figure 3.3:   Diagram of the Uniform/Variable mesh refinement technique**
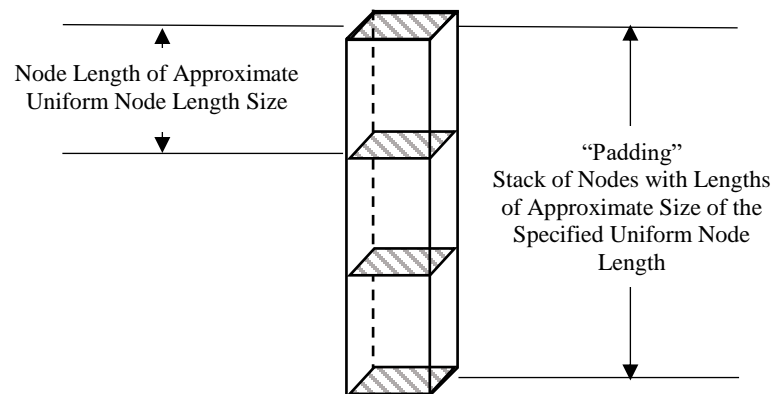


**Figure 3.4:   Diagram of the padding in proximity of a grid spacer**

### 3.5.4   Mesh Refinement Cases

The mesh refinement cases are categorized by the number of times the original node size seen

in *figure 2.5* is sub-divided.

$$Uniform\ Node\ Length = \frac{H_{fuel}}{DN} \tag{12}$$

$H_{fuel}$ = Axial length of the electrically heated rod

$D$ = Number divisions per node

$N$ = Number original nodes

| Table 3.5:   Mesh Refinement Case Uniform Node Length | | | | | | |
|---|---|---|---|---|---|---|
| Mesh Refinement Case | | | | | | |
| 1X24 | 3X24 | 4X24 | 5X24 | 6X24 | 7X24 | 8X24 |
| Uniform Node Length | | | | | | |
| Metric (m) | | | | | | |
| 0.1545 | 0.0515 | 0.038625 | 0.0309 | 0.02575 | **0.02207** | 0.0193125 |
| Standard (in) | | | | | | |
| **6.08268** | **2.02756** | **1.52067** | **1.21654** | **1.01378** | **0.86895** | **0.76033** |

*\* Bold indicates approximates values*

*Table 3.6* reflects the mesh refinement technique used to produce the results for each test case

for each mesh refinement case.

| Table 3.6:   Test Case Mesh Refinement Technique Legend | | | | | | | |
|---|---|---|---|---|---|---|---|
| Test Case | Mesh Refinement Case | | | | | | |
| | 1X24 | 3X24 | 4X24 | 5X24 | 6X24 | 7X24 | 8X24 |
| P60001 | Base | Base | Base | *Base | *Base | *Base | Base |
| P60007 | Base | Base | Base | *Base | *Base | *Base | U/V |
| P60015 | Base | Base | Base | *Base | *Base | U/V | U/V |

*\*Modifications to mesh refinement technique*

### 3.5.5   Adjustment to 5X24

Applying the Base technique results in the spaces before and after the fifth grid spacer seen in *table 3.7*. The axial positions are defined by the node edges. Axial position 2.503m, is the fifth grid spacer position while 2.472m and 2.5338m are axial positions shared by all the mesh refinement cases.

| Table 3.7:   5X24 Adjustment, Evaluation of 0.1mm Node Before 5th Grid Spacer | | | | | |
|---|---|---|---|---|---|
| Node Length (m) | | | | | |
| Uniform Node | Previous Uniform Node | Before Grid Spacer | After Grid Spacer | Next Uniform Node | Uniform Node |
| 0.0309 | 0.0309 | **0.0001** | 0.0308 | 0.0309 | 0.0309 |
| Axial Position (m) | | | | | |
| **2.472** | 2.5029 | **2.503** | **2.5338** | 2.5647 | |

*Figures 3.5* and *3.6* are plots of the time steps versus percent total energy storage for both techniques for mesh refinement case 5X24. *Figure 3.5* illustrates that after 40,000 steps the solution does not appear to be reaching convergence after a force quit was applied. This may reach a converged solution, but it would have taken excessive run times.
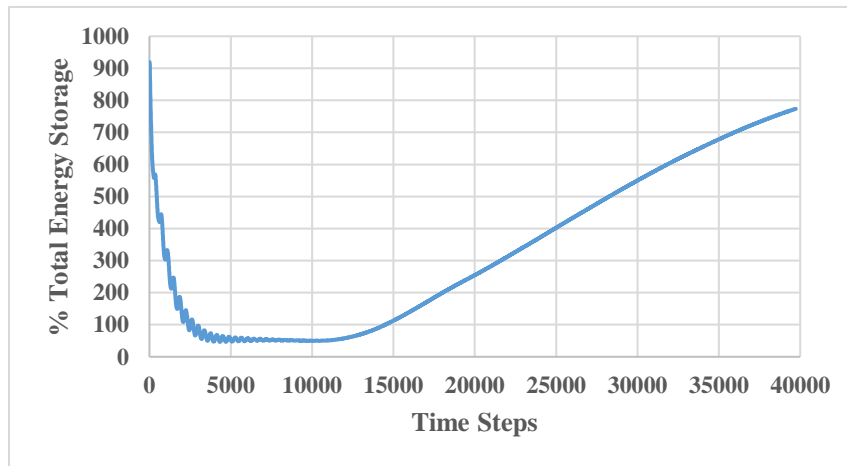


Figure 3.5:   Plot of failed solution convergence for P60001 5X24 with the 0.1mm node

A solution was obtained once the 0.1mm before the grid spacer is adjusted. *Table 3.8* reflects

that the 0.1mm space was absorbed in the next uniform space after the 2.472m position.

This preserves the positions of interest, 2.472m, 2.503m, and 2.5338m. in addition, all the

nodes in this area are approximately the same size. This correction allows for the run to

converge on a solution.

$$2.472m + 0.031m = 2.503m$$

| Table 3.8:   5X24 Adjustment, Change in Node Before 5th Grid Spacer | | | | | |
|---|---|---|---|---|---|
| Node Length (m) | | | | | |
| Uniform Node | Previous Uniform Node | Before Grid Spacer | After Grid Spacer | Next Uniform Node | Uniform Node |
| 0.0309 | 0.0309 | **0.031** | 0.0309 | 0.0309 | 0.0309 |
| Axial Position (m) | | | | | |
| 2.4411 | **2.472** | | **2.503** | **2.5338** | 2.5647 |

*Figure 3.6* illustrates that the solution is achieved at 4610 steps.
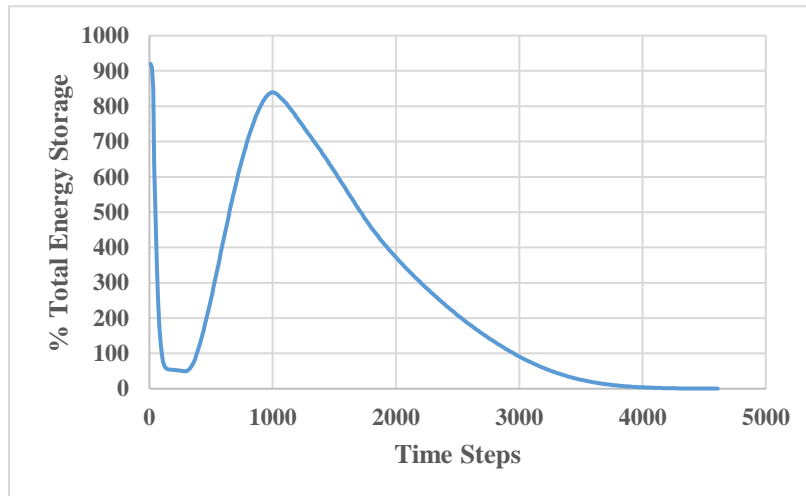


**Figure 3.6:   Plot of solution convergence for P60001 5X24 without the 0.1mm node**

### 3.5.6 Adjustment to 6X24

Applying the Base technique results in the space before and after the seventh grid spacer seen in *table 3.9*. Axial position, 3.527m, is the seventh grid spacer position while 3.5535m is an axial position shared by all the mesh refinement cases.

| Table 3.9: 6X24 Adjustment, Evaluation of 0.75mm Node After 7th Grid Spacer | | | | | |
|---|---|---|---|---|---|
| Node Length (m) | | | | | |
| Uniform Node | Previous Uniform Node | Before Grid Spacer | After Grid Spacer | Next Uniform Node | Uniform Node |
| 0.02575 | 0.02575 | 0.025 | **0.00075** | 0.02575 | 0.02575 |
| Axial Position (m) | | | | | |
| 2.47625 | 3.502 | **3.527** | 3.52775 | **3.5535** | |

*Table 3.10* shows that the 0.75mm space is absorbed with the following uniform distance starting at 3.52775m. This preserves the positions of interest 3.527m, and 3.5535m. in addition, all the nodes in this area are approximately the same size. All three test cases can use both methods to converge on a solution.

| Table 3.10: 6X24 Adjustment, Change in Node After 7th Grid Spacer | | | | | |
|---|---|---|---|---|---|
| Node Length (m) | | | | | |
| Uniform Node | Previous Uniform Node | Before Grid Spacer | After Grid Spacer | Next Uniform Node | Uniform Node |
| 0.02575 | 0.02575 | 0.025 | **0.0265** | 0.02575 | 0.02575 |
| Axial Position (m) | | | | | |
| 3.47625 | 3.502 | **3.527** | **3.5535** | 3.57925 | |

Including the 0.75mm after the grid spacer, the run for P60001 takes 24,810 steps to reach a converged solution. When the distance of 0.75mm is absorbed, the solution converges after 8,557 steps. The same acceleration is seen on P60007 and P60015.

### 3.5.7 Adjustment to 7X24

Applying the Base technique to P60001 test case results in the space before and after the third

grid spacer seen in *table 3.11*. Axial position, 1.479m, is the third grid spacer position. The

uniform mesh size of approximately 0.022071m, allows for four nodes before and one node

after the two spaces surrounding the grid spacer which results in the two axial positions shared

by all the mesh refinement cases, 1.3905m and 1.545m respectively.

| Table 3.11: 7X24 Adjustment, Evaluation of 0.214mm Node Before 3rd Grid Spacer | | | | | |
|---|---|---|---|---|---|
| Node Length (m) | | | | | |
| Uniform Node | Previous Uniform Node | Before Grid Spacer | After Grid Spacer | Next Uniform Node | Uniform Node |
| 0.022071 | 0.022071 | **0.000214** | 0.021857 | 0.022071 | 0.022071 |
| Axial Position (m) | | | | | |
| 1.4567 | 1.4788 | **1.479** | 1.50086 | 1.5229 | |

*Table 3.12* shows that the 0.214mm space is absorbed with the previous uniform distance

starting at 1.4567m. This preserves the grid spacer position 1.479m. In addition, all the nodes

in this area are approximately the same size.

| Table 3.12: 7X24 Adjustment, Change in Node Before 3rd Grid Spacer | | | | | |
|---|---|---|---|---|---|
| Node Length (m) | | | | | |
| Uniform Node | Previous Uniform Node | Before Grid Spacer | After Grid Spacer | Next Uniform Node | Uniform Node |
| 0.022071 | 0.022071 | **0.022286** | 0.021857 | 0.022071 | 0.022071 |
| Axial Position (m) | | | | | |
| 1.4346 | 1.4567 | **1.479** | 1.50086 | 1.5229 | |

The same acceleration is observed as the mesh refinement case 6X24. Including the 0.214mm

after the grid spacer, the run for P60001 takes 56,632 steps to reach a converged solution. The

solution converges after 4,192 steps when the distance of 0.214mm is removed.

The Base technique used in the P60001 test case did not converge on a solution and exhibited an oscillatory behavior for P60007 until a user force quit applied at 80,000 steps. This lead to more adjustments to the Base technique labeled "*Test 1*" where further attempts to ensure node lengths are more similar in size to nodes in proximity. *Table 3.13* reflects the location of further adjustments made compared to the Base technique for the 7X24 mesh refinement case labeled "With 0.241mm." The locations marked in bold red indicate quantity of nodes, JLEV, with node lengths, VARDX, prior to adjustments while the bold black text marks the adjustments. Further adjustments to the 7x24 mesh refinement case labeled "*Test 1*" include modifications to node lengths near the second and seventh grid spacer.

| Table 3.13: Further Adjustment to 7X24 Base Technique | | | | | |
|---|---|---|---|---|---|
| **With 0.214mm** | | **Without 0.214mm** | | **7X24 Test 1** | |
| **JLEV** | **VARDX** | **JLEV** | **VARDX** | **JLEV** | **VARDX** |
| No Change | | | | | |
| 46 | 0.017928571429 | 46 | 0.017928571429 | 46 | 0.017928571429 |
| 47 | 0.004142857143 | *47* | *0.004142857143* | *47* | *0.026214285714* |
| 70 | 0.022071428571 | 69 | 0.022071428571 | 68 | 0.022071428571 |
| *71* | *0.000214285714* | *70* | *0.022285714286* | **69** | **0.022285714286** |
| 72 | 0.021857142857 | 71 | 0.021857142857 | 70 | 0.021857142857 |
| No Change | | | | | |
| 167 | 0.017642857143 | 166 | 0.017642857143 | 165 | 0.017642857143 |
| 168 | 0.004428571429 | *167* | *0.004428571429* | *166* | *0.026500000000* |
| 176 | 0.022071428571 | 175 | 0.022071428571 | 174 | 0.022071428571 |

*JLEV is a numbering system used by COBRA-CTF to determine a quantity of nodes of the same size, VARDX. The actual value for JLEV is determined by subtracting the previous value from the next in sequence. Example:*

$$JLEV(71) - JLEV(70) = 1$$

*Table 3.14* provides a closer look at the node spacing near the second grid spacer located at 0.967m where the node length before is 0.0179m and after is 0.00414m in the "Without 0.214mm" case.

| Table 3.14: 7X24 Test 1, Evaluation of Node After 2nd Grid Spacer | | | | | |
|---|---|---|---|---|---|
| Node Length (m) | | | | | |
| Uniform Node | Previous Uniform Node | Before Grid Spacer | After Grid Spacer | Next Uniform Node | Uniform Node |
| 0.022071 | 0.022071 | 0.017929 | **0.004143** | 0.022071 | 0.022071 |
| Axial Position (m) | | | | | |
| 0.927 | 0.94907 | **0.967** | 0.97114 | 0.99321 | |

*Table 3.15* shows the adjustment to the 4.14mm space is absorbed with the next uniform distance starting at 0.971m seen in *table 3.14*.

| Table 3.15: 7X24 Test 1, Change in Node After 2nd Grid Spacer | | | | | |
|---|---|---|---|---|---|
| Node Length (m) | | | | | |
| Uniform Node | Previous Uniform Node | Before Grid Spacer | After Grid Spacer | Next Uniform Node | Uniform Node |
| 0.022071 | 0.022071 | 0.017929 | **0.026214** | 0.022071 | 0.022071 |
| Axial Position (m) | | | | | |
| 0.927 | 0.94907 | **0.967** | 0.99321 | 1.01529 | |

*Table 3.16* provides the node spacing near the seventh grid spacer located at 3.527m where the

node length before is 0.0176m and after is 4.43mm in the "Without 0.214mm" case.

| Table 3.16: 7X24 Test 1, Evaluation of Node After 7th Grid Spacer | | | | | |
|---|---|---|---|---|---|
| Node Length (m) | | | | | |
| Uniform Node | Previous Uniform Node | Before Grid Spacer | After Grid Spacer | Next Uniform Node | Uniform Node |
| 0.022071 | 0.022071 | 0.017643 | **0.004429** | 0.022071 | 0.022071 |
| Axial Position (m) | | | | | |
| 3.4873 | | 3.5094 | **3.527** | 3.5314 | **3.5535** |

*Table 3.17* shows that the 4.43mm space is absorbed with the next uniform distance starting at

3.5314m seen in *table 3.16*. This preserves the grid spacer position 3.527m, and the position

3.5535m shared by other mesh refinement cases.

| Table 3.17: 7X24 Test 1, Change in Node After 7th Grid Spacer | | | | | |
|---|---|---|---|---|---|
| Node Length (m) | | | | | |
| Uniform Node | Previous Uniform Node | Before Grid Spacer | After Grid Spacer | Next Uniform Node | Uniform Node |
| 0.022071 | 0.022071 | 0.017643 | **0.0265** | 0.022071 | 0.022071 |
| Axial Position (m) | | | | | |
| 3.4873 | | 3.5094 | **3.527** | **3.5535** | 3.5756 |

The adjustments made near the second and seventh grid spacers in the 7x24 *Test 1* mesh

refinement case ensures that all the nodes are similar in size to nodes in proximity which can

be seen in *table 3.5*. The adjustments made in the 7X24 Test 1 case do result in a converged

solution after 4,684 steps for test case P60007.

The P60015 test case did not converge on a solution with the modified Base technique described in the 7X24 *Test 1* mesh refinement case. There is a listing of failed 7X24 mesh refinement cases conducted for the P60015 test case in *appendix D*. Failure of the further modifications to the Base technique led to the development of the U/V technique. The first attempt of the U/V technique for the 7X24 mesh refinement case labeled *Test 6* did not reach a converged solution and exhibited oscillatory behavior. Further manipulation of the node lengths within the "padding" before and after grid spacers resulted in the successful 7X24 *Test 8* mesh refinement case. *Table 3.18* illustrates the similarity between variations in mesh refinement cases 7X24 *Test 6* and *Test 8*.

| Table 3.18: Uniform/Variable Technique, 7X24 Test 6 and Test 8 | | | |
|---|---|---|---|
| **7X24 Test 6** | | **7X24 Test 8** | |
| **JLEV** | **VARDX** | **JLEV** | **VARDX** |
| No Change | | | |
| 92 | 0.022833333333 | 92 | 0.022833333333 |
| *93* | *0.017500000000* | *98* | *0.028666666667* |
| 114 | 0.022071428571 | 112 | 0.022071428571 |
| *116* | *0.015500000000* | *113* | *0.031000000000* |
| 122 | 0.020583333333 | 119 | 0.020583333333 |
| 136 | 0.022071428571 | 133 | 0.022071428571 |
| 140 | 0.019875000000 | 137 | 0.019875000000 |
| 144 | 0.018750000000 | 141 | 0.018750000000 |
| 158 | 0.022071428571 | 158 | 0.022071428571 |
| *164* | *0.021333333333* | *161* | *0.020595238095* |
| 165 | 0.026500000000 | 162 | 0.026500000000 |
| 172 | 0.022071428571 | 169 | 0.022071428571 |

*Table 3.19* list the uniform node length for the 7X24 mesh refinement case, grid spacer axial

positions, and the quantity of same size nodes used to build the padding before and after the

grid spacers. Test case P60015 converges on a solution with mesh refinement 7X24 *Test 8*

in 4,536 steps.

| Table 3.19: Uniform/Variable Grid Spacer Padding for 7X24 Test 8 | | | | |
|---|---|---|---|---|
| Uniform Node Length for 7X24 (m) | | | | |
| 0.0220714286 | | | | |
| Padding Before Grid Spacer | | Grid Spacer Axial Position (m) | Padding After Grid Spacer | |
| Quantity of Nodes | ΔZ of Adjusted Nodes (m) | | Quantity of Nodes | ΔZ of Adjusted Nodes (m) |
| 7 | 0.02086 | 0.455 | 1 | 0.00850 |
| 2 | 0.02000 | 0.967 | 5 | 0.02290 |
| 1 | 0.02229 | 1.479 | 3 | 0.02200 |
| 6 | 0.02283 | 1.991 | 6 | 0.02867 |
| 1 | 0.03100 | 2.503 | 6 | 0.02058 |
| 4 | 0.01988 | 3.015 | 4 | 0.01875 |
| 3 | 0.02060 | 3.527 | 1 | 0.02650 |

### 3.5.8 Adjustment to 8X24

The P60001 test case uses the Base technique while test cases P60007 and P60015 require the Uniform/Variable technique. Test case P60007 uses the 8X24 *Test 1* setup and P60015 uses the 8X24 *Test 2* seen in *table 3.20*, and in *appendix D*. Other attempts were made to make these comparable to the previous mesh refinement tests, but the 8X24 case appears to be extremely sensitive to node size which affects the placement of axial positions. This sensitivity is especially noticeable in the proximity of the grid spacer positions. In addition, the more problematic P60007 and P60015 test cases do exhibit the transition from the "small-to-large bubble" to the "churn/turbulent" flow regimes at the 0.5 vapor fraction value. P60007 8X24 *Test 1* and P60015 8X24 *Test 2* converges on a solution at 5,068 and 6,358 steps respectively.

| Table 3.20: 8X24 Test 1 and Test 2 | | | |
|---|---|---|---|
| **8X24 Test 1** | | **8X24 Test 2** | |
| **JLEV** | **VARDX** | **JLEV** | **VARDX** |
| No Change | | | |
| 104 | 0.019861111111 | 104 | 0.019861111111 |
| **114** | **0.019312500000** | **112** | **0.030000000000** |
| **131** | **0.018757352941** | **126** | **0.019428571429** |
| 148 | 0.019312500000 | 145 | 0.019312500000 |
| **158** | **0.018368750000** | **153** | **0.018132812500** |
| **161** | **0.032785714286** | 168 | 0.019312500000 |
| **168** | **0.018734693878** | **180** | **0.018526041667** |
| 180 | 0.019312500000 | 188 | 0.019312500000 |
| **183** | **0.016916666667** | **189** | **0.026500000000** |
| 191 | 0.019312500000 | | |
| **192** | **0.027000000000** | | |

## 3.6    Total Power Forcing Function

COBRA-CTF calculates the local linear heat rate transferred through the rod surface to the

coolant with *equation 13* [3]:

$$\dot{q}(rod, x, t) = (1 - d)\dot{q}f_{time}(t)f_{axial}(x, t)f_{radial}(rod, t) \qquad (13)$$

where:

$\dot{q}$ = average linear heat rate per rod.

$d$ = Fraction of local heat rate generated by the heater rods which is released directly into the

    coolant, not the vapor.

$f_{time}(t)$ = Power factor, *FQ(N)*.

$$FQ(N) = \frac{power\ at\ tme\ YQ(N)}{initial\ power} \qquad (14)$$

$f_{axial}(x, t)$ = Relative axial power factor.

$f_{radial}(rod, t)$ = Radial power factors for all rods.


The axial peaking factors in *figure 2.5* are used to build the power table. These values are

interpolated linearly for axial power factors at that axial positions along the heated assembly.

The profile is re-integrated over each cell to obtain on average linear heat rate for the cell [3].
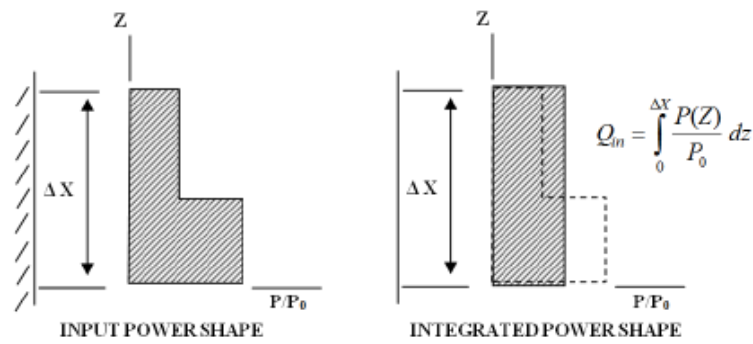


Figure 3.7:   Heat input over one fluid node

### 3.6.1 Axial Power Profile

The power profile is entered in *card 11* for COBRA-CTF. The axial peaking factors illustrated in *figure 2.5* and radial peaking factors illustrated in *figure 2.6* provided in the NUPEC BFBT benchmark database are entered in *card 11.4* and *card 11.8* respectively. There were no values provided at the ends of the heated rod. Typically, this axial peaking factor can be determined using the power profile function. Using a fit function built from the trendline feature in EXCEL for both a fifth and twelfth degree polynomials offers plausible values of 0.373 and 0.397 respectively. These values provide a computed supplied power close to the desired power indicated in the NUPEC BFBT database.

*Table 3.21* shows the computed COBRA-CTF power compared to the NUPEC BFBT test case operating power when the extrapolated axial peaking factor for the ends of the heated rod is selected to be 0.3125. This value was determined by trial and error.

| Table 3.21: Powers with 0.3125 Extrapolated Axial Peaking Factor | | |
|---|---|---|
| Computed Supplied Power (kW) | | |
| P60001 | P60007 | P60015 |
| 86300.1254 | 237500.3451 | 534000.7758 |
| Desired Power (MW) | | |
| P60001 | P60007 | P60015 |
| 0.863 | 2.375 | 5.34 |

Value for computed power supplied 86300.1254kW, 237500.3451kW, and 534000.7758kW appears to be a mistake with the output file, "ctf.heat". Refer to *table 3.2* for the test case total thermal powers and the average linear heat rates per rod.

**3.7    Mesh Convergence Study Pressure and Vapor Fraction Plots**

*Figures 3.9, 3.11,* and *3.13* are plots of vapor fraction for test cases P60001, P60007, and P60015. There are noticeable dips in predicted vapor fraction at the grid spacer locations. This behavior is nonphysical and appears to be a result of how COBRA-CTF manages local losses due to obstructions. There is an observable increase in the magnitude of the drop for vapor fraction in the "small-to-large bubble" region of the "normal wall" flow regime map defined as the vapor fraction between 0.2 to 0.5. There is an approximate 10 to 20 percent decrease in vapor fraction at the grid spacer locations illustrated in *figures 3.9, 3.11,* and *3.13* with in the "small-to-large bubble" region. There are zoomed in plots of the vapor fraction and pressure at the grid spacer positions for the test case P60007 in *appendix E*. These zoomed in plots for vapor fraction illustrate that the magnitude of the drop appears to be dependent on the axial position before the grid spacer position. There does not seem to be a consistent pattern to identify whether this dependence is directly related to the axial position, or in some connection to the node length that yields the node edge resulting in the axial position. This behavior appears to be more dominant at void fractions near transitions between flow regimes, especially near 0.5. Only observable trends are mentioned as there is no benchmark data to compare vapor fraction for the NUPEC BFBT Phase II, "*Critical Power Benchmark*", Exercise 0, "*Steady State Pressure Drop Benchmark*."

### 3.7.1    P60001, Mesh Convergence Study Pressure and Vapor Fraction Plots
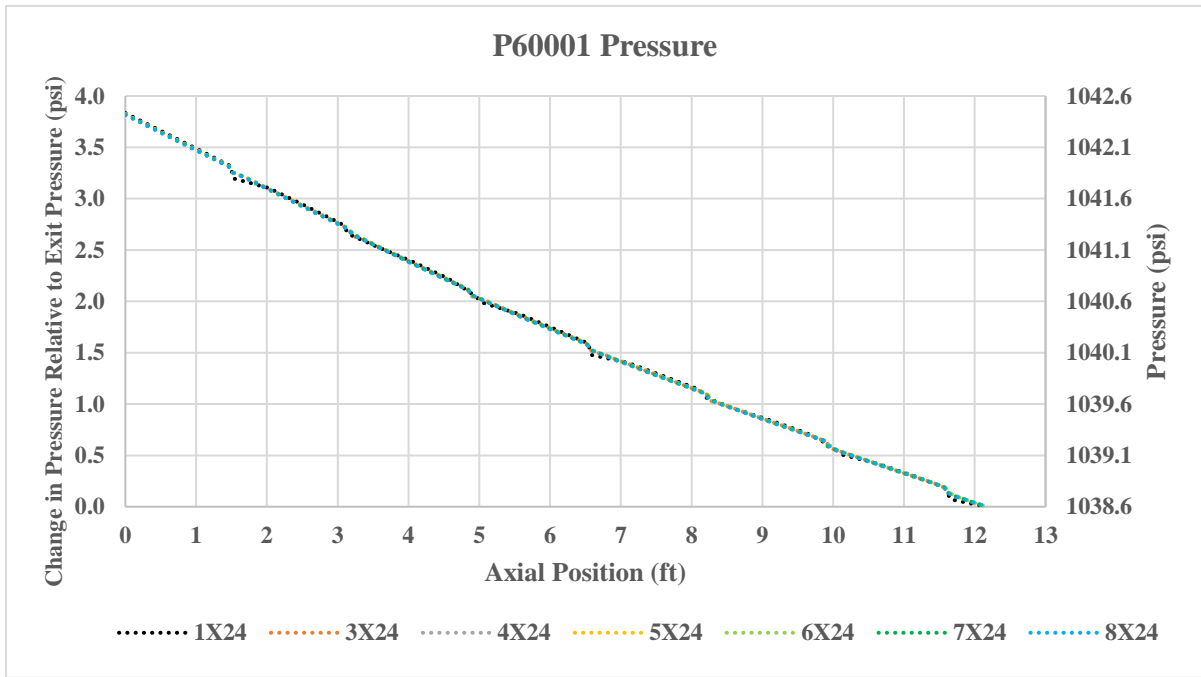


**Figure 3.8:   P60001, Pressure at axial positions for the convergence study mesh refinement cases**
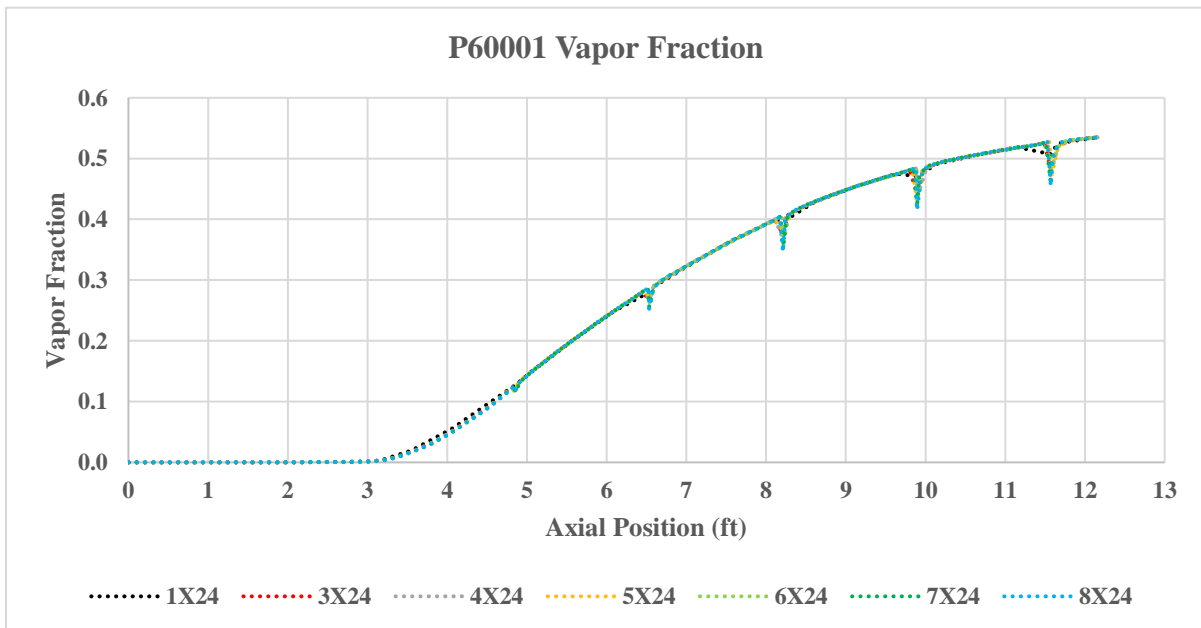


**Figure 3.9:   P60001, Vapor fraction at axial positions for the convergence study mesh refinement cases**
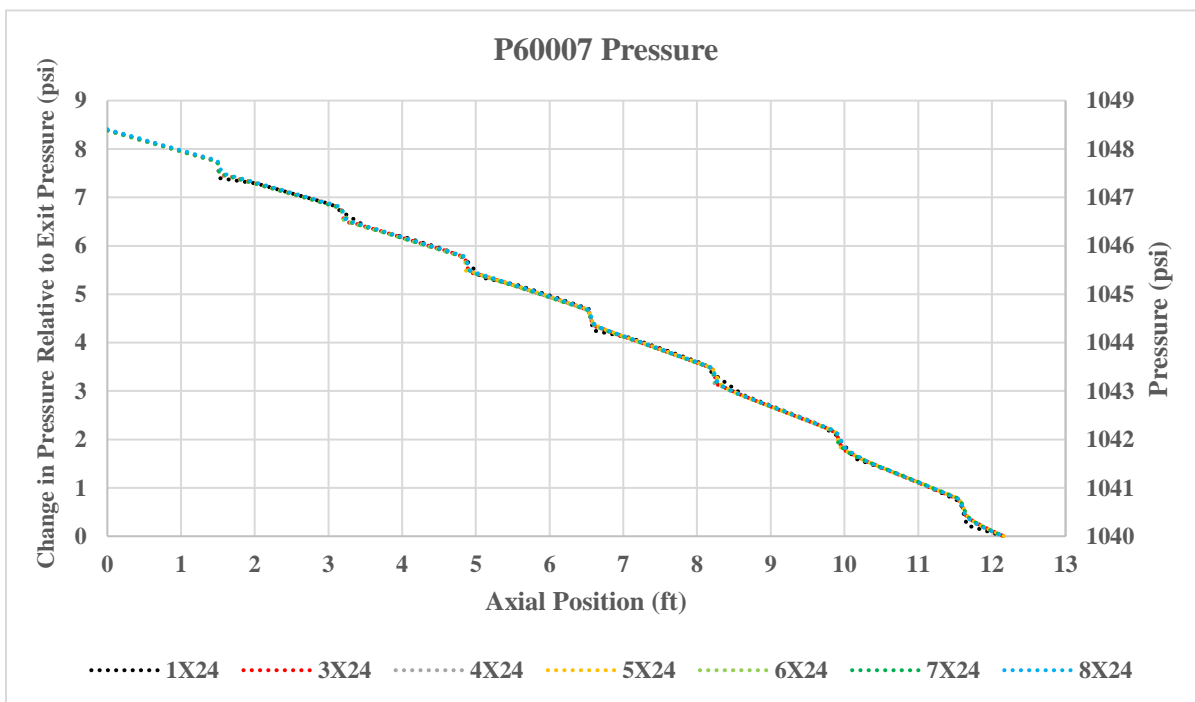
### 3.7.3    P60015, Mesh Convergence Study Pressure and Vapor Fraction Plots
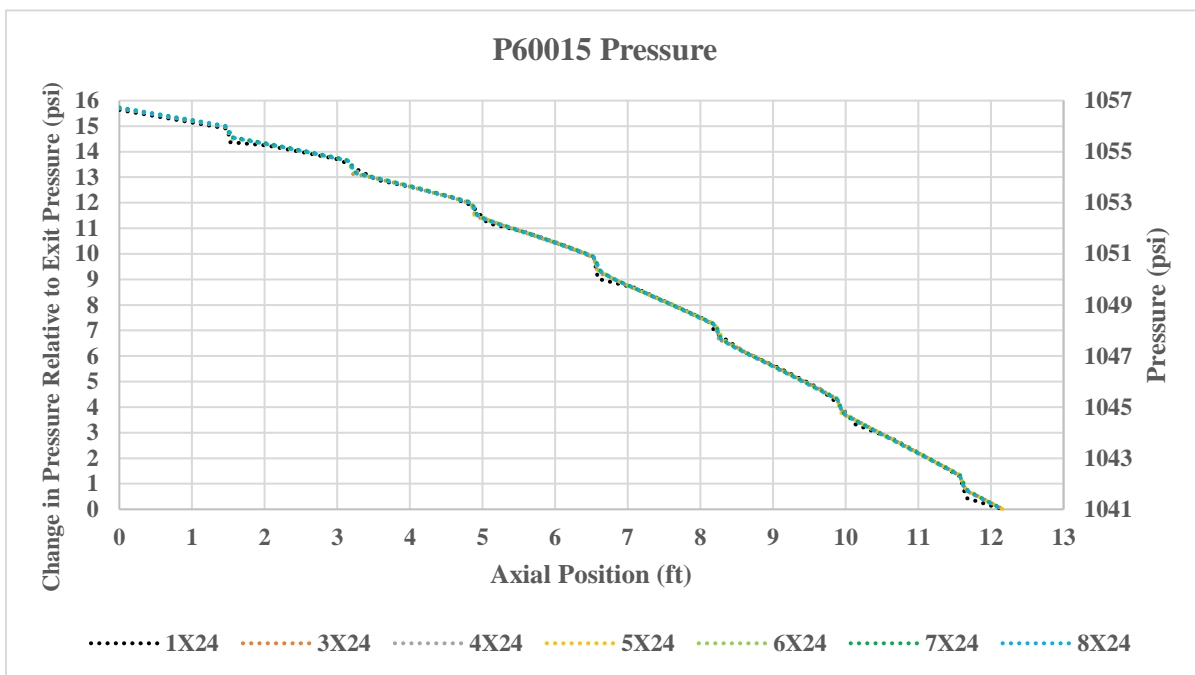


**Figure 3.12: P60015, Vapor fraction at axial positions for the convergence study mesh refinement cases**
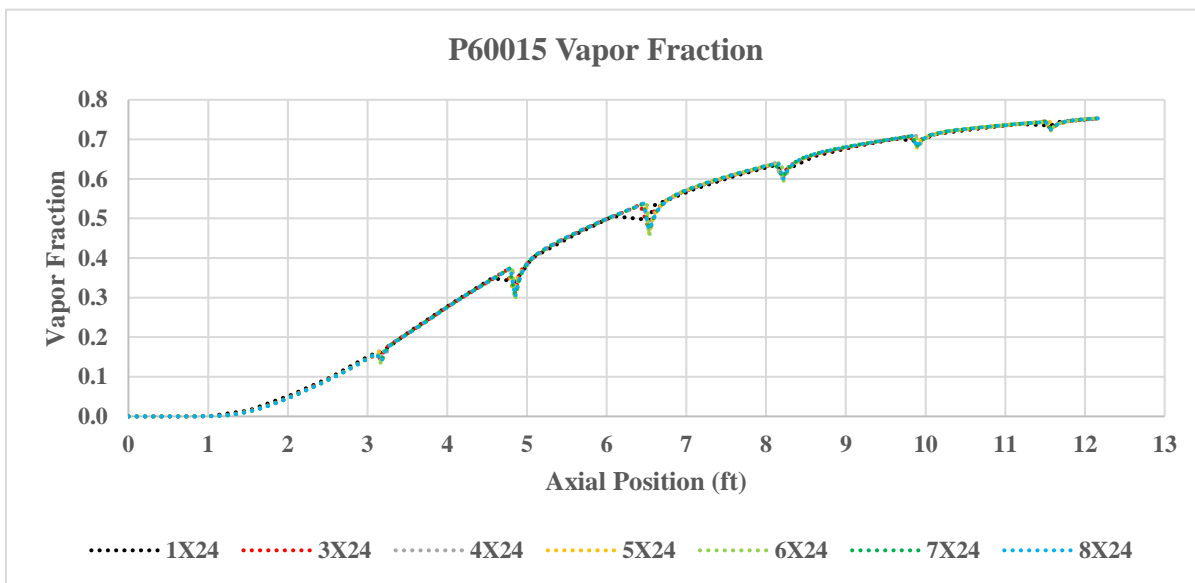


**Figure 3.13: P60015, Pressure at axial positions for the convergence study mesh refinement cases**

## 3.8 Mesh Convergence Study Analysis

The mesh refinement study was conducted to determine the sensitivity of simulation results to axial node length. Data is collected for all the mesh refinement cases for three benchmark cases. The primary parameter of interest is the pressures calculated by COBRA-CTF at the shared axial positions. In addition, vapor fraction, and flow quality have also been collected. Once this data has been tabulated, the absolute relative difference is calculated between two mesh refinement cases at each shared axial position.

$$Absolute\ Relative\ Difference = \frac{|Value - Value_{Reference}|}{Value_{Reference}} \tag{15}$$

This calculation is performed in ascending order from 1X24 to 3X24, 3X24 to 4X24, and so on until 7X24 to 8X24. The reference value is the preceding mesh reference case value. The $L_{\infty Norm}$ and the $L_{2Norm}$ is determined for a column of absolute relative differences between two mesh refinement cases. The $L_{\infty Norm}$ is the maximum value in the column and the $L_{2Norm}$ is defined in *equation 16*.

$$L_{2Norm} = \sqrt{(x_1{}^2 + x_2{}^2 + \cdots + x_n{}^2)} \tag{16}$$

There is a table containing an example of the absolute relative differences for test case P60001 shown in *appendix F* for reference.

An isolated example shown in *Table 3.22* consist of absolute relative differences from the results of the mesh refinement cases 1X24 and 3X24 involving the test case P60001. The rows marked in green indicate the grid spacer axial positions with their associated absolute relative difference values for pressure, vapor fraction, and flow quality.

| Table 3.22: P60001 Absolute Relative Difference for 1X24 to 3X24 | | | |
|---|---|---|---|
| **Axial Position (ft)** | **Pressure** | **Vapor Fraction** | **Flow Quality** |
| 0.000 | 0.008% | 0.000% | 0.000% |
| 0.154 | 0.008% | 0.000% | 0.200% |
| 0.309 | 0.008% | 70.470% | 68.901% |
| 0.455 | 0.008% | 15.209% | 14.902% |
| 0.464 | 0.003% | 13.668% | 13.929% |
| 0.618 | 0.008% | 10.744% | 11.017% |
| 0.773 | 0.008% | 9.015% | 9.122% |
| 0.927 | 0.008% | 7.568% | 6.995% |
| 0.967 | 0.003% | 4.202% | 3.429% |
| 1.082 | 0.006% | 8.808% | 9.406% |
| 1.236 | 0.009% | 7.428% | 7.932% |
| 1.391 | 0.009% | 4.851% | 4.878% |
| 1.479 | 0.006% | 4.724% | 2.275% |
| 1.545 | 0.004% | 0.667% | 0.917% |
| 1.700 | 0.009% | 0.000% | 0.000% |
| 1.854 | 0.009% | 0.000% | 0.481% |
| 1.991 | 0.009% | 3.214% | 0.394% |
| 2.009 | 0.004% | 0.346% | 0.385% |
| 2.163 | 0.009% | 0.304% | 0.321% |
| 2.317 | 0.009% | 0.272% | 0.000% |
| 2.472 | 0.009% | 0.000% | 0.241% |
| 2.503 | 0.004% | 5.051% | 0.235% |
| 2.627 | 0.007% | 0.000% | 0.216% |
| 2.781 | 0.008% | 0.000% | 0.000% |
| 2.936 | 0.008% | 0.211% | 0.182% |
| 3.015 | 0.006% | 5.945% | 0.000% |
| 3.090 | 0.005% | 0.204% | 0.000% |
| 3.245 | 0.008% | 0.000% | 0.163% |
| 3.399 | 0.008% | 0.193% | 0.156% |
| 3.527 | 0.008% | 5.128% | 0.000% |
| 3.554 | 0.003% | 0.762% | 0.151% |
| 3.708 | 0.008% | 0.000% | 0.147% |
| $L_{\infty Norm}$ | 0.00009 | 0.70470 | 0.68901 |
| $L_{2Norm}$ | 0.00042 | 0.77028 | 0.74905 |

**3.8.1   Absolute Relative Differences for the Mesh Refinement Convergence Study**

The tabulated absolute relative differences for the mesh refinement convergence study with the three test cases is categorized to convey different information based on the axial positions chosen. The motivation for this evaluation is the variability in void fraction in the vicinity of the grid spacers. In addition, this evaluation will provide insight on where the largest contribution of error is located. The absolute relative difference determined for pressure is based on bars as a unit of measure in *tables 3.23, 3.26*, and *3.29*.

- *All Shared Axial Positions:* All the values at the shared axial positions are evaluated. This indicates whether the change in node length contributes to a significant change in a quantity of interest. The information from this category is used in the selection of the appropriate mesh size to compare to COBRA-EN.

- *Only Grid Spacers Remain:* All values at the shared axial positions have been removed except at the grid spacer positions. This category represents whether the grid spacer values alone are converging as the mesh size decreases.

- *Only Grid Spacers Removed:* The values at the shared grid spacer axial positions have been removed. This indicates if the values are converging without the grid spacer values included.

- *Grid Spacer, and Space Before and After Removed:* The values at the shared grid spacer, plus the nodes before and after the spacer have been removed.

- *Grid Spacer and Space Before Removed:* The values at the shared grid spacer, plus the node before the spacer have been removed.

- *Grid Spacer and Space After Removed:* The values at the shared grid spacer, plus the node after the spacer have been removed.

### 3.8.2 P60001, Axial Position Influence on Absolute Relative Differences

| Table 3.23: COBRA-CTF, P60001 Convergence Study Error Results for Pressure | | | | | | |
|---|---|---|---|---|---|---|
| **Error** | **1 to 3** | **3 to 4** | **4 to 5** | **5 to 6** | **6 to 7** | **7 to 8** |
| | **All Shared Axial Positions** | | | | | |
| $L_{\infty Norm}$ | 8.75E-05 | 2.65E-05 | 6.84E-06 | 1.45E-05 | 8.92E-06 | 1.06E-05 |
| $L_{2Norm}$ | 4.20E-04 | 7.01E-05 | 3.10E-05 | 3.21E-05 | 2.65E-05 | 1.98E-05 |
| **Error** | **Only Grid Spacers Remain** | | | | | |
| $L_{\infty Norm}$ | 8.73E-05 | 2.65E-05 | 6.42E-06 | 1.45E-05 | 8.92E-06 | 1.06E-05 |
| $L_{2Norm}$ | 1.78E-04 | 4.26E-05 | 1.29E-05 | 2.25E-05 | 1.31E-05 | 1.42E-05 |
| **Error** | **Only Grid Spacers Removed** | | | | | |
| $L_{\infty Norm}$ | 8.75E-05 | 1.24E-05 | 6.84E-06 | 5.58E-06 | 6.70E-06 | 3.21E-06 |
| $L_{2Norm}$ | 3.80E-04 | 5.57E-05 | 2.82E-05 | 2.29E-05 | 2.31E-05 | 1.38E-05 |
| **Error** | **Grid Spacer, and Space Before and After Removed** | | | | | |
| $L_{\infty Norm}$ | 8.70E-05 | 1.24E-05 | 6.56E-06 | 5.58E-06 | 5.02E-06 | 3.21E-06 |
| $L_{2Norm}$ | 2.78E-04 | 3.88E-05 | 1.94E-05 | 1.61E-05 | 1.51E-05 | 9.51E-06 |
| **Error** | **Grid Spacer and Space Before Removed** | | | | | |
| $L_{\infty Norm}$ | 8.73E-05 | 2.65E-05 | 6.84E-06 | 1.45E-05 | 8.92E-06 | 1.06E-05 |
| $L_{2Norm}$ | 3.55E-04 | 6.27E-05 | 2.67E-05 | 2.95E-05 | 2.34E-05 | 1.82E-05 |
| **Error** | **Grid Spacer and Space After Removed** | | | | | |
| $L_{\infty Norm}$ | 8.75E-05 | 1.24E-05 | 6.56E-06 | 5.58E-06 | 5.02E-06 | 3.21E-06 |
| $L_{2Norm}$ | 3.57E-04 | 4.99E-05 | 2.50E-05 | 2.05E-05 | 1.96E-05 | 1.22E-05 |

| Error | 1 to 3 | 3 to 4 | 4 to 5 | 5 to 6 | 6 to 7 | 7 to 8 |
|---|---|---|---|---|---|---|
| **Table 3.24: COBRA-CTF, P60001 Convergence Study Error Results for Void Fraction** | | | | | | |
| **Error** | **1 to 3** | **3 to 4** | **4 to 5** | **5 to 6** | **6 to 7** | **7 to 8** |
| **All Shared Axial Positions** | | | | | | |
| $L_{\infty Norm}$ | 0.7047 | 0.0468 | 0.0480 | 0.0656 | 0.0478 | 0.0132 |
| $L_{2Norm}$ | 0.7703 | 0.0840 | 0.0800 | 0.0848 | 0.0611 | 0.0308 |
| **Error** | **Only Grid Spacers Remain** | | | | | |
| $L_{\infty Norm}$ | 0.1521 | 0.0263 | 0.0480 | 0.0656 | 0.0478 | 0.0117 |
| $L_{2Norm}$ | 0.1920 | 0.0534 | 0.0661 | 0.0792 | 0.0558 | 0.0244 |
| **Error** | **Only Grid Spacers Removed** | | | | | |
| $L_{\infty Norm}$ | 0.7047 | 0.0468 | 0.0307 | 0.0190 | 0.0194 | 0.0132 |
| $L_{2Norm}$ | 0.7460 | 0.0649 | 0.0451 | 0.0303 | 0.0248 | 0.0189 |
| **Error** | **Grid Spacer, and Space Before and After Removed** | | | | | |
| $L_{\infty Norm}$ | 0.1074 | 0.0139 | 0.0094 | 0.0095 | 0.0048 | 0.0040 |
| $L_{2Norm}$ | 0.1588 | 0.0223 | 0.0144 | 0.0125 | 0.0070 | 0.0044 |
| **Error** | **Grid Spacer and Space Before Removed** | | | | | |
| $L_{\infty Norm}$ | 0.1521 | 0.0263 | 0.0480 | 0.0656 | 0.0478 | 0.0117 |
| $L_{2Norm}$ | 0.2977 | 0.0654 | 0.0719 | 0.0822 | 0.0573 | 0.0266 |
| **Error** | **Grid Spacer and Space After Removed** | | | | | |
| $L_{\infty Norm}$ | 0.7047 | 0.0468 | 0.0307 | 0.0190 | 0.0194 | 0.0132 |
| $L_{2Norm}$ | 0.7279 | 0.0572 | 0.0378 | 0.0243 | 0.0222 | 0.0162 |

| Error | 1 to 3 | 3 to 4 | 4 to 5 | 5 to 6 | 6 to 7 | 7 to 8 |
|---|---|---|---|---|---|---|
| **Table 3.25: COBRA-CTF, P60001 Convergence Study Error Results for Flow Quality** | | | | | | |
| **Error** | **1 to 3** | **3 to 4** | **4 to 5** | **5 to 6** | **6 to 7** | **7 to 8** |
| **All Shared Axial Positions** | | | | | | |
| $L_{\infty Norm}$ | 0.6890 | 0.0470 | 0.0485 | 0.0216 | 0.0169 | 0.0106 |
| $L_{2Norm}$ | 0.7491 | 0.0760 | 0.0703 | 0.0361 | 0.0288 | 0.0208 |
| **Error** | **Only Grid Spacers Remain** | | | | | |
| $L_{\infty Norm}$ | 0.1490 | 0.0276 | 0.0485 | 0.0191 | 0.0130 | 0.0067 |
| $L_{2Norm}$ | 0.1547 | 0.0364 | 0.0509 | 0.0214 | 0.0168 | 0.0106 |
| **Error** | **Only Grid Spacers Removed** | | | | | |
| $L_{\infty Norm}$ | 0.6890 | 0.0470 | 0.0308 | 0.0216 | 0.0169 | 0.0106 |
| $L_{2Norm}$ | 0.7329 | 0.0667 | 0.0486 | 0.0291 | 0.0234 | 0.0179 |
| **Error** | **Grid Spacer, and Space Before and After Removed** | | | | | |
| $L_{\infty Norm}$ | 0.1102 | 0.0190 | 0.0113 | 0.0064 | 0.0098 | 0.0038 |
| $L_{2Norm}$ | 0.1636 | 0.0263 | 0.0187 | 0.0097 | 0.0111 | 0.0050 |
| **Error** | **Grid Spacer and Space Before Removed** | | | | | |
| $L_{\infty Norm}$ | 0.1490 | 0.0276 | 0.0485 | 0.0191 | 0.0130 | 0.0087 |
| $L_{2Norm}$ | 0.2811 | 0.0544 | 0.0610 | 0.0275 | 0.0217 | 0.0157 |
| **Error** | **Grid Spacer and Space After Removed** | | | | | |
| $L_{\infty Norm}$ | 0.6890 | 0.0470 | 0.0308 | 0.0216 | 0.0169 | 0.0106 |
| $L_{2Norm}$ | 0.7133 | 0.0592 | 0.0397 | 0.0253 | 0.0219 | 0.0145 |
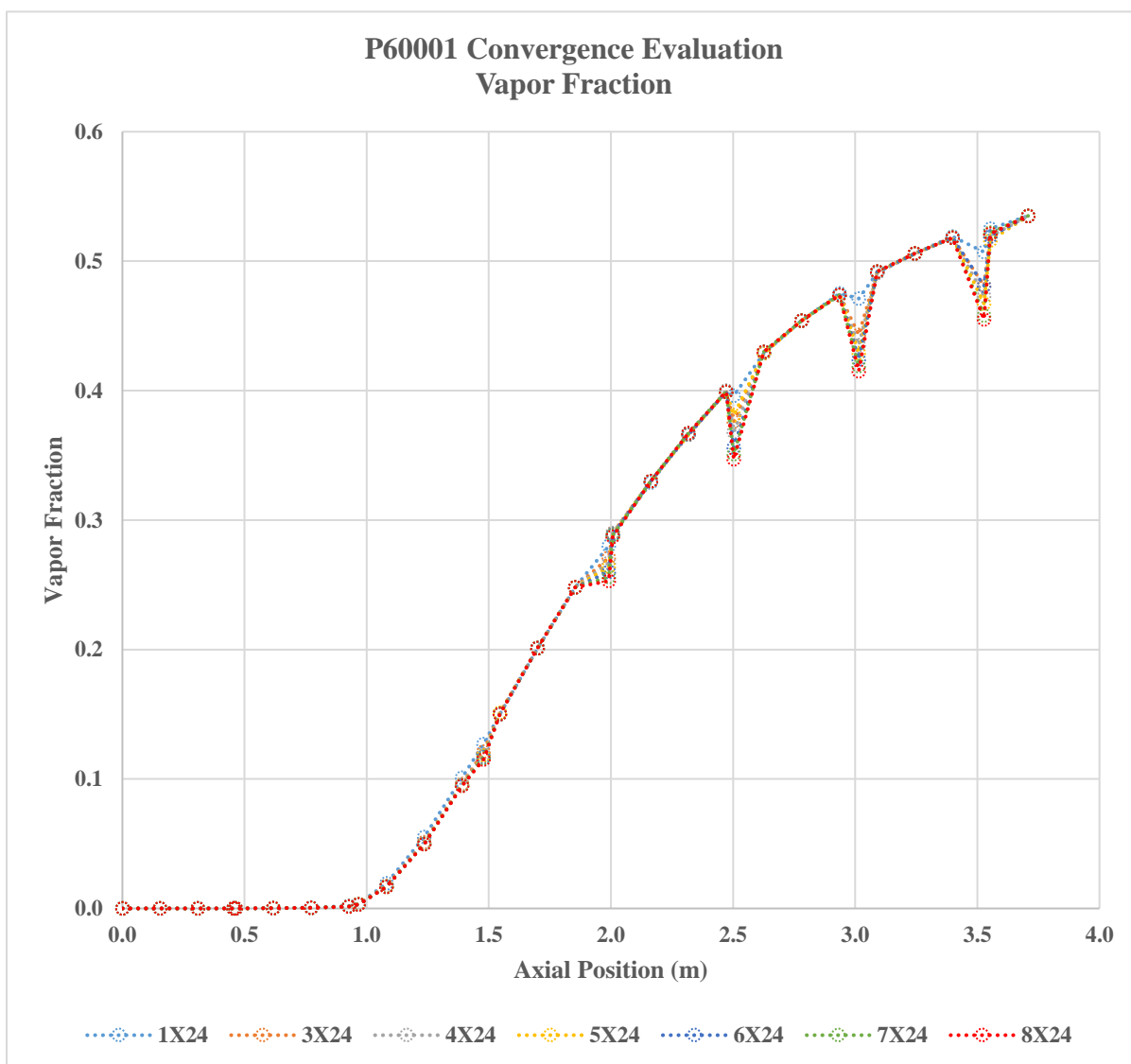
**Figure 3.14: P60001 Vapor fractions at shared axial position for all mesh refinement cases**

### 3.8.3  P60007, Axial Position Influence on Absolute Relative Differences

| Table 3.26: COBRA-CTF, P60007 Convergence Study Error Results for Pressure | | | | | | |
|---|---|---|---|---|---|---|
| **Error** | **1 to 3** | **3 to 4** | **4 to 5** | **5 to 6** | **6 to 7** | **7 to 8** |
| | **All Shared Axial Positions** | | | | | |
| $L_{\infty Norm}$ | 2.43E-04 | 5.61E-05 | 2.77E-05 | 4.39E-05 | 1.35E-05 | 1.54E-04 |
| $L_{2Norm}$ | 1.15E-03 | 1.81E-04 | 5.51E-05 | 1.23E-04 | 2.87E-05 | 2.13E-04 |
| **Error** | **Only Grid Spacers Remain** | | | | | |
| $L_{\infty Norm}$ | 2.43E-04 | 5.61E-05 | 1.26E-05 | 4.39E-05 | 1.35E-05 | 4.76E-05 |
| $L_{2Norm}$ | 5.04E-04 | 1.03E-04 | 2.44E-05 | 7.32E-05 | 2.14E-05 | 8.54E-05 |
| **Error** | **Only Grid Spacers Removed** | | | | | |
| $L_{\infty Norm}$ | 2.38E-04 | 3.45E-05 | 2.77E-05 | 2.45E-05 | 1.23E-05 | 1.54E-04 |
| $L_{2Norm}$ | 1.03E-03 | 1.49E-04 | 4.95E-05 | 9.90E-05 | 1.91E-05 | 1.95E-04 |
| **Error** | **Grid Spacer, and Space Before and After Removed** | | | | | |
| $L_{\infty Norm}$ | 2.35E-04 | 3.42E-05 | 1.58E-05 | 2.44E-05 | 7.39E-06 | 2.99E-05 |
| $L_{2Norm}$ | 7.34E-04 | 1.04E-04 | 2.98E-05 | 6.78E-05 | 1.07E-05 | 8.04E-05 |
| **Error** | **Grid Spacer and Space Before Removed** | | | | | |
| $L_{\infty Norm}$ | 2.35E-04 | 3.42E-05 | 2.77E-05 | 2.44E-05 | 1.23E-05 | 1.54E-04 |
| $L_{2Norm}$ | 8.44E-04 | 1.24E-04 | 4.39E-05 | 8.28E-05 | 1.78E-05 | 1.84E-04 |
| **Error** | **Grid Spacer and Space After Removed** | | | | | |
| $L_{\infty Norm}$ | 2.38E-04 | 3.45E-05 | 1.58E-05 | 2.45E-05 | 7.39E-06 | 2.99E-05 |
| $L_{2Norm}$ | 9.42E-04 | 1.34E-04 | 3.75E-05 | 8.69E-05 | 1.27E-05 | 1.02E-04 |

| Table 3.27: COBRA-CTF, P60007 Convergence Study Error Results for Vapor Fraction | | | | | | |
|---|---|---|---|---|---|---|
| **Error** | **1 to 3** | **3 to 4** | **4 to 5** | **5 to 6** | **6 to 7** | **7 to 8** |
| | **All Shared Axial Positions** | | | | | |
| $L_{\infty Norm}$ | 0.1713 | 0.0741 | 0.0345 | 0.0639 | 0.0794 | 0.0644 |
| $L_{2 Norm}$ | 0.3501 | 0.1061 | 0.0740 | 0.0870 | 0.0864 | 0.1010 |
| **Error** | **Only Grid Spacers Remain** | | | | | |
| $L_{\infty Norm}$ | 0.1139 | 0.0360 | 0.0345 | 0.0639 | 0.0794 | 0.0644 |
| $L_{2 Norm}$ | 0.2230 | 0.0621 | 0.0573 | 0.0809 | 0.0830 | 0.0967 |
| **Error** | **Only Grid Spacers Removed** | | | | | |
| $L_{\infty Norm}$ | 0.1713 | 0.0741 | 0.0320 | 0.0248 | 0.0141 | 0.0173 |
| $L_{2 Norm}$ | 0.2699 | 0.0861 | 0.0468 | 0.0319 | 0.0240 | 0.0291 |
| **Error** | **Grid Spacer, and Space Before and After Removed** | | | | | |
| $L_{\infty Norm}$ | 0.1401 | 0.0741 | 0.0320 | 0.0248 | 0.0085 | 0.0043 |
| $L_{2 Norm}$ | 0.1646 | 0.0760 | 0.0329 | 0.0253 | 0.0098 | 0.0068 |
| **Error** | **Grid Spacer and Space Before Removed** | | | | | |
| $L_{\infty Norm}$ | 0.1401 | 0.0741 | 0.0320 | 0.0248 | 0.0103 | 0.0173 |
| $L_{2 Norm}$ | 0.2003 | 0.0801 | 0.0384 | 0.0297 | 0.0178 | 0.0215 |
| **Error** | **Grid Spacer and Space After Removed** | | | | | |
| $L_{\infty Norm}$ | 0.1713 | 0.0741 | 0.0320 | 0.0248 | 0.0141 | 0.0166 |
| $L_{2 Norm}$ | 0.2446 | 0.0822 | 0.0424 | 0.0278 | 0.0189 | 0.0208 |

| Table 3.28: COBRA-CTF, P60007 Convergence Study Error Results for Flow Quality | | | | | | |
|---|---|---|---|---|---|---|
| **Error** | **1 to 3** | **3 to 4** | **4 to 5** | **5 to 6** | **6 to 7** | **7 to 8** |
| | **All Shared Axial Positions** | | | | | |
| $L_{\infty Norm}$ | 0.1748 | 0.0674 | 0.0337 | 0.0233 | 0.0153 | 0.0157 |
| $L_{2Norm}$ | 0.3116 | 0.0823 | 0.0495 | 0.0318 | 0.0227 | 0.0237 |
| **Error** | **Only Grid Spacers Remain** | | | | | |
| $L_{\infty Norm}$ | 0.1129 | 0.0182 | 0.0185 | 0.0094 | 0.0095 | 0.0061 |
| $L_{2Norm}$ | 0.1482 | 0.0234 | 0.0207 | 0.0112 | 0.0113 | 0.0076 |
| **Error** | **Only Grid Spacers Removed** | | | | | |
| $L_{\infty Norm}$ | 0.1748 | 0.0674 | 0.0337 | 0.0233 | 0.0153 | 0.0157 |
| $L_{2Norm}$ | 0.2741 | 0.0789 | 0.0449 | 0.0297 | 0.0197 | 0.0224 |
| **Error** | **Grid Spacer, and Space Before and After Removed** | | | | | |
| $L_{\infty Norm}$ | 0.1414 | 0.0674 | 0.0337 | 0.0233 | 0.0153 | 0.0091 |
| $L_{2Norm}$ | 0.1689 | 0.0689 | 0.0357 | 0.0234 | 0.0154 | 0.0118 |
| **Error** | **Grid Spacer and Space Before Removed** | | | | | |
| $L_{\infty Norm}$ | 0.1414 | 0.0674 | 0.0337 | 0.0233 | 0.0153 | 0.0091 |
| $L_{2Norm}$ | 0.2020 | 0.0713 | 0.0385 | 0.0262 | 0.0170 | 0.0142 |
| **Error** | **Grid Spacer and Space After Removed** | | | | | |
| $L_{\infty Norm}$ | 0.1748 | 0.0674 | 0.0337 | 0.0233 | 0.0153 | 0.0157 |
| $L_{2Norm}$ | 0.2507 | 0.0767 | 0.0425 | 0.0273 | 0.0184 | 0.0210 |
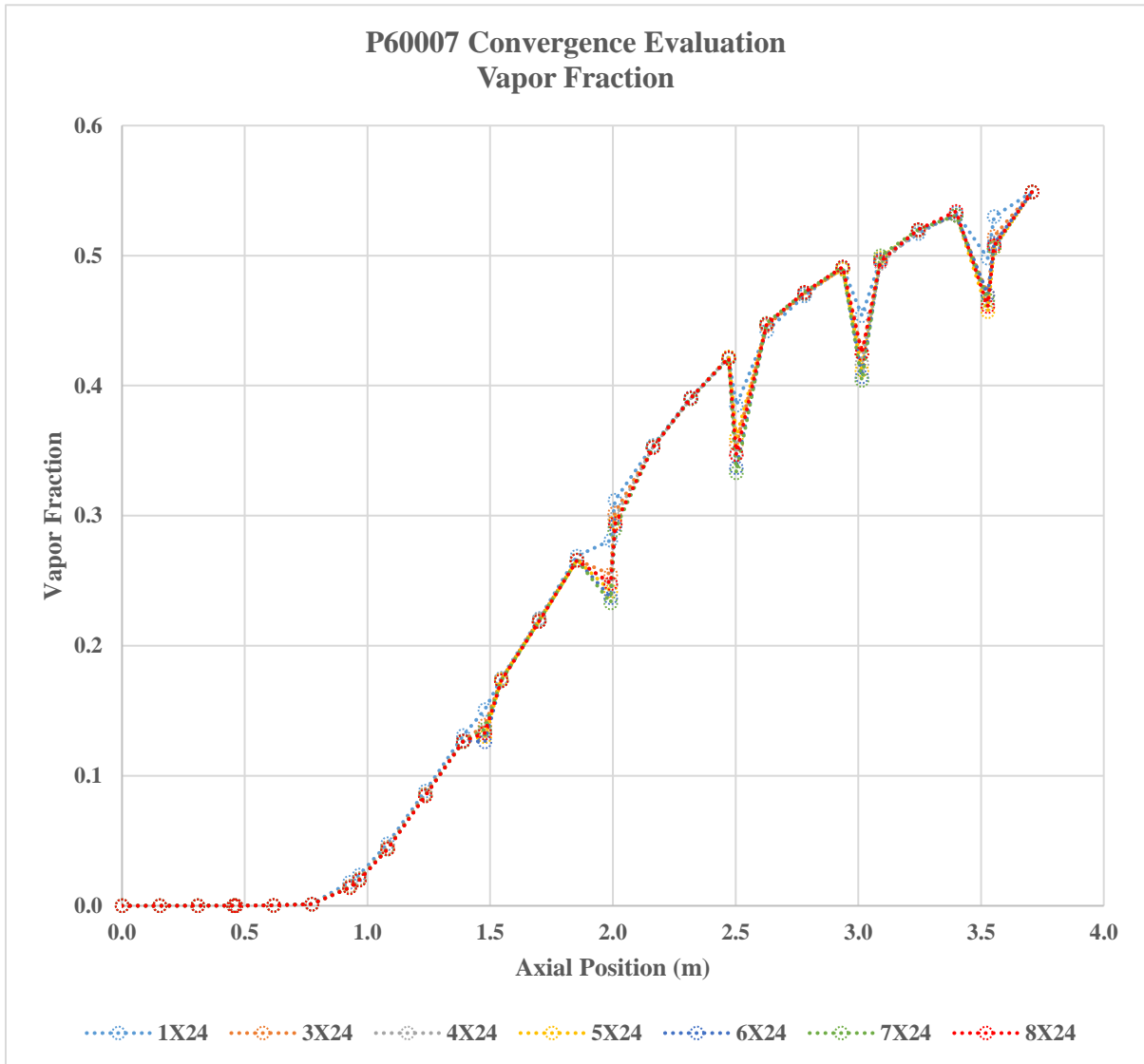
**Figure 3.15: P60007 Vapor fractions at shared axial position for all mesh refinement cases**

**3.8.4  P60015, Axial Position Influence on Absolute Relative Differences**

| Table 3.29: COBRA-CTF, P60015 Convergence Study Error Results for Pressure | | | | | | |
|---|---|---|---|---|---|---|
| **Error** | **1 to 3** | **3 to 4** | **4 to 5** | **5 to 6** | **6 to 7** | **7 to 8** |
| | **All Shared Axial Positions** | | | | | |
| $L_{\infty Norm}$ | 5.05E-04 | 9.83E-05 | 5.82E-05 | 7.33E-05 | 1.38E-04 | 2.00E-04 |
| $L_{2Norm}$ | 2.40E-03 | 2.84E-04 | 2.01E-04 | 1.56E-04 | 1.75E-04 | 2.05E-04 |
| **Error** | **Only Grid Spacers Remain** | | | | | |
| $L_{\infty Norm}$ | 4.98E-04 | 9.83E-05 | 4.25E-05 | 7.33E-05 | 5.11E-05 | 2.38E-05 |
| $L_{2Norm}$ | 1.06E-03 | 1.68E-04 | 7.52E-05 | 1.13E-04 | 7.11E-05 | 2.49E-05 |
| **Error** | **Only Grid Spacers Removed** | | | | | |
| $L_{\infty Norm}$ | 5.05E-04 | 6.13E-05 | 5.82E-05 | 2.44E-05 | 1.38E-04 | 2.00E-04 |
| $L_{2Norm}$ | 2.16E-03 | 2.29E-04 | 1.86E-04 | 1.07E-04 | 1.60E-04 | 2.03E-04 |
| **Error** | **Grid Spacer, and Space Before and After Removed** | | | | | |
| $L_{\infty Norm}$ | 5.05E-04 | 6.13E-05 | 4.22E-05 | 2.38E-05 | 2.26E-05 | 2.01E-05 |
| $L_{2Norm}$ | 1.53E-03 | 1.58E-04 | 1.24E-04 | 7.40E-05 | 4.73E-05 | 2.21E-05 |
| **Error** | **Grid Spacer and Space Before Removed** | | | | | |
| $L_{\infty Norm}$ | 5.05E-04 | 6.13E-05 | 5.82E-05 | 2.38E-05 | 1.38E-04 | 2.00E-04 |
| $L_{2Norm}$ | 1.77E-03 | 1.90E-04 | 1.58E-04 | 8.88E-05 | 1.54E-04 | 2.03E-04 |
| **Error** | **Grid Spacer and Space After Removed** | | | | | |
| $L_{\infty Norm}$ | 5.05E-04 | 6.13E-05 | 4.22E-05 | 2.44E-05 | 2.26E-05 | 2.01E-05 |
| $L_{2Norm}$ | 1.96E-03 | 2.03E-04 | 1.58E-04 | 9.45E-05 | 6.34E-05 | 2.44E-05 |

| Table 3.30: COBRA-CTF, P60015 Convergence Study Error Results for Vapor Fraction | | | | | | |
|---|---|---|---|---|---|---|
| **Error** | **1 to 3** | **3 to 4** | **4 to 5** | **5 to 6** | **6 to 7** | **7 to 8** |
| | **All Shared Axial Positions** | | | | | |
| $L_{\infty Norm}$ | 0.4681 | 0.0668 | 0.0360 | 0.0299 | 0.0846 | 0.0142 |
| $L_{2Norm}$ | 0.5604 | 0.0968 | 0.0599 | 0.0524 | 0.1073 | 0.0270 |
| **Error** | **Only Grid Spacers Remain** | | | | | |
| $L_{\infty Norm}$ | 0.1757 | 0.0414 | 0.0360 | 0.0299 | 0.0846 | 0.0142 |
| $L_{2Norm}$ | 0.2309 | 0.0594 | 0.0478 | 0.0462 | 0.1059 | 0.0230 |
| **Error** | **Only Grid Spacers Removed** | | | | | |
| $L_{\infty Norm}$ | 0.4681 | 0.0668 | 0.0286 | 0.0203 | 0.0113 | 0.0122 |
| $L_{2Norm}$ | 0.5106 | 0.0765 | 0.0362 | 0.0247 | 0.0170 | 0.0142 |
| **Error** | **Grid Spacer, and Space Before and After Removed** | | | | | |
| $L_{\infty Norm}$ | 0.0839 | 0.0121 | 0.0078 | 0.0062 | 0.0045 | 0.0023 |
| $L_{2Norm}$ | 0.1184 | 0.0177 | 0.0111 | 0.0079 | 0.0067 | 0.0028 |
| **Error** | **Grid Spacer and Space Before Removed** | | | | | |
| $L_{\infty Norm}$ | 0.1615 | 0.0296 | 0.0153 | 0.0079 | 0.0078 | 0.0050 |
| $L_{2Norm}$ | 0.2027 | 0.0366 | 0.0221 | 0.0140 | 0.0126 | 0.0063 |
| **Error** | **Grid Spacer and Space After Removed** | | | | | |
| $L_{\infty Norm}$ | 0.4681 | 0.0668 | 0.0286 | 0.0203 | 0.0113 | 0.0122 |
| $L_{2Norm}$ | 0.4834 | 0.0695 | 0.0308 | 0.0218 | 0.0133 | 0.0131 |

| Table 3.31: COBRA-CTF, P60015 Convergence Study Error Results for Flow Quality | | | | | | |
|---|---|---|---|---|---|---|
| **Error** | **1 to 3** | **3 to 4** | **4 to 5** | **5 to 6** | **6 to 7** | **7 to 8** |
| | **All Shared Axial Positions** | | | | | |
| $L_{\infty Norm}$ | 0.4806 | 0.0656 | 0.0316 | 0.0181 | 0.0148 | 0.0144 |
| $L_{2Norm}$ | 0.5524 | 0.0850 | 0.0409 | 0.0262 | 0.0225 | 0.0212 |
| **Error** | **Only Grid Spacers Remain** | | | | | |
| $L_{\infty Norm}$ | 0.1779 | 0.0337 | 0.0182 | 0.0118 | 0.0103 | 0.0069 |
| $L_{2Norm}$ | 0.1800 | 0.0350 | 0.0182 | 0.0122 | 0.0104 | 0.0071 |
| **Error** | **Only Grid Spacers Removed** | | | | | |
| $L_{\infty Norm}$ | 0.4806 | 0.0656 | 0.0316 | 0.0181 | 0.0148 | 0.0144 |
| $L_{2Norm}$ | 0.5223 | 0.0775 | 0.0366 | 0.0233 | 0.0200 | 0.0200 |
| **Error** | **Grid Spacer, and Space Before and After Removed** | | | | | |
| $L_{\infty Norm}$ | 0.0840 | 0.0144 | 0.0073 | 0.0045 | 0.0045 | 0.0045 |
| $L_{2Norm}$ | 0.1228 | 0.0238 | 0.0105 | 0.0061 | 0.0062 | 0.0060 |
| **Error** | **Grid Spacer and Space Before Removed** | | | | | |
| $L_{\infty Norm}$ | 0.1594 | 0.0304 | 0.0149 | 0.0106 | 0.0092 | 0.0081 |
| $L_{2Norm}$ | 0.2019 | 0.0398 | 0.0183 | 0.0122 | 0.0111 | 0.0114 |
| **Error** | **Grid Spacer and Space After Removed** | | | | | |
| $L_{\infty Norm}$ | 0.4806 | 0.0656 | 0.0316 | 0.0181 | 0.0148 | 0.0144 |
| $L_{2Norm}$ | 0.4971 | 0.0706 | 0.0333 | 0.0207 | 0.0177 | 0.0174 |
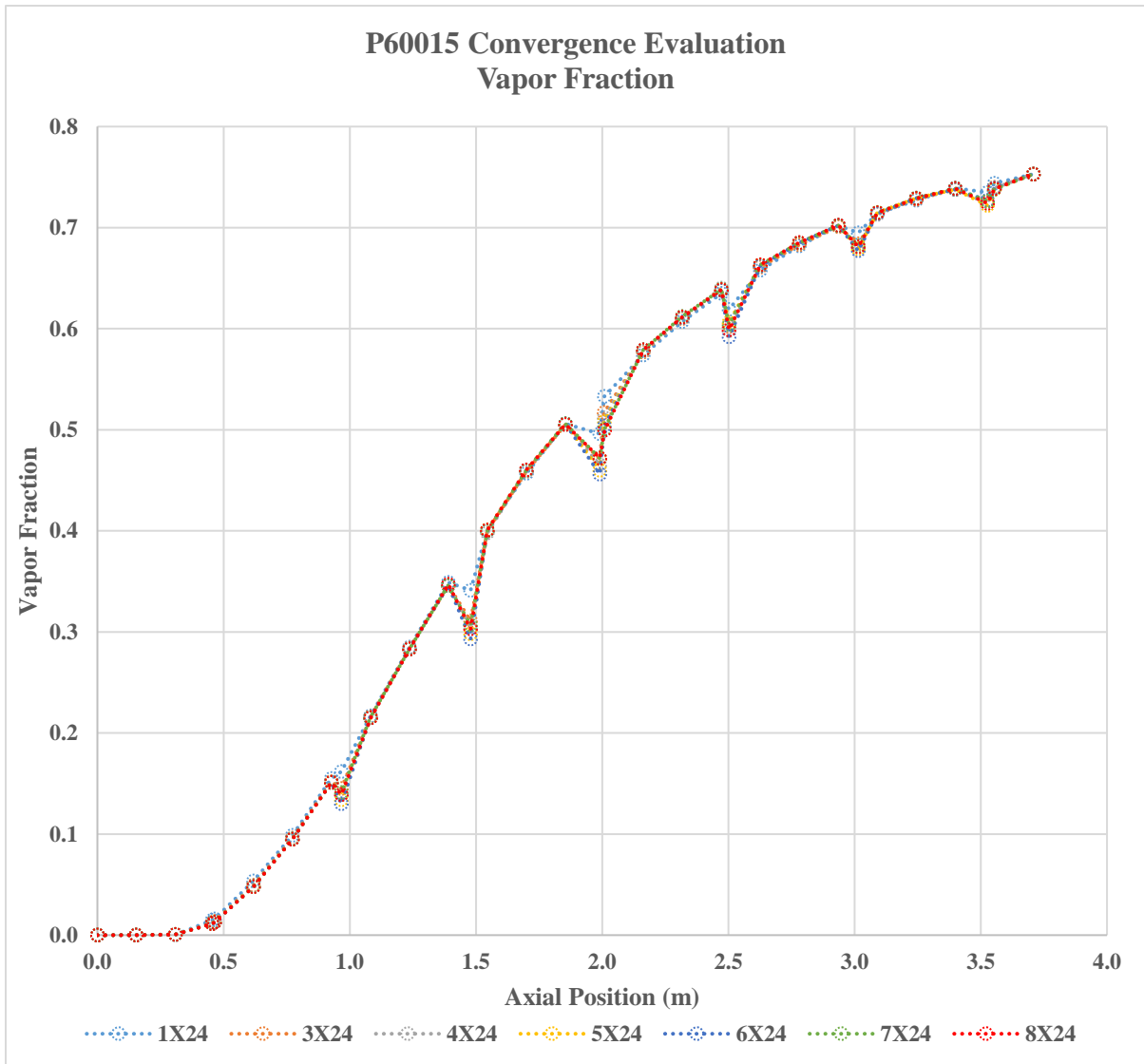
**Figure 3.16: P60015 Vapor fractions at shared axial position for all mesh refinement cases**

**3.9   Convergence Study Conclusion**

The reduction in mesh size negligibly contributes to a change in pressure for all three test cases. The change is between the fourth and fifth decimal place for pressure in bars. The relative difference between the mesh refinement cases appears to be due to numerical noise, and its negligible contribution is beyond the 1% accuracy [7] associated with the instrumentation to measure the pressure during the data collection process. This would indicate that using the COBRA-CTF 1X24 mesh refinement case will be sufficient for comparing pressure drop with COBRA-EN results.

A definitive selection of mesh refinement based on vapor fraction cannot be made in this study considering two major factors:

1. No consistent indication of convergence on void fraction with decreasing mesh size was observed in the "*All Shared Axial Positions*" category.

2. The NUPEC BFBT Phase II, "*Critical Power Benchmark*", Exercise 0, "*Steady State Pressure Drop Benchmark*" does not provide vapor fraction measurements to compare with COBRA-CTF results.

However, the behavior of vapor fraction based on the absolute relative differences observed in *tables 3.24*, *3.27*, and *3.20* do consistently exhibit the following trends:

- The largest contributor to the inconsistency appears in the values collected at the grid spacer positions seen in the "*Only Grid Spacers Remain*" category.

- The space before and after the grid spacers exhibit a large contribution in the magnitude of absolute relative difference between subsequent mesh refinement cases.

- Ignoring the information at the grid spacer, and space before and after does provide two consistent trends.

  1. A converging pattern between subsequent mesh refinements cases.

  2. An acceptable absolute relative difference for vapor fraction.

More research with the other test conditions will be required to determine a pattern if the larger contribution in the magnitude and inconsistency of absolute relative difference between subsequent mesh refinement cases is due to the grid spacer, or space before or after the grid spacer.

As the vapor volume fraction results were inconclusive, the 1X24 mesh refinement case was deemed sufficient for comparing pressure drop with COBRA-EN results. The ETD case is a modified version of the 1X24 nodalization where the pressure tap positions are introduced in the same manner as performed in COBRA-EN. The purpose of the ETD case is to ensure that both codes are comparing data at the same axial positions, and to reduce the need to use interpolation.

## 3.10 Axial Peaking Factors

*Table 3.32* contain the node center axial positions with associated axial peaking factors for both the 1X24 and the modified ETD cases. These values can be compared to the respective values provided in the NUPEC BFBT database seen in *figure 2.5*. The values bolded and italicized are node centers for introduced nodes to capture the pressure tap positions.

| Table 3.32: COBRA-CTF Center Points with Associated Axial Peaking Factors | | | | | |
|---|---|---|---|---|---|
| **1X24** | | | **ETD** | | |
| **Axial Position (m)** | **Axial Position (ft)** | **FZ** | **Axial Position (m)** | **Axial Position (ft)** | **FZ** |
| 0.0000 | 0.0000 | 0.352 | 0.0000 | 0.0000 | 0.352 |
| 0.0772 | 0.2533 | 0.468 | 0.0772 | 0.2533 | 0.468 |
| 0.2318 | 0.7605 | 0.579 | 0.2318 | 0.7605 | 0.579 |
| 0.3820 | 1.2533 | 0.686 | 0.3820 | 1.2533 | 0.686 |
| 0.4592 | 1.5066 | 0.737 | 0.4592 | 1.5066 | 0.737 |
| 0.5408 | 1.7743 | 0.789 | 0.5408 | 1.7743 | 0.789 |
| 0.6953 | 2.2812 | 0.882 | *0.6500* | *2.1325* | *0.854* |
| 0.8498 | 2.7881 | 0.989 | *0.7273* | *2.3862* | *0.903* |
| 0.9470 | 3.1070 | 1.053 | 0.8498 | 2.7881 | 0.989 |
| 1.0243 | 3.3606 | 1.108 | 0.9470 | 3.1070 | 1.053 |
| 1.1587 | 3.8015 | 1.204 | 1.0243 | 3.3606 | 1.108 |
| 1.3133 | 4.3087 | 1.235 | 1.1587 | 3.8015 | 1.204 |
| 1.4347 | 4.7070 | 1.314 | 1.3133 | 4.3087 | 1.235 |
| 1.5120 | 4.9606 | 1.340 | 1.4347 | 4.7070 | 1.314 |
| 1.6222 | 5.3222 | 1.347 | 1.5120 | 4.9606 | 1.340 |
| 1.7768 | 5.8294 | 1.392 | 1.6222 | 5.3222 | 1.347 |
| 1.9225 | 6.3074 | 1.395 | *1.7027* | *5.5863* | *1.371* |
| 1.9997 | 6.5607 | 1.373 | *1.7800* | *5.8399* | *1.393* |
| 2.0857 | 6.8428 | 1.347 | 1.9225 | 6.3074 | 1.395 |
| 2.2403 | 7.3501 | 1.325 | 1.9997 | 6.5607 | 1.373 |
| 2.3948 | 7.8570 | 1.235 | 2.0857 | 6.8428 | 1.348 |
| 2.4875 | 8.1611 | 1.220 | *2.1905* | *7.1867* | *1.340* |
| 2.5648 | 8.4147 | 1.200 | *2.2677* | *7.4400* | *1.317* |
| 2.7037 | 8.8704 | 1.094 | 2.3947 | 7.8566 | 1.235 |
| 2.8583 | 9.3776 | 0.989 | 2.4875 | 8.1611 | 1.220 |
| 2.9752 | 9.7612 | 0.907 | 2.5647 | 8.4144 | 1.200 |
| 3.0525 | 10.0148 | 0.857 | *2.6782* | *8.7867* | *1.112* |
| 3.1673 | 10.3914 | 0.789 | *2.7555* | *9.0404* | *1.057* |
| 3.3218 | 10.8983 | 0.689 | 2.8582 | 9.3773 | 0.989 |
| 3.4630 | 11.3615 | 0.589 | *2.9607* | *9.7136* | *0.917* |
| 3.5403 | 11.6152 | 0.530 | *3.0005* | *9.8442* | *0.889* |
| 3.6308 | 11.9121 | 0.468 | 3.0525 | 10.0148 | 0.857 |
| 3.7080 | 12.1654 | 0.352 | *3.1660* | *10.3871* | *0.790* |
| | | | *3.2432* | *10.6404* | *0.741* |
| | | | 3.3217 | 10.8980 | 0.689 |
| | | | *3.4485* | *11.3140* | *0.600* |
| | | | *3.5125* | *11.5240* | *0.552* |
| | | | 3.5402 | 11.6148 | 0.530 |
| | | | 3.6307 | 11.9117 | 0.468 |
| | | | 3.7080 | 12.1654 | 0.352 |

The forcing function used by COBRA-CTF changes the user supplied axial peaking factors and attempts to smooth out the power profile seen in *figure 3.17*. This is more dominant in the higher values where the provided axial peaking factors are similar as seen in *figure 2.5*.
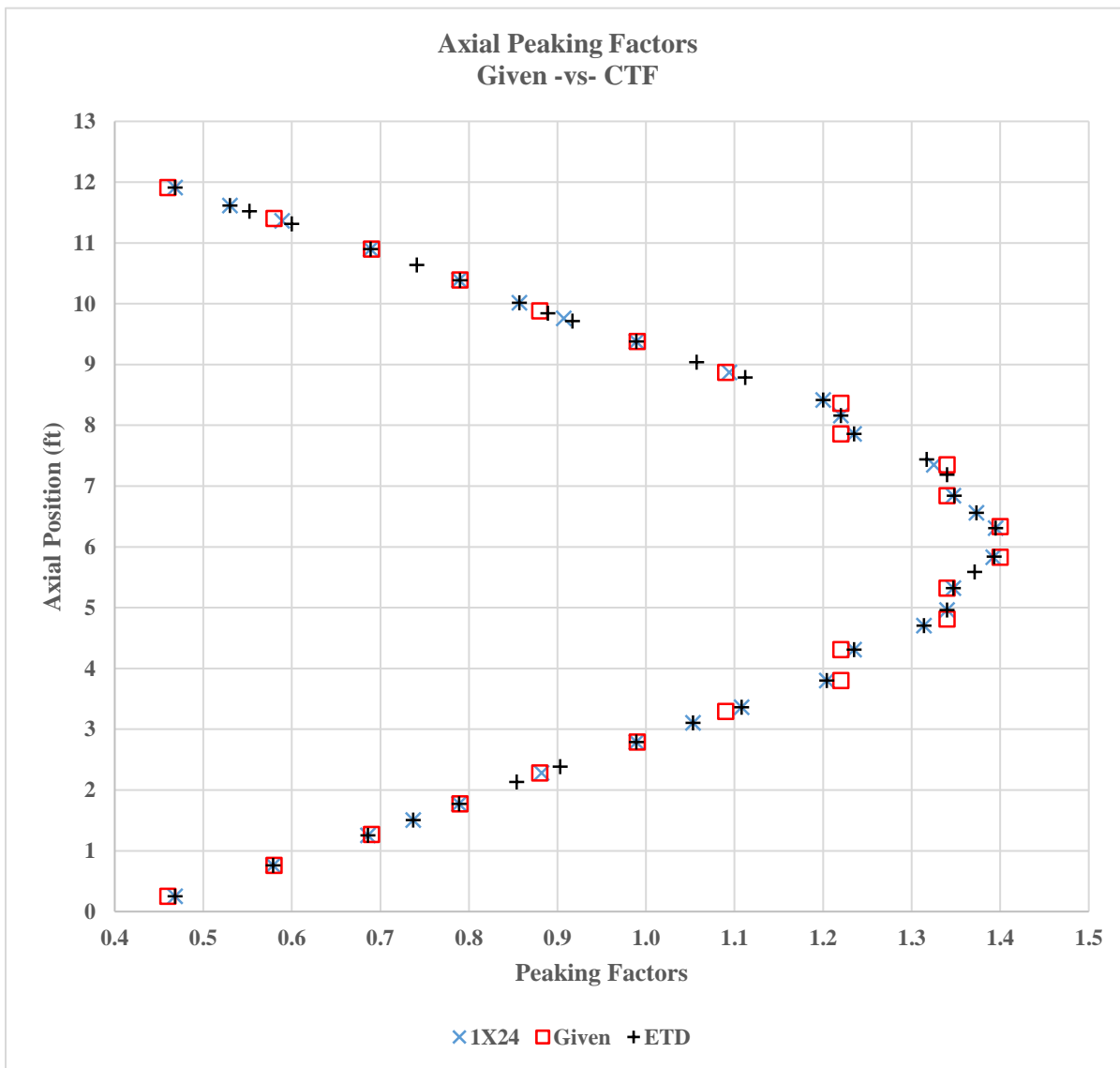


**Figure 3.17: Axial peaking factors for COBRA-CTF 1X24 and ETD compared to the given values**

## 3.11  Evaluation of the 1X24 and ETD Mesh Refinement Cases

The *figures 3.18, 3.20*, and *3.22* reveal that the code calculated values for pressure along the axial length of the fuel assembly match in most locations as expected. However, there are a few locations where the ETD mesh refinement case display a slight difference in calculated pressure in comparison with the 1X24 mesh refinement case. This behavior occurs at positions that are between grid spacers where there are no other form or local losses effecting the position. These downward shifts in pressure do not appear in the other mesh refinement cases where the node lengths are kept uniform. This is more noticeable when the neighboring axial nodes are noticeably larger than the one that creates the node edge that yields a pressure tap position. This behavior is similar in nature to the variable node lengths required to introduce the grid spacer positions in the convergence study. These outliers appear to slightly affect the outcome of the pressure drop calculations during the comparison with code calculated values to the NUPEC BFBT benchmarks. *Tables 3.33* tabulates the slight differences in simulation results between the mesh refinement cases 1X24 and the modified ETD for total pressure drop.

| Table 3.33: Measured Total Pressure Drop (psi) | | | | | |
|---|---|---|---|---|---|
| P60001 | | P60007 | | P60015 | |
| 3.974 | | 8.396 | | 16.530 | |
| Calculated Total Pressure Drop (psi) | | | | | |
| P60001 | | P60007 | | P60015 | |
| 1X24 | ETD | 1X24 | ETD | 1X24 | ETD |
| 3.834 | 3.827 | 8.388 | 8.319 | 15.612 | 15.482 |
| Absolute Relative Difference Between Measured and Calculated Total Pressure Drop | | | | | |
| 3.517% | 3.704% | 0.102% | 0.916% | 5.551% | 6.339% |
| Difference Between Measured and Calculated Total Pressure Drop (psi) | | | | | |
| -0.140 | -0.147 | -0.009 | -0.077 | -0.918 | -1.048 |

### 3.11.1 P60001, Pressure and Vapor Fraction Plots of 1X24 and ETD Cases
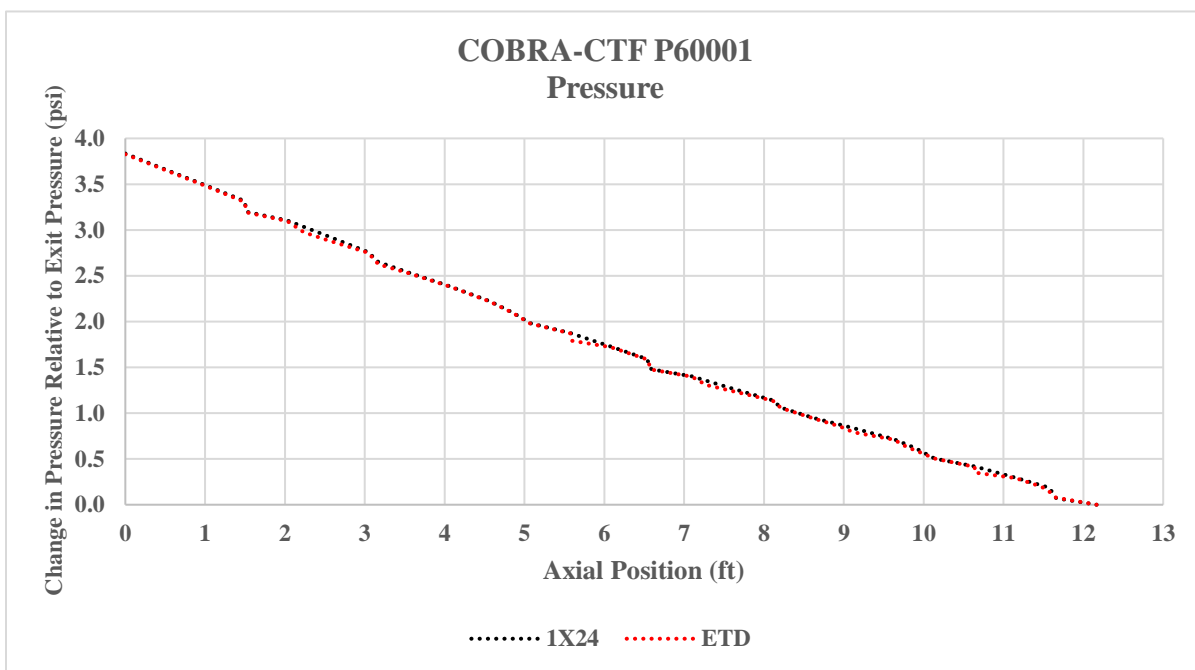


Figure 3.18: P60001, Pressures of the COBRA-CTF 1X24 and ETD mesh refinement cases
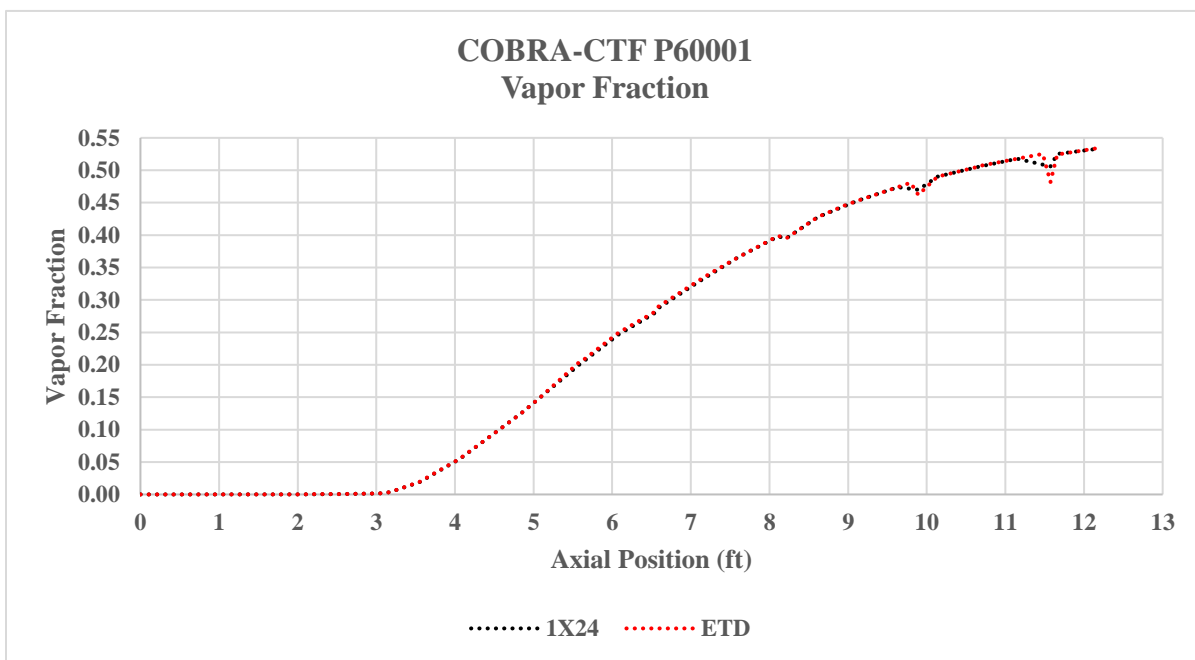


Figure 3.19: P60001, Vapor Fractions of the COBRA-CTF 1X24 and ETD mesh refinement cases

**3.11.2   P60007, Pressure and Vapor Fraction Plots of 1X24 and ETD Cases**
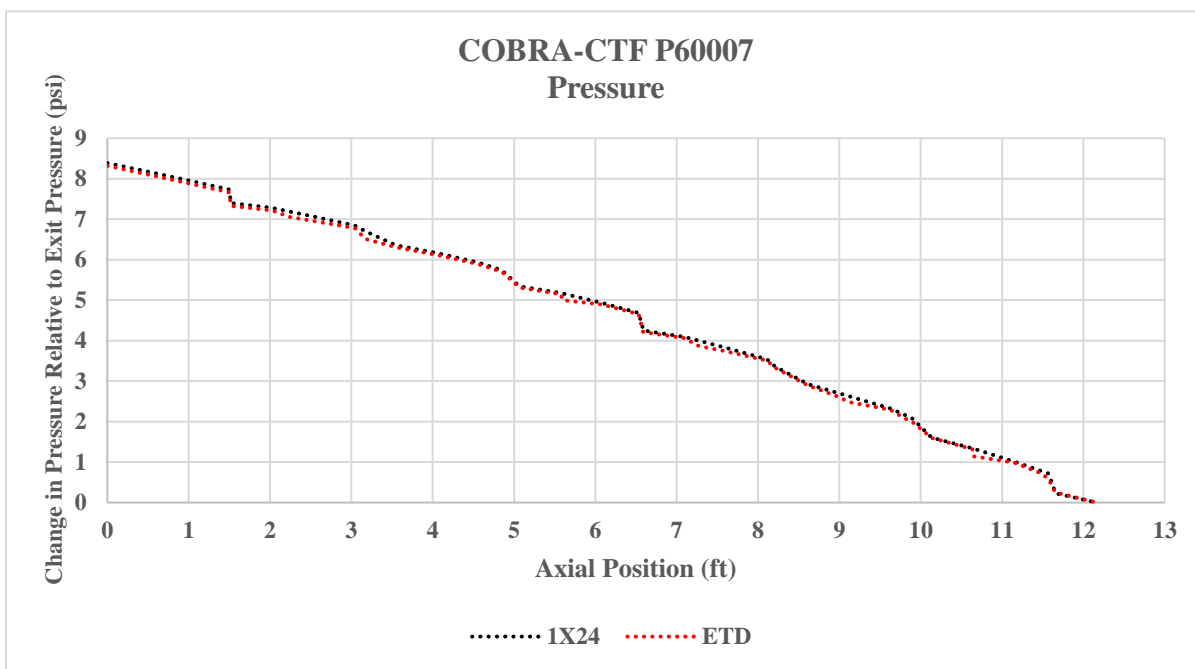


**Figure 3.20: P60007, Pressures of the COBRA-CTF 1X24 and ETD mesh refinement cases**
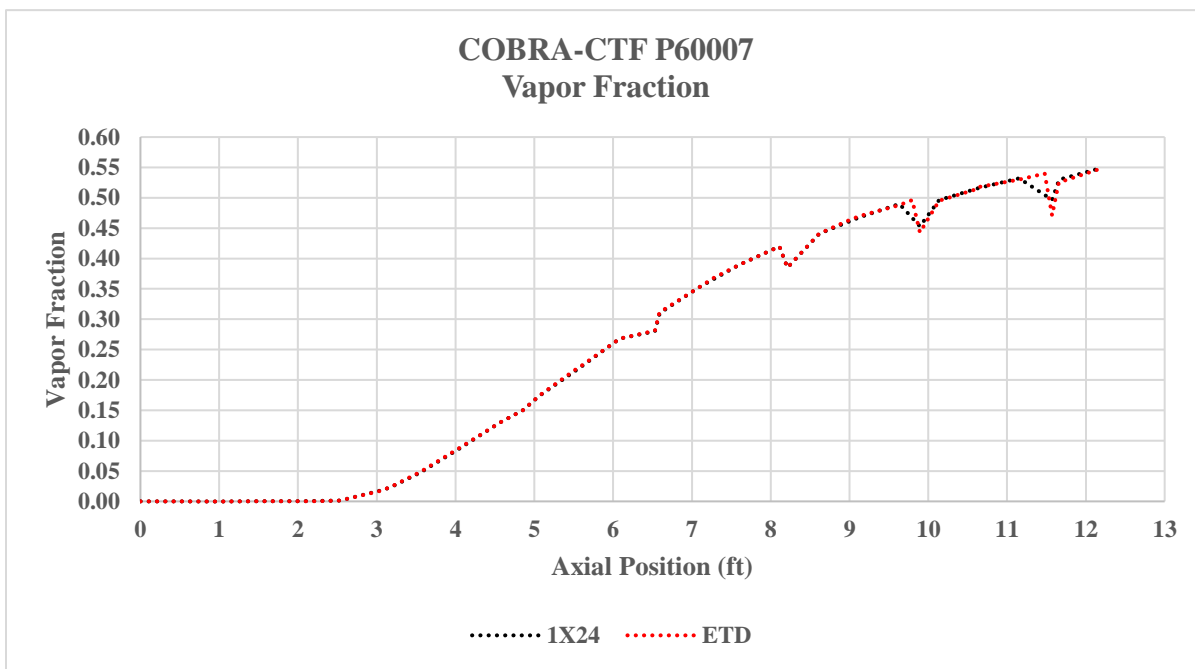


**Figure 3.21: P60007, Vapor Fractions of the COBRA-CTF 1X24 and ETD mesh refinement cases**

### 3.11.3 P60015, Pressure and Vapor Fraction Plots of 1X24 and ETD Cases

**COBRA-CTF P60015**
**Pressure**

*Change in Pressure Relative to Exit Pressure (psi)*

*Axial Position (ft)*

········ 1X24    ········ ETD
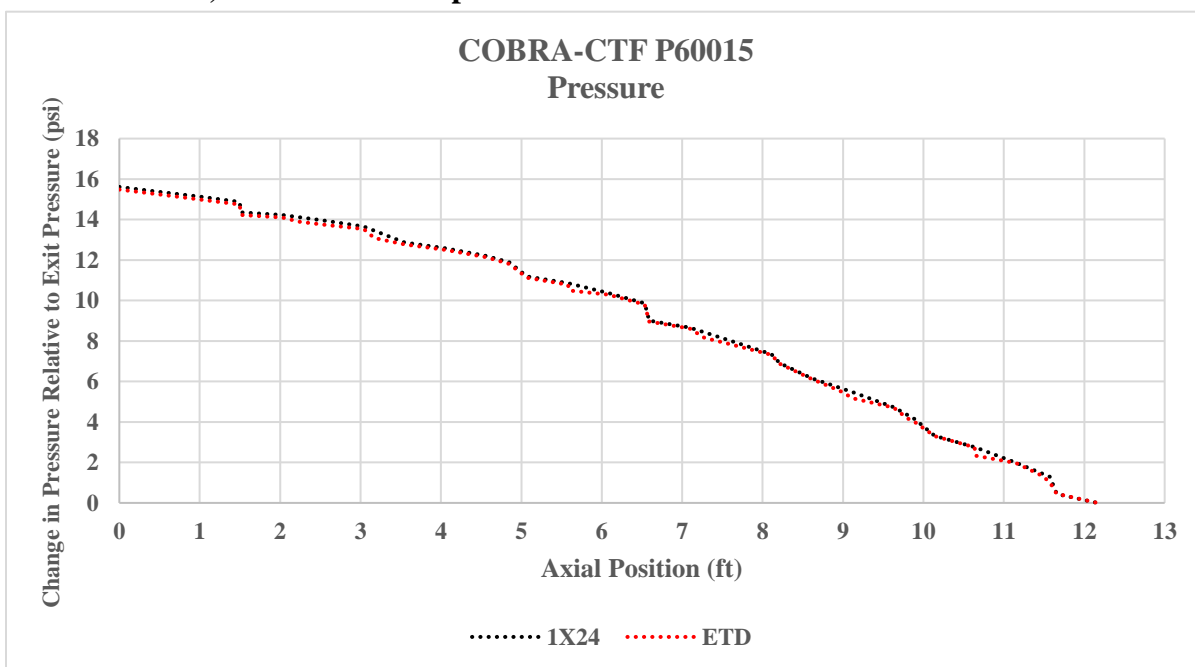
**Figure 3.22: P60015, Pressures of the COBRA-CTF 1X24 and ETD mesh refinement cases**

**COBRA-CTF P60015**
**Vapor Fraction**

*Vapor Fraction*

*Axial Position (ft)*

········ 1X24    ········ ETD
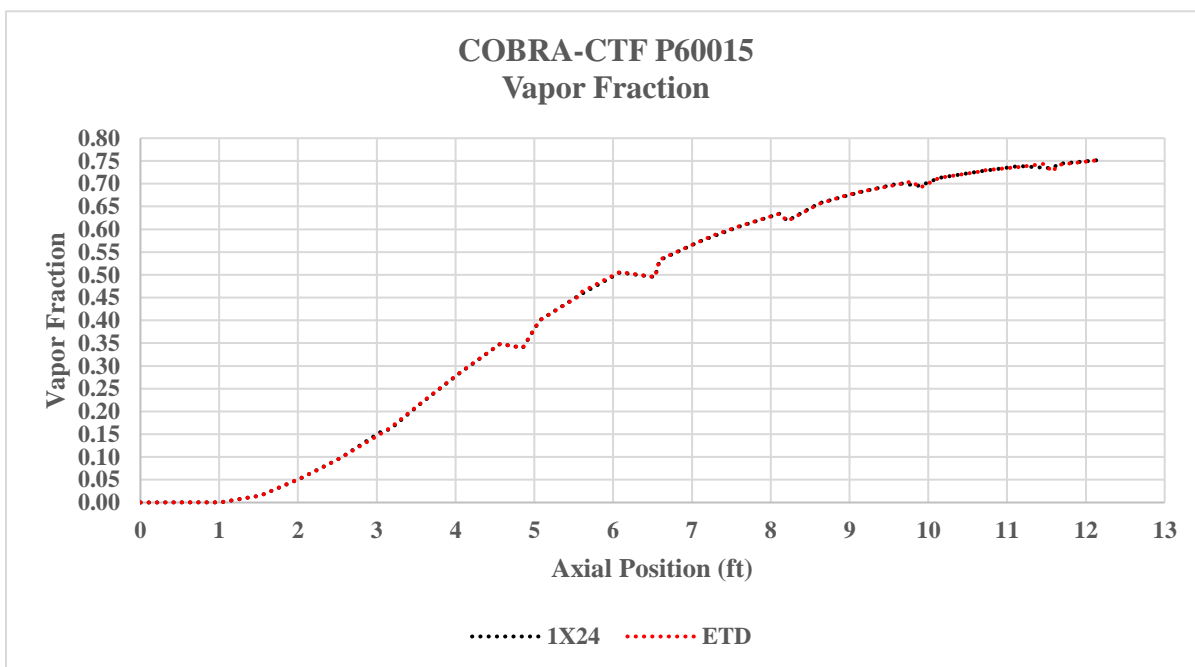
**Figure 3.23: P60015, Vapor Fractions of the COBRA-CTF 1X24 and ETD mesh refinement cases**

**3.11.4   P60015, Example of Differences in Pressure for 1X24 and ETD Cases**

*Figures 3.24, 3.25*, and *3.26* are zoomed in plots of the test case P60015 pressure drop for the

1X24 and ETD mesh refinements. These noticeable differences are observed in the other two

test cases P60001, and P60007. *Figure 3.24* illustrates a slight shift in predicted values for

pressure before reaching the axial position of 3.5499ft. The circled region on *figure 3.24*

illustrates a location where the pressure tap position at 2.2375ft will yield a different value for

pressure than an interpolated value at the same location with the 1X24 case.
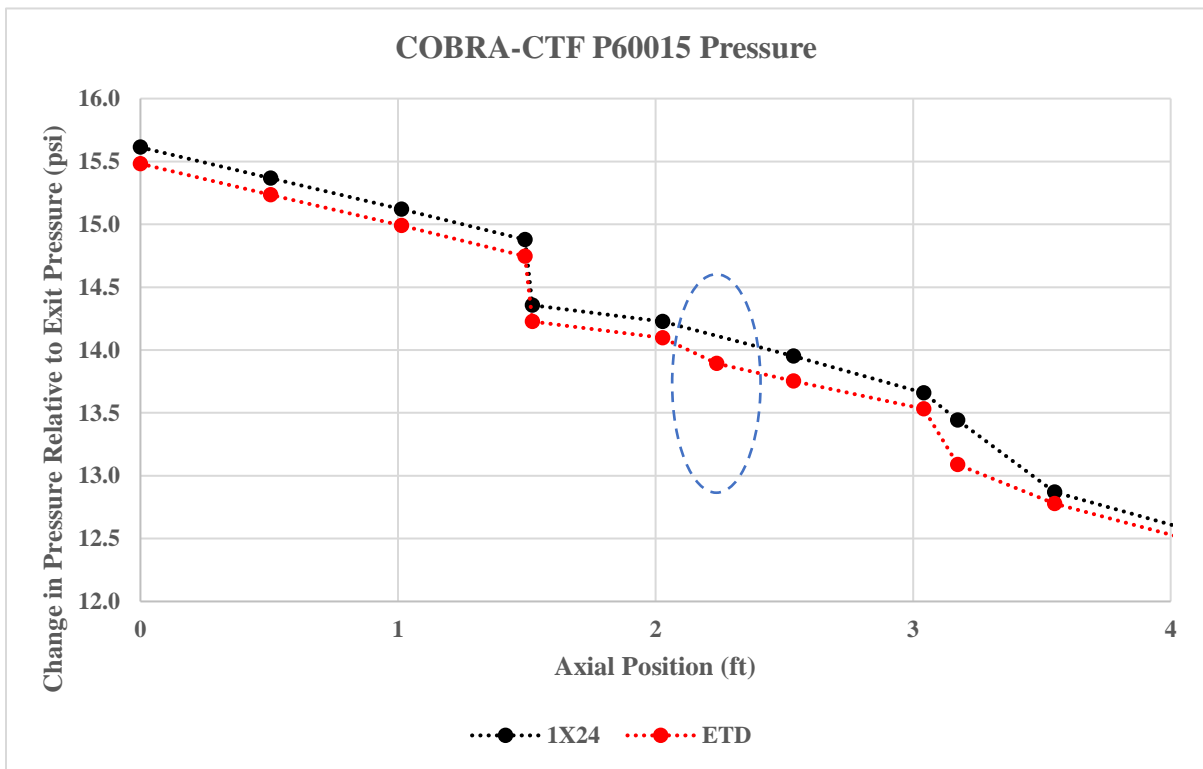


**Figure 3.24: Shift in pressure predictions observed in lower assembly positions for 1X24 and ETD cases**
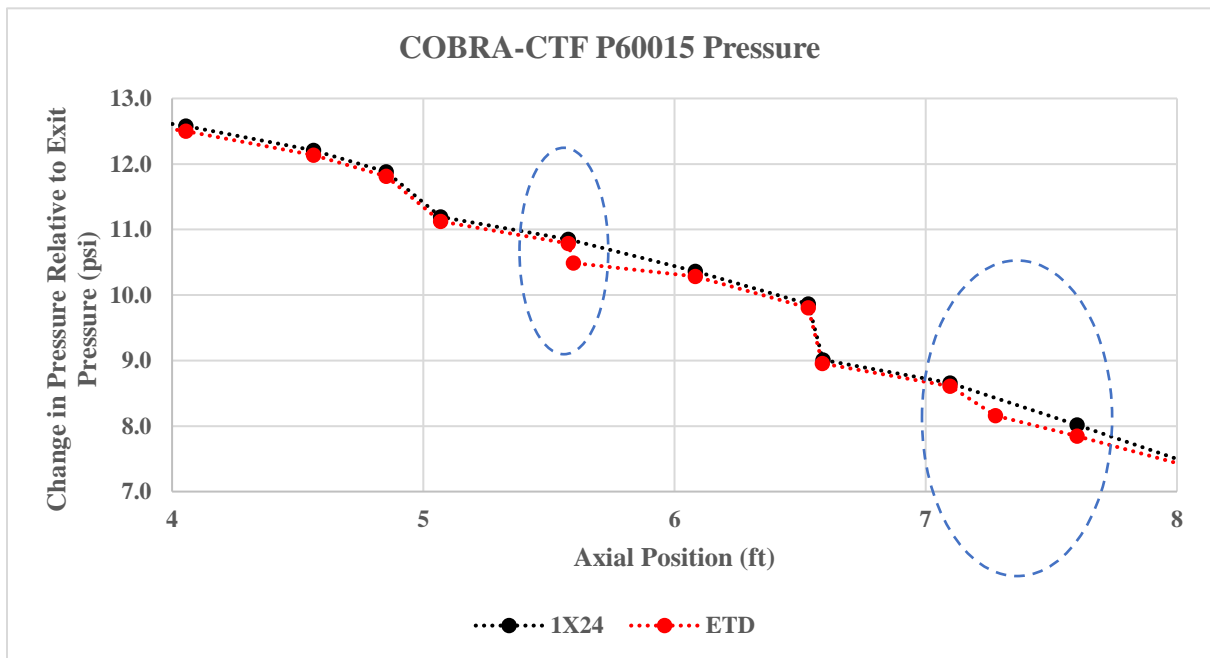
**Figure 3.25: Shift in pressure predictions observed at 5.587ft and 7.27ft for 1X24 and ETD cases**

The pressure tap position of 5.5971ft is between the grid spacer positions of 4.852ft and 6.532ft. There is an observable shift in the predicted pressure value at the pressure tap positions at 5.5971ft directly after the shared position of 5.5774ft. *Table 3.24* indicates the node length between the pressure tap position and the next shared position is significantly smaller that the surrounding node lengths. This effect is also observed at the pressure tap position 7.2769ft after the shared position of 7.0965ft. This last shift in predicted values does appear to affect the pressure determined at the shared axial position at 7.6017ft.

| Table 3.34: P60015, Smaller Node Size Between 5.577ft and 5.597ft in ETD Case | | | | | |
|---|---|---|---|---|---|
| **Axial Positions (ft)** | | | | | |
| **4.8524** | 5.0689 | 5.5774 | 5.5971 | 6.0827 | **6.5322** |
| **Distance Between Axial Positions (ft)** | | | | | |
| 0.2164 | | 0.5069 | 0.021213 | 0.4857 | 0.5069 |
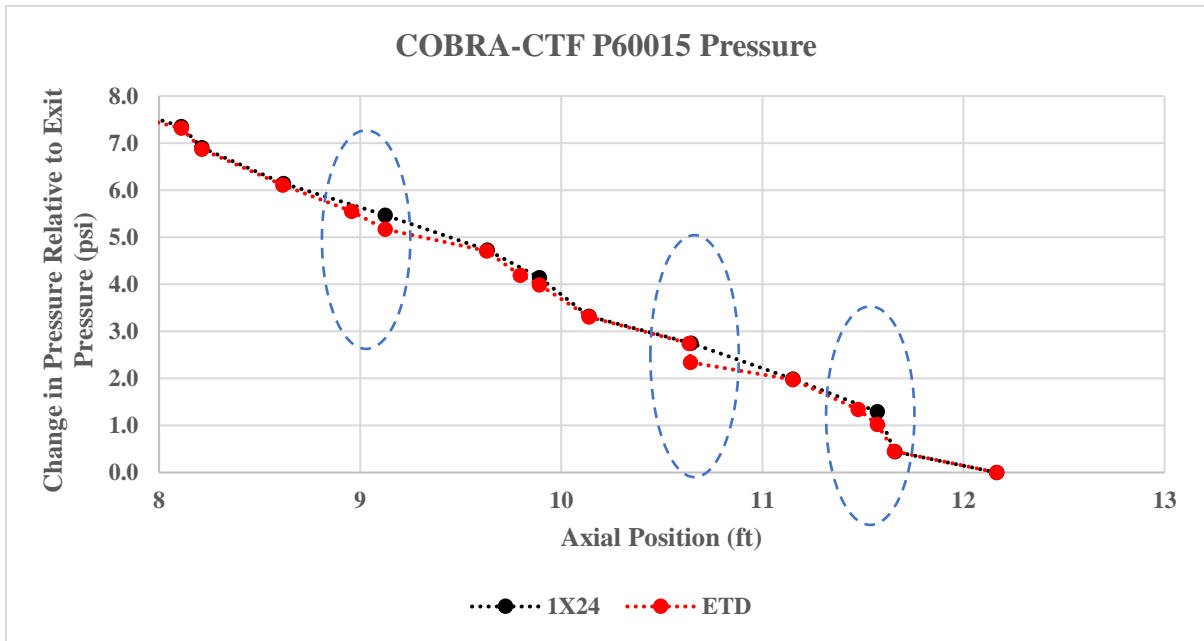
**Figure 3.26: Shift in pressure predictions observed at 9.124ft, 10.646ft, and 11.57ft for 1X24 and ETD cases**

The pressure tap position at 10.636ft is between the grid spacers positions at 9.892ft and 11.572ft. There is an observable shift in the predicted pressure value at the shared axial position of 10.6463ft that appears to be affected by the introduction of the 10.636ft pressure tap position in the ETD case. *Table 3.35* indicates the node length between the pressure tap position and the next shared position is significantly smaller that the surrounding node lengths. This effect can is also observed at the shared axial positions at 9.1240ft and 11.5715ft with the introduction of the pressure tap positions at 8.9567ft and 11.4764ft respectively.

| Table 3.35: P60015, Smaller Node Size Between 10.6463ft and 10.636ft in ETD Case | | | | | |
|---|---|---|---|---|---|
| Axial Positions (ft) | | | | | |
| 9.8917 | 10.1378 | 10.6365 | 10.6463 | 11.1516 | 11.4764 |
| Distance Between Axial Positions (ft) | | | | | |
| 0.2461 | 0.4982 | 0.008685 | 0.5069 | 0.3244 | |

### 3.12  COBRA-CTF Results

*Table 3.36* list the measured and calculated total pressure drop along with the absolute relative differences for individual pressure drop identifiers for each test case with the ETD mesh refinement case. The instrumentation to measure the pressure during the data collection process is recorded to exhibit a 1% accuracy [7]. The pressure drop identifier, *dp09*, is the absolute relative difference associated with the total pressure drop. These values will be compared to the results from COBRA-EN.

| Table 3.36: COBRA-CTF Results for Pressure Drop | | | | | | |
|---|---|---|---|---|---|---|
| **Total Pressure Drop (psi)** | | | **Absolute Relative Difference in Pressure Drop for Individual Pressure Drop Identifiers** | | | |
| **Measured** | **P60001** | **P60007** | **P60015** | **Identifier** | **P60001** | **P60007** | **P60015** |
| | 3.974 | 8.396 | 16.530 | dp01 | 16.72% | 10.38% | 38.09% |
| **Calculated** | **P60001** | **P60007** | **P60015** | dp02 | 24.37% | 21.02% | 41.33% |
| | 3.827 | 8.319 | 15.482 | dp03 | 12.35% | 11.86% | 2.17% |
| | | | | dp04 | 12.98% | 4.47% | 7.58% |
| | | | | dp05 | 14.32% | 6.50% | 11.70% |
| | | | | dp06 | 15.11% | 7.12% | 7.56% |
| | | | | dp07 | 6.27% | 3.63% | 4.06% |
| | | | | dp08 | 6.72% | 5.26% | 4.61% |
| | | | | dp09 | 3.70% | 0.92% | 6.34% |
| | | | | Average | 12.51% | 7.91% | 13.71% |

**CHAPTER 4: COBRA-EN**

COBRA-EN is a combination of COBRA-IV-I, and VIPRE-01 which both evolved from the original COBRA-3C subchannel analysis code developed in 1973 [4]. The main purpose of COBRA-EN was to verify the SBWR and AP600 designs in safety studies relating to reactivity transients [4]. The version of COBRA-EN used in this study is from the Radiation Safety Information Computational Center (RSICC) code package PSR-507 that is written in FORTRAN-77 and compiled to run on a Window platform in a DOS shell.

COBRA-EN can simulate steady-state or transient conditions with user supplied inputs such as total power, outlet pressure, inlet enthalpy or coolant temperature, and mass flowrate. It has the capability to evaluate an assembly with closed (no crossflow) or open channels (crossflow), or at the core level. COBRA-EN allows the user to choose either a three-equation or four-equation thermal-hydraulic model [4]. Both thermal-hydraulic models begin with the mixture conservation equations for mass, energy, and momentum where the interfacial terms between phases cancel [4]. The momentum vector is in both the axial and lateral directions for the water liquid/vapor mixture allowing for simulation of crossflow [4]. These conservation equations are approximated by finite differences in each control volume to produce a system of coupled nonlinear equations that are solved by an implicit iterative scheme based on the calculation of the pressure gradients in the axial direction or Newton-Raphson iteration procedure [4]. This study utilizes the three-equation model with open channels to allow for lateral momentum through the gaps between the heated rods. The equations are solved by an implicit iterative scheme which includes a Gauss forward elimination and backward substitution used in the original COBRA-3C package [4]. Nonhomogeneous flow conditions

can be accounted for through appropriate void quality models and non-thermal equilibrium conditions with subcooled boiling models. In this study, heat transfer models have been omitted as the linear heat rates at selected axial positions are supplied as a user input. Forty-five runs per test case were evaluated with various combinations of correlation options for the two-phase flow models provided by COBRA-EN. The four-equation model where void fraction can be computed directly from an additional vapor continuity equation was not used and is documented to have known issues [4].

## 4.1 Subchannel Conservation Equations

The differential form of the mixture conservation equations employed in COBRA-EN.

Mass Equation [5]:

$$A_k \frac{\partial}{\partial t}(\rho_k) + \frac{\partial}{\partial z}(G_k A_k) = \sum_j \dot{w}'_{j,k} \tag{17}$$

where:

$\dot{w}'_{j,k}$ = Pressure driven lateral mass flow rate per unit length from adjacent subchannel $j$ to subchannel $k$.

$G_k A_k = \dot{m}_k$ = Axial mass flow rate in subchannel $k$ is the product of the mass flux, and cross-sectional flow area of subchannel $k$.

Energy Equation [5]:

$$A_k \frac{\partial \rho_k u_k}{\partial t} + \frac{\partial}{\partial z}(G_k h_k A_k) - \sum_j \dot{w}'_{j,k} h^* - \sum_j \widetilde{w}'_{j,k}(h_j - h_k) = \dot{q}'_k \tag{18}$$

The enthalpy, $h^*$, due to energy exchange between subchannel $k$ and the adjacent subchannels $j$ seen in the convective cross flow term is defined as [5]:

$$h^* = \begin{cases} h_j & \dot{w}'_{j,k} > 0 \\ h_k & \dot{w}'_{j,k} < 0 \end{cases} \tag{19}$$

The parameter $\widetilde{w}'_{j,k}$, is an empirical turbulent mixing crossflow, independent of the lateral pressure gradient [5]. The axial linear heat rate over the length, $\Delta z$, of subchannel $k$, is $\dot{q}'_k$.

Axial Momentum Subchannel Equation [5]:

$$A_k \frac{\partial G_k}{\partial t} + \frac{\partial}{\partial z}\left[ G_k{}^2 \left( \frac{(1-x)^2}{\alpha_l \rho_l} + \frac{x^2}{\alpha_g \rho_g} \right)_k A_k \right] - \sum_j \dot{w}'_{j,k}\, v^* - \sum_j \widetilde{w}'_{j,k}\left( v_j - v_k \right) =$$

$$- A_k \frac{\partial P_k}{\partial z} - \frac{G_k{}^2}{2}\left[ \frac{f\phi^2}{D_h \rho_l} + K_{form,z}\left( \frac{(1-x)^2}{\alpha_l \rho_l} + \frac{x^2}{\alpha_g \rho_g} \right) \Delta z \right]_k - \rho_k A_k g$$

(20)

The momentum velocity, $v^*$, due to exchange between subchannel $k$ and the adjacent subchannels $j$ is seen in the convective cross flow term is defined as [5]:

$$v^* = \begin{cases} v_j & \dot{w}'_{j,k} > 0 \\ v_k & \dot{w}'_{j,k} < 0 \end{cases}$$

(21)

and in the turbulent cross flow term. The forces acting on the fluid in the axial direction are defined in *equation 22* in the order of pressure, friction, and weight:

$$- A_k \frac{\partial P_k}{\partial z} - \frac{G_k{}^2}{2}\left[ \frac{f\phi^2}{D_h \rho_l} + K_{form,z}\left( \frac{(1-x)^2}{\alpha_l \rho_l} + \frac{x^2}{\alpha_g \rho_g} \right) \Delta z \right]_k - \rho_k A_k g$$

(22)

where:

$K_{form,z}$ = The local obstruction loss coefficient, typically a grid spacer loss coefficient

$x$ = Flow quality determined by user selected subcooled boiling model

$f$ = Single-phase friction factor

$\alpha_g$ = Vapor fraction determined by the user selected void quality relationship correlation

$\phi^2$ = Two-phase friction multiplier determined by the user selected correlation

Lateral Momentum Equation [5]:

$$l\Delta z \frac{\partial \dot{w}'_{j,k}}{\partial t} + \dot{w}'_{j,k} l v_z \Big|_{z+\Delta z} - \dot{w}'_{j,k} l v_z \Big|_z =$$

$$S\Delta z (P_j - P_k) - \frac{\dot{w}'^2_{j,k}}{2lS} \left[ K_{form,x} \left( \frac{(1-x)^2}{\alpha_l \rho_l} + \frac{x^2}{\alpha_g \rho_g} \right) \Delta z \right]_k \tag{23}$$

The dimensions for the lateral control volume are illustrated in *figure 4.1* [5].

$l$ =Total length of the lateral momentum control volume that equates to the sum of the length

from the center of subchannel $k$ to the center of subchannel $j$.

$S$ =Width of the lateral momentum control volume. The length of the gap between fuel rods

in a lattice, or fuel rod to structural surface such as the wall of a BWR canister.
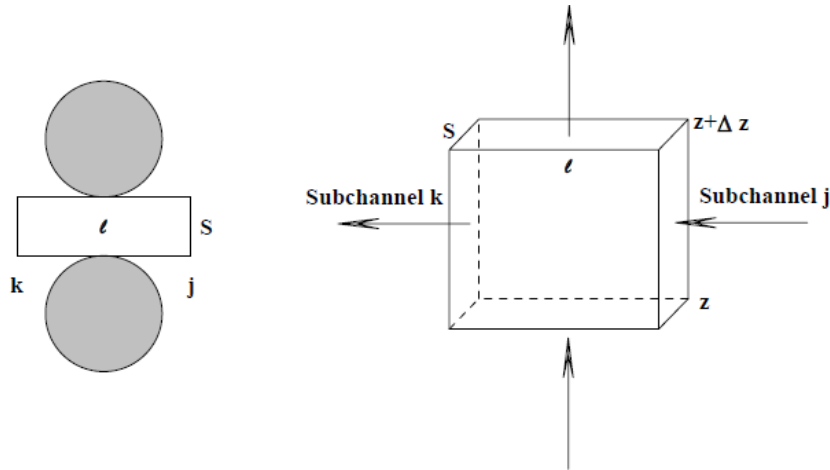


**Figure 4.1:   Diagram of the lateral momentum control volume**

The forces acting on the fluid in the lateral direction are defined in *equation 24* in the order

of gap pressure, and friction:

$$S\Delta z (P_j - P_k) - \frac{\dot{w}'^2_{j,k}}{2lS} \left[ K_{form,x} \left( \frac{(1-x)^2}{\alpha_l \rho_l} + \frac{x^2}{\alpha_g \rho_g} \right) \Delta z \right]_k \tag{24}$$

where:

$K_{form,x}$ = The cross-flow resistance loss coefficient

**4.2 Subcooled Boiling Models**

Thermal non-equilibrium can be accounted for in the three-equation model using an empirical subcooled boiling model which relates the flow quality to the equilibrium quality. There is a list of the model parameters in the subcooled boiling models section in *appendix G.* The following options for the subcooled models are available [4]:

- Homogeneous model,
- Levy correlation,
- EPRI correlation

The flow quality is the flow fraction of the vapor phase and is equal to the equilibrium quality only under equilibrium conditions. The equilibrium quality, $x_e$, is defined as:

$$x_e = \frac{h - h_f}{h_g - h_f} \tag{25}$$

The COBRA-EN homogenous subcooled boiling model refers to the phases in thermal equilibrium where the flow quality is equal to equilibrium quality and does not imply equal phase velocities [4]:

$$x = x_e = \frac{h - h_f}{h_g - h_f} \tag{26}$$

The Levy and EPRI models relate the flow quality to the equilibrium quality by introducing the bubble departure quality $x_d$, which is defined to be the equilibrium quality at the bubble departure point [4].

The Levy model defines the flow quality as [4]:

$$x = x_e - x_d \exp\left(\frac{x_e}{x_d} - 1\right) \qquad if \ x_e \geq x_d \qquad (27)$$

$$x = 0 \qquad if \ x_e < x_d$$

where the bubble departure quality is defined as [4]:

$$x_d = -\frac{C_{pf} \Delta T_d}{h_{fg}} \qquad (28)$$

Flow quality in the EPRI model is given as [4]:

$$x = \frac{x_e - x_d \left[1 - \tanh\left(1 - \frac{x_e}{x_d}\right)\right]}{1 - x_d \left[1 - \tanh\left(1 - \frac{x_e}{x_d}\right)\right]} \qquad if \ x_e \geq x_d \qquad (29)$$

$$x = 0 \qquad if \ x_e < x_d$$

where the bubble departure quality is defined as [4]:

$$x_d = -\frac{C_{pl} Z}{h_{fg}} \qquad (30)$$

## 4.3 Void Quality Relations

Relative phase velocity can be accounted for with a void quality relationship based on slip ratio or through drift flux models. The following options for the void quality relationships available [4]:

- EPRI correlation
- Zuber-Findlay correlation
- Homogeneous model
- Armand-Messena correlation
- Smith correlation
- Slip ratio given as polynomial in quality
- Void fraction given as polynomial in quality

The polynomial options were not explored in this study. Vapor volume fraction (void fraction) can be determined using a void model with flow quality from a sub-cooled boiling model. Slip ratio, $S$, defined as the ratio of vapor-to-liquid phase velocity can be used to account for the effects of relative phase velocity on the void fraction. Void fraction, quality, and slip ratio can be related through the Fundamental Void-Quality-Slip relation.

$$\alpha = \frac{xv_g}{(1-x)v_f S + xv_g}$$
(31)

For the void-quality model, homogenous flow assumes the liquid and vapor velocities are equal and the slip ratio is one:

$$S = \frac{V_g}{V_f} = 1$$
(32)

where:

$V_g$ = vapor phase velocity,

$V_l$ = liquid phase velocity,

$v_f$ = liquid specific volume,

$v_g$ = vapor specific volume

Empirical void-quality, or equivalent slip quality relations are given below.

Smith correlation [4]:

$$S = 0.4 + 0.6\sqrt{\frac{0.4 + x\left(\frac{v_g}{v_f} - 0.4\right)}{0.4 + 0.6x}} \tag{33}$$

Armand-Messena correlation [4]:

$$\alpha = x v_g \frac{(0.833 + 0.167x)}{(1-x)v_f + x v_g} \tag{34}$$

Zuber-Findlay relation [4]:

$$\alpha = \frac{x}{1.13\left[x + \frac{\rho_g}{\rho_l}(1-x)\right] + \frac{\rho_g V_{gj}}{G}} \tag{35}$$

where the drift velocity $V_{gj}$ is given by [4]:

$$V_{gj} = 1.18\left[\frac{\sigma g g_c(\rho_f - \rho_g)}{\rho_f^2}\right]^{\frac{1}{4}} \tag{36}$$

EPRI void/quality correlation [4]:

$$\alpha = \frac{x}{C_0\left[x+\frac{\rho_g}{\rho_l}(1-x)\right]+\frac{\rho_g V_{gj}}{G}} \tag{37}$$

where:

$$C_0 = \frac{L(\alpha,P)}{K_0+(1-K_0)\alpha^r} \tag{38}$$

$$L(\alpha,P) = \frac{1-e^{-C_1\alpha}}{1-e^{-C_1}} \tag{39}$$

$$K_0 = K_1 + (1-K_1)\left(\frac{\rho_g}{\rho_f}\right)^{\frac{1}{4}} \tag{40}$$

$$r = \frac{1+1.57\left(\frac{\rho_g}{\rho_f}\right)}{1-K_1} \tag{41}$$

$$C_1 = \frac{4}{\frac{P}{P_c}\left(1-\frac{P}{P_c}\right)} \tag{42}$$

$$K_1 = min(0.8, K_1^F) \tag{43}$$

$$K_1^F = \frac{1}{1+e^{-Re/10^5}} \tag{44}$$

And the drift velocity $V_{gj}$ has been corrected so that it becomes zero if $\alpha = 1$ [4]:

$$V_{gj} = 1.41\left[\frac{\sigma g g_c(\rho_f-\rho_g)}{\rho_f^2}\right]^{\frac{1}{4}}\frac{\sqrt{1-\alpha}}{1+\alpha}\cos\theta \tag{45}$$

**4.4 Two Phase Friction Model**

The two-phase pressure drop is modeled by introducing a two-phase friction multiplier. The two-phase multiplier is defined as the ratio between friction pressure drop in two-phase flow to the friction pressure drop assuming all the fluid flows as a saturated liquid. The following options for the two-phase friction multiplier are available [4]:

- Homogeneous model,
- EPRI correlation (default),
- Armand correlation,
- a polynomial in quality up to sixth degree, specified in input.

The polynomial options for two-phase friction multiplier were not explored in this study. There is a list of the model parameters in the two-phase friction models section in *appendix G*. For the momentum equation, homogenous flow is defined as having equal phase velocities, independent of the relative states of the phases. The homogeneous two-phase friction multiplier can be derived assuming homogenous flow conditions and is given as function of the flow quality by [4]:

$$\phi^2 = \frac{\rho_l}{\rho_m}\left[\frac{\mu_f}{x\mu_g + \mu_f(1-x)}\right]^b \tag{46}$$

The EPRI correlation is a function of the flow quality, mass flux, and pressure [4]:

$$\phi^2 = 1.0 + \left(\frac{v_g}{v_f} - 1\right) x C_F \tag{47}$$

The Armand correlation is a function of flow quality and vapor fraction [4]:

$$\phi^2 = \frac{(1-x)^2}{(1-\alpha)^{1.42}} \quad if\ 0 < \alpha < 0.6 \tag{48}$$

$$\phi^2 = 0.478\frac{(1-x)^2}{(1-\alpha)^{2.2}} \quad if\ 0.6 < \alpha < 0.9 \tag{49}$$

$$\phi^2 = 1.73\frac{(1-x)^2}{(1-\alpha)^{1.64}} \quad if\ 0.9 < \alpha < 1.0 \tag{50}$$

## 4.5   Pressure Drop

The two-phase wall friction pressure drop for axial flow is represented as:

$$\frac{dP}{dX} = \frac{fG^2}{2D_h\rho_l g_c}\phi^2 \tag{51}$$

where the wall friction factor, $f$, is defined as [4]:

$$f = aRe^b + c, \quad where\ Re = \frac{GD_h}{\mu_{bulk}} \tag{52}$$

The list of parameters for the pressure drop is in *appendix H.* COBRA-EN can assign specific sub-channels with user specified sets of constants a, b, and c for both laminar and turbulent flow. The smooth tube friction factor is based on the fully developed laminar flow and the McAdams relation for turbulent flow conditions [4].

Fully Developed Laminar Flow

$$a = 64.0, \quad b = -1.0, \quad c = 0; \quad for\ laminar\ flow$$

McAdams Relation [8]

$$a = 0.184, \quad b = -0.2, \quad c = 0; \quad for\ turbulent\ flow$$

Pressure loss for flow across grid spacers or through lower and upper grid plates is given by *equation 54* [4]:

$$\Delta P_{axial,form} = K_D \frac{G^2 v'}{2g_c}$$

(53)

The local pressure loss due to the grid spacers seen in *equation 53* contain the user specified grid spacer loss coefficient, $K_D$, and the effective specific volume for momentum transport, $v'$, represented by *equation 54*:

$$v' = \frac{x^2}{\alpha \rho_v} + \frac{(1-x)^2}{(1-\alpha)\rho_l}$$

(54)

The effective specific volume for momentum transport term acts as a two-phase multiplier for the local pressure drop.

Pressure drop in the lateral direction through channel boundary gaps from both friction and form drag are treated with a cumulative drag loss coefficient [4]:

$$\Delta P_{lat,drag} = K_G \frac{|w|wv'}{2slg_c} \tag{55}$$

The COBRA-EN default value 0.5 was used for the user specified cross-flow resistance loss coefficient, $K_G$ [4]. The effective specific volume for momentum transport again acts as a two-phase multiplier for the pressure drop.

## 4.6 Water Properties

To estimate the required water properties in COBRA-EN, the functions developed by EPRI for RETRAN-02 computer program have been coded [4].

**4.7    COBRA-EN Axial Nodes**

Computational nodes are stacked along the axial length of the assembly. The positions of interest such as pressure tap and shared axial positions are defined by the edges of these stacked nodes with associated axial peaking factors supplied by the user. A decision was made to define the provided axial peaking factors in *figure 2.5* for an entire node length at the node center. The axial peaking factors used as inputs in COBRA-EN have been tabulated in *table 4.3*. Linear interpolation of given nearest nodes' axial peaking factors are used in this study. This technique is used to introduce pressure tap positions and during the process of introducing additional nodes in the convergence study. Pressure tap positions are introduced to reduce error while determining the pressure drop values between the pressure tap positions indicated on *figure 2.4*. Otherwise, there are occurrences where a grid spacer position is between two pressure tap positions used in the determination of a pressure drop calculation. Linear interpolation over this range is problematic considering the nonlinear behavior of the pressure drop over the range where a local obstruction occurs at some arbitrary location between the pressure tap measurements such as a grid spacer. Furthermore, the introduction of the pressure tap positions allow the code to generate values at this location for evaluation instead of introducing interpolation errors.

*Figures 4.2* and *4.3* illustrate the techniques used to determine the center of a node. These node centers are first used to resolve the axial peaking factor at that location. Then, the previously determined axial peaking factor is used as an input in the *equation 56* to generate the linear fission power, linear heat rate, at that position. Also, these node centers are used to determine the node edges which are the positions of interest located in the output file. COBRA-EN requires an input of the node size that is used in conjunction with the node centers. The node centers are designated in increasing increments along the axial length of the heated rod, and half the node sized is used to determine the lower and upper edges of the node. *Figure 4.2* reflects a normal node. *Figure 4.3* illustrates the extra steps taken to resolve the node centers required for positions to approximate axial peaking factors, and to node edges for the positions of interest such as pressure tap positions and subdivision of nodes during the convergence study.

### 4.7.1 Description of the Normal Axial Nodes in COBRA-EN

The figure below illustrates the normal (uniform) axial node:

$$\Delta z = \frac{Height_{Fuel}}{Axial_{Intervals}} = \frac{12.165 ft}{24} = 0.50689 ft$$

For example, the given axial peaking factor $F_z(J) = 0.46$, located at the center of the node

position $XTAB(J) = 0.25344 ft$, and length of the axial interval $DX(J) = 0.50689 ft$.

*Values are examples seen in the table between the bottom to the first edge value of 0.50689ft

Next
Node

Upper Edge
of Node

XTAB(J)

Known Value for
Axial Peaking
Factor, Fz(J)

DX(J)=2*XTAB(J)

XTAB(J)

Lower Edge
of Node

Previous
Node
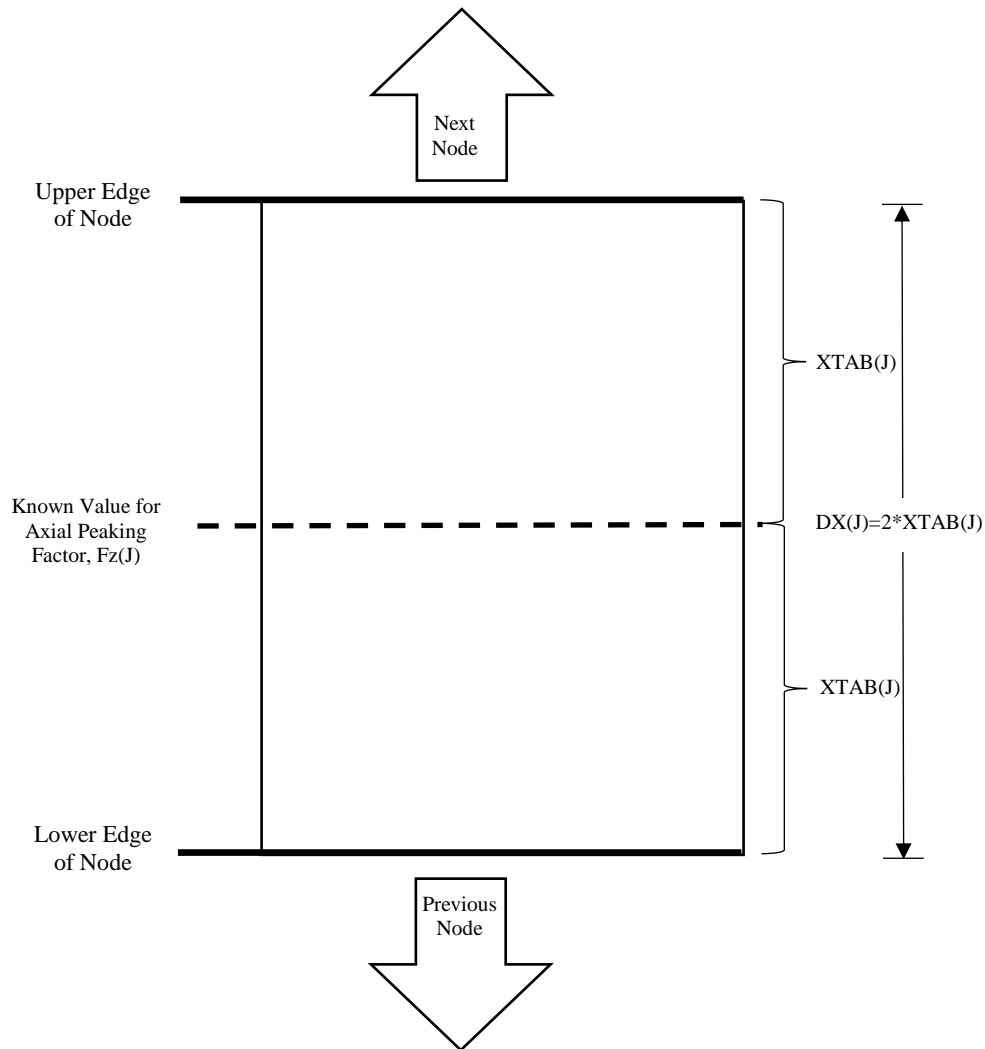
**Figure 4.2:   Diagram to illustrate the construction of a normal COBRA-EN axial node**

## 4.7.2   Illustration of the Introduced Axial Nodes in COBRA-EN
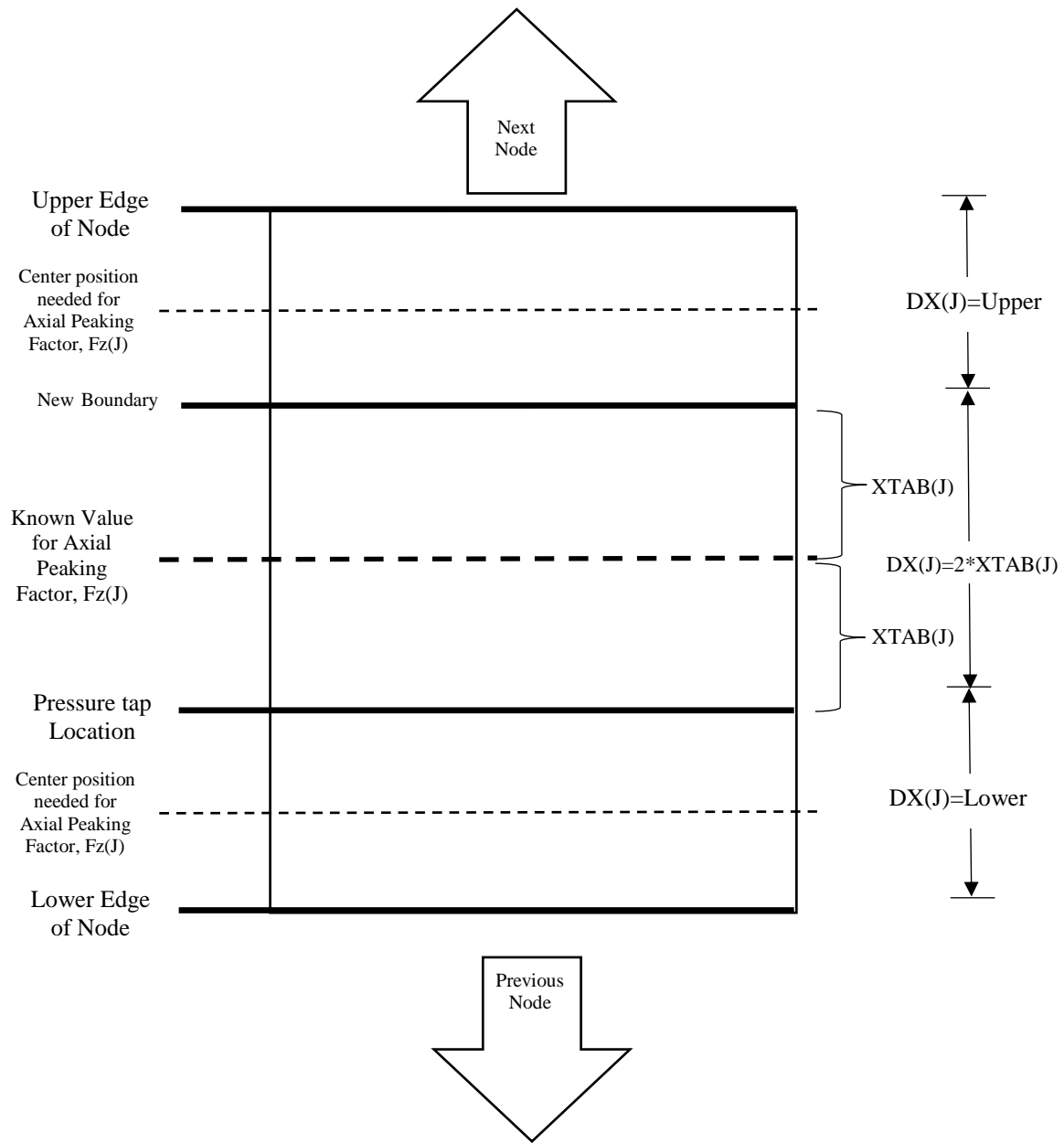


**Figure 4.3:   Diagram to illustrate the construction of an introduced COBRA-EN axial node.**

*These are required to introduced pressure tap positions and subdividing node for the convergence study*

*Table 4.1* lists the node lengths along the heated length of the assembly that results in the axial positions where COBRA-EN will generate results. The blue cells are marked to display the created edges, and the orange cells indicate the pressure tap positions.

| | Table 4.1: COBRA-EN Node Edges | | |
|---|---|---|---|
| Node Length (ft) | Outfile Axial Position (ft) | Calculated Axial Position (ft) | Calculated Axial Position (m) |
| | 0.000 | 0.0000 | 0.0000 |
| 0.50689 | 0.507 | 0.5069 | 0.1545 |
| 0.50689 | 1.014 | 1.0138 | 0.3090 |
| 0.50689 | 1.521 | 1.5207 | 0.4635 |
| 0.50689 | 2.028 | 2.0276 | 0.6180 |
| 0.21000 | 2.238 | 2.2375 | 0.6820 |
| 0.08695 | 2.325 | 2.3245 | 0.7085 |
| 0.21000 | 2.535 | 2.5344 | 0.7725 |
| 0.50689 | 3.041 | 3.0413 | 0.9270 |
| 0.50689 | 3.548 | 3.5482 | 1.0815 |
| 0.50689 | 4.055 | 4.0551 | 1.2360 |
| 0.50689 | 4.562 | 4.5620 | 1.3905 |
| 0.50689 | 5.069 | 5.0689 | 1.5450 |
| 0.50689 | 5.576 | 5.5758 | 1.6995 |
| 0.02132 | 5.597 | 5.5971 | 1.7060 |
| 0.46424 | 6.061 | 6.0614 | 1.8475 |
| 0.02132 | 6.083 | 6.0827 | 1.8540 |
| 0.50689 | 6.590 | 6.5896 | 2.0085 |
| 0.50689 | 7.097 | 7.0965 | 2.1630 |
| 0.18044 | 7.277 | 7.2769 | 2.2180 |
| 0.14600 | 7.423 | 7.4229 | 2.2625 |
| 0.18044 | 7.603 | 7.6033 | 2.3175 |
| 0.50689 | 8.110 | 8.1102 | 2.4720 |
| 0.50689 | 8.617 | 8.6171 | 2.6265 |
| 0.16733 | 8.784 | 8.7844 | 2.6775 |
| 0.17224 | 8.957 | 8.9567 | 2.7300 |
| 0.16733 | 9.124 | 9.1240 | 2.7810 |
| 0.50689 | 9.631 | 9.6309 | 2.9355 |
| 0.16568 | 9.797 | 9.7966 | 2.9860 |
| 0.17553 | 9.972 | 9.9721 | 3.0395 |
| 0.16568 | 10.138 | 10.1378 | 3.0900 |
| 0.00821 | 10.146 | 10.1460 | 3.0925 |
| 0.49048 | 10.637 | 10.6365 | 3.2420 |
| 0.00821 | 10.645 | 10.6447 | 3.2445 |
| 0.50689 | 11.152 | 11.1516 | 3.3990 |
| 0.18209 | 11.334 | 11.3337 | 3.4545 |
| 0.14271 | 11.476 | 11.4764 | 3.4980 |
| 0.18209 | 11.659 | 11.6585 | 3.5535 |
| 0.50689 | 12.165 | 12.1654 | 3.7080 |

**4.8 Power Profile**

The power profile is built by determining the local power distribution at positions along the axial length of the heated rod. This is accomplished with the small FORTRAN code attached in *appendix I* written to generate the linear fission power at each axial position along the axial length of each heated rod in the bundle. *Equation 59* for linear fission power is calculated at each node's center point.

$$q' = \frac{QF_zF_q\gamma}{NH}$$ (56)

$q'$ = Linear fission power (linear heat rate) at axal location,

$Q$ = Total thermal output,

$F_z$ = Axial peaking factor at axial location,

$F_q$ = Radial peaking factor for the sub-channel,

$\gamma$ = Fraction of heat directly deposited in the bulk fluid of the sub-channel,

$N$ = Number of heated rods in the bundle,

$H$ = Height of the heated rod.

There are marginal differences between the NUPEC BFBT given test case thermal outputs in comparison to the COBRA-EN generated values for thermal outputs seen in the output file. There is a slight round off error contribution due to the linear heat rates that are entered at each axial position along the heated rods. This is captured in the *tables 4.2* for each test case.

| Table 4.2: COBRA-EN Thermal Output (MW) | | | |
|---|---|---|---|
| Test Case | P60001 | P60007 | P60015 |
| Given Thermal Output | 0.863 | 2.375 | 5.340 |
| Code Calculated Thermal Output | 0.8647068 | 2.379696 | 5.350603 |
| Absolute Relative Difference | 0.198% | 0.198% | 0.199% |
| Difference | -0.00171 | 0.00470 | -0.01060 |

*Table 4.3* lists the node centers along the heated length of the assembly with asscoiated axial

peaking factors, $F_z$. The blue cells are marked to display the node centers with created edges,

and the orange cells to indicate the node centers for pressure tap positions where the axial

peaking factors were approximated.

| Table 4.3:   COBRA-EN Center Points | | | |
|---|---|---|---|
| **Outfile Axial Position (ft)** | **Input Axial Position (ft)** | **Input Axial Position (m)** | **FZ** |
| 0.253 | 0.2534 | 0.0773 | 0.46 |
| 0.760 | 0.7603 | 0.2318 | 0.58 |
| 1.267 | 1.2672 | 0.3863 | 0.69 |
| 1.774 | 1.7741 | 0.5408 | 0.79 |
| 2.133 | 2.1325 | 0.6500 | 0.85 |
| 2.281 | 2.2810 | 0.6953 | 0.88 |
| 2.430 | 2.4295 | 0.7405 | 0.91 |
| 2.788 | 2.7879 | 0.8498 | 0.99 |
| 3.295 | 3.2948 | 1.0043 | 1.09 |
| 3.802 | 3.8017 | 1.1588 | 1.22 |
| 4.309 | 4.3086 | 1.3133 | 1.22 |
| 4.816 | 4.8155 | 1.4678 | 1.34 |
| 5.322 | 5.3223 | 1.6223 | 1.34 |
| 5.587 | 5.5864 | 1.7027 | 1.37 |
| 5.829 | 5.8292 | 1.7768 | 1.40 |
| 6.072 | 6.0720 | 1.8508 | 1.40 |
| 6.336 | 6.3361 | 1.9313 | 1.40 |
| 6.843 | 6.8430 | 2.0858 | 1.34 |
| 7.187 | 7.1867 | 2.1905 | 1.34 |
| 7.350 | 7.3499 | 2.2403 | 1.34 |
| 7.513 | 7.5131 | 2.2900 | 1.30 |
| 7.857 | 7.8568 | 2.3948 | 1.22 |
| 8.364 | 8.3637 | 2.5493 | 1.22 |
| 8.701 | 8.7008 | 2.6520 | 1.13 |
| 8.871 | 8.8706 | 2.7038 | 1.09 |
| 9.040 | 9.0404 | 2.7555 | 1.06 |
| 9.378 | 9.3775 | 2.8583 | 0.99 |
| 9.714 | 9.7137 | 3.0913 | 0.92 |
| 9.884 | 9.8844 | 3.0128 | 0.88 |
| 10.055 | 10.0550 | 3.2432 | 0.85 |
| 10.142 | 10.1419 | 3.9607 | 0.83 |
| 10.391 | 10.3912 | 3.1673 | 0.79 |
| 10.641 | 10.6406 | 3.0648 | 0.74 |
| 10.898 | 10.8981 | 3.3218 | 0.69 |
| 11.243 | 11.2426 | 3.4268 | 0.62 |
| 11.405 | 11.4050 | 3.4763 | 0.58 |
| 11.567 | 11.5674 | 3.5257 | 0.54 |
| 11.912 | 11.9119 | 3.6308 | 0.46 |

### 4.9 COBRA-EN Boundary Conditions

The given parameters are entered on *card 29, operating conditions,* which are used for boundary conditions in COBRA-EN.

### 4.9.1 Inlet Boundary Conditions

The inlet boundary conditions are a total inlet mass flux, *GIN*, used to calculate subchannel mass flow rates for the user specified subchannels flow areas, and inlet fluid temperature, *HIN*. This study chooses to use a constant inlet fluid temperature for all subchannels.

| Table 4.4: Inlet Fluid Temperature, HIN | | |
|---|---|---|
| **P60001** | **P60007** | **P60015** |
| °C | | |
| 277.3 | 277.8 | 278.2 |
| °F | | |
| 531.14 | 532.04 | 532.76 |

Average inlet mass flux is constant over the cross-sectional flow area for a given mass flow is:

$$G = \frac{\dot{m}}{Area_X} \tag{57}$$

| Table 4.5: Total Inlet Mass Flux Rate, GIN | | |
|---|---|---|
| **P60001** | **P60007** | **P60015** |
| $kg/m^2 s$ | | |
| 592.889 | 1614.30 | 2054.57 |
| $lb_m/ft^2 hr$ | | |
| $4.3716 \times 10^5$ | $1.19029 \times 10^6$ | $1.51491 \times 10^6$ |
| Given Mass Flow Rate (t/hr) | | |
| 20.2 | 55.0 | 70.0 |
| Bundle Cross-Sectional Area, $A_x$ | | |
| $14.668 in^2$ | $9463 mm^2$ | |

### 4.9.2 Outlet Boundary Conditions

The outlet boundary condition is the system exit pressure, *PEXIT*. This is set as system reference

pressure [4].

| Table 4.6: Exit Pressure, PEXIT | | |
|---|---|---|
| **P60001** | **P60007** | **P60015** |
| **MPa** | | |
| 7.16 | 7.17 | 7.17 |
| **psi** | | |
| 1038.4702 | 1039.9206 | 1039.9206 |

### 4.10 Case Studies for COBRA-EN

Two studies were performed with COBRA-EN prior to comparing COBRA-EN and

COBRA-CTF predictions with the NUPEC BFBT benchmark data. Unlike COBRA-CTF,

COBRA-EN allows the user to select combinations of correlations for computing two-phase

flow conditions. The first study determines the appropriate combinations of correlations to

compare to the benchmark data. The criteria involved during this process were:

- Determine the appropriate set of correlations with the least amount of error compared
  to the NUPEC BFBT benchmark measured data.

- Select a set of correlations that will apply to typical BWR operating conditions.

- Use the selected set of correlations to compare to equivalent COBRA-CTF results.

The second study involves a mesh convergence study performed in the same fashion as

previously done for COBRA-CTF. The purpose for this procedure is to recognize sensitivity

of simulation results to node length in COBRA-EN and determine an appropriate uniform node

length that both COBRA-EN and COBRA-CTF have in common to compare the results of

both codes at the same axial positions along the heated channel.

**4.10.1 Combination of Correlations for COBRA-EN**

*Table 4.7* is a list of the combinations of correlations used in COBRA-EN:

| Table 4.7: Legend for Combinations of Correlations Used in COBRA-EN | | | | |
|---|---|---|---|---|
| **Card 18: Two Phase Friction Model** | | | **Card 20: Void Fraction Model** | |
| **J4: Two Phase Friction Multiplier** | | | **J2: Subcooled Boiling** | **J3: Indicator of Bulk Void/Quality Relationship** |
| **EPRI** | **Homogenous** | **Armand** | | |
| **Identifier** | | | | |
| 1 | 16 | 31 | EPRI | EPRI |
| 2 | 17 | 32 | EPRI | Zuber-Findlay |
| 3 | 18 | 33 | EPRI | Homogeneous |
| 4 | 19 | 34 | EPRI | Armand-Messena |
| 5 | 20 | 35 | EPRI | Smith |
| 6 | 21 | 36 | Levy | EPRI |
| 7 | 22 | 37 | Levy | Zuber-Findlay |
| 8 | 23 | 38 | Levy | Homogeneous |
| 9 | 24 | 39 | Levy | Armand-Messena |
| 10 | 25 | 40 | Levy | Smith |
| 11 | 26 | 41 | Homogeneous | EPRI |
| 12 | 27 | 42 | Homogeneous | Zuber-Findlay |
| 13 | 28 | 43 | Homogeneous | Homogeneous |
| 14 | 29 | 44 | Homogeneous | Armand-Messena |
| 15 | 30 | 45 | Homogeneous | Smith |

The COBRA-EN manual suggest the following combinations of consistent correlations [4]:

- All the EPRI correlations making up together the EPRI void model (default option)
  *Identifier 1*
- Homogeneous void model with the possible inclusion of the Smith correlation
  *Identifier 45*
- Armand correlation for two-phase friction multiplier, homogenous subcooled boiling, and Armand-Messena correlation for void fraction
  *Identifier 44*
- EPRI correlation for the two-phase friction multiplier, Levy subcooled boiling, and Zuber-Findlay void relations.
  *Identifier 7*

### 4.10.2 P60001, Evaluation of Total Pressure Drop

The cells marked in a darker shade of blue (less than 2%) indicate that *sets 11,* and *12* consist of correlations that provide predicted values that match the measured value for total pressure drop with absolute relative differences of 1.925% and 1.979% respectively. Both *sets 11,* and *12* are using the EPRI two-phase friction correlation, and the homogenous (equilibrium) subcooled boiling model. The void/quality relationship model used for *set 11* is the EPRI correlation while *set 12* uses the Zuber-Findley correlation.

| Table 4.8: P60001 Evaluation for Total Pressure Drop of Measured Value 3.974 psi | | | | | | | | | | | | | | |
|---|---|---|---|---|---|---|---|---|---|---|---|---|---|---|
| **EPRI Two-Phase Friction Multiplier Suite** | | | | | | | | | | | | | | |
| 1 | 2 | 3 | 4 | 5 | 6 | 7 | 8 | 9 | 10 | 11 | 12 | 13 | 14 | 15 |
| **Total Pressure Drop (psi)** | | | | | | | | | | | | | | |
| 3.877 | 3.879 | 3.752 | 3.857 | 3.866 | 3.878 | 3.879 | 3.753 | 3.858 | 3.866 | 3.897 | 3.895 | 3.775 | 3.875 | 3.885 |
| **Absoulte Relative Difference** | | | | | | | | | | | | | | |
| 2.43% | 2.39% | 5.58% | 2.94% | 2.73% | 2.41% | 2.39% | 5.57% | 2.93% | 2.72% | 1.93% | 1.98% | 5.01% | 2.49% | 2.24% |
| **Difference** | | | | | | | | | | | | | | |
| -0.0966 | -0.0950 | -0.2216 | -0.1167 | -0.1085 | -0.0958 | -0.0949 | -0.2213 | -0.1165 | -0.1080 | -0.0765 | -0.0786 | -0.1993 | -0.0989 | -0.0890 |
| **Homogenous Two-Phase Friction Multiplier Suite** | | | | | | | | | | | | | | |
| 16 | 17 | 18 | 19 | 20 | 21 | 22 | 23 | 24 | 25 | 26 | 27 | 28 | 29 | 30 |
| **Total Pressure Drop (psi)** | | | | | | | | | | | | | | |
| 3.711 | 3.713 | 3.613 | 3.694 | 3.700 | 3.712 | 3.713 | 3.613 | 3.695 | 3.700 | 3.736 | 3.734 | 3.640 | 3.717 | 3.724 |
| **Absoulte Relative Difference** | | | | | | | | | | | | | | |
| 6.61% | 6.57% | 9.08% | 7.04% | 6.91% | 6.59% | 6.57% | 9.08% | 7.03% | 6.89% | 5.99% | 6.04% | 8.41% | 6.47% | 6.30% |
| **Difference** | | | | | | | | | | | | | | |
| -0.2627 | -0.2613 | -0.3610 | -0.2797 | -0.2744 | -0.2618 | -0.2611 | -0.3607 | -0.2795 | -0.2739 | -0.2379 | -0.2401 | -0.3344 | -0.2573 | -0.2503 |
| **Armand Two-Phase Friction Multiplier Suite** | | | | | | | | | | | | | | |
| 31 | 32 | 33 | 34 | 35 | 36 | 37 | 38 | 39 | 40 | 41 | 42 | 43 | 44 | 45 |
| **Total Pressure Drop (psi)** | | | | | | | | | | | | | | |
| 3.738 | 3.740 | 3.665 | 3.724 | 3.727 | 3.739 | 3.740 | 3.666 | 3.724 | 3.727 | 3.762 | 3.760 | 3.691 | 3.746 | 3.750 |
| **Absoulte Relative Difference** | | | | | | | | | | | | | | |
| 5.94% | 5.89% | 7.77% | 6.29% | 6.23% | 5.92% | 5.89% | 7.76% | 6.28% | 6.21% | 5.33% | 5.37% | 7.12% | 5.74% | 5.64% |
| **Difference** | | | | | | | | | | | | | | |
| -0.236 | -0.234 | -0.309 | -0.250 | -0.247 | -0.235 | -0.234 | -0.308 | -0.250 | -0.247 | -0.212 | -0.214 | -0.283 | -0.228 | -0.224 |

### 4.10.3   P60001, Evaluation of Pressure Drop for the Pressure Drop Identifiers

The darker blue cells (less than 2%) indicate code calculated values closer to the measured data for individual pressure drop identifiers. The EPRI two-phase friction multiplier suite indicates less absolute relative difference in the predicted value compared to the measured data for a majority of the pressure drop identifiers. Also, the column averages suggest the EPRI two-phase friction multiplier suite match the measured data better than the Armand and homogenous suites. S*ets 11*, and *12* represent the closest code predicted values to the measured data with column averages of 9.14% and 9.10% respectively. All three two-phase friction multiplier suites display a larger absolute relative difference near the upper portion of the assembly, especially at the top of the assembly labeled *dpt01*. The subcooled boiling models exhibit a minor contribution to the results under these conditions. The EPRI two-phase friction multiplier in combination with either the EPRI, or Zuber-Findley void/quality relationship models will yield the better results for lower than nominal BWR operating power and mass flow rates seen in test cast P60001.

**Table 4.9: P60001 Absolute Relative Difference for Pressure Drop at Pressure Drop Identifiers**

**EPRI Two-Phase Friction Multiplier Suite**

| Pressure Tap | Measured | 1 | 2 | 3 | 4 | 5 | 6 | 7 | 8 | 9 | 10 | 11 | 12 | 13 | 14 | 15 |
|---|---|---|---|---|---|---|---|---|---|---|---|---|---|---|---|---|
| dp01 | 0.167 | 31.74% | 31.74% | 25.75% | 31.74% | 31.74% | 31.74% | 31.74% | 25.75% | 31.74% | 31.74% | 31.74% | 31.74% | 25.75% | 31.74% | 31.74% |
| dp02 | 0.284 | 8.45% | 8.45% | 11.97% | 8.45% | 8.45% | 8.45% | 8.45% | 11.97% | 8.45% | 8.45% | 8.45% | 8.45% | 11.97% | 8.45% | 8.45% |
| dp03 | 0.367 | 14.44% | 14.44% | 6.27% | 14.44% | 17.17% | 14.44% | 14.44% | 6.27% | 14.44% | 17.17% | 14.44% | 14.44% | 6.27% | 14.44% | 17.17% |
| dp04 | 0.505 | 6.93% | 6.93% | 12.87% | 8.91% | 6.93% | 6.93% | 6.93% | 12.87% | 8.91% | 6.93% | 6.93% | 6.93% | 12.87% | 8.91% | 6.93% |
| dp05 | 0.531 | 7.72% | 7.72% | 13.37% | 7.72% | 9.60% | 7.72% | 7.72% | 13.37% | 7.72% | 9.60% | 5.84% | 7.72% | 13.37% | 7.72% | 9.60% |
| dp06 | 0.570 | 7.02% | 7.02% | 12.28% | 8.77% | 8.77% | 7.02% | 8.77% | 12.28% | 10.53% | 8.77% | 8.77% | 7.02% | 12.28% | 8.77% | 8.77% |
| dp07 | 1.780 | 4.49% | 4.49% | 6.74% | 5.06% | 5.06% | 4.49% | 4.49% | 6.74% | 5.06% | 5.06% | 3.93% | 3.37% | 5.06% | 3.93% | 3.93% |
| dp08 | 0.798 | 0.25% | 0.25% | 0.25% | 0.25% | 0.25% | 0.25% | 0.25% | 0.25% | 0.25% | 0.25% | 0.25% | 0.25% | 1.00% | 0.25% | 1.00% |
| dp09 | 3.974 | 2.43% | 2.39% | 5.58% | 2.94% | 2.73% | 2.41% | 2.39% | 5.57% | 2.93% | 2.72% | 1.93% | 1.98% | 5.01% | 2.49% | 2.24% |
| Average | | 9.27% | 9.27% | 10.56% | 9.81% | 10.08% | 9.27% | 9.47% | 10.56% | 10.00% | 10.08% | 9.14% | 9.10% | 10.40% | 9.63% | 9.98% |

**Homogenous Two-Phase Friction Multiplier Suite**

| Pressure Tap | Measured | 16 | 17 | 18 | 19 | 20 | 21 | 22 | 23 | 24 | 25 | 26 | 27 | 28 | 29 | 30 |
|---|---|---|---|---|---|---|---|---|---|---|---|---|---|---|---|---|
| dp01 | 0.167 | 19.76% | 19.76% | 19.76% | 19.76% | 19.76% | 19.76% | 19.76% | 19.76% | 19.76% | 19.76% | 19.76% | 19.76% | 19.76% | 19.76% | 19.76% |
| dp02 | 0.284 | 15.49% | 15.49% | 19.01% | 19.01% | 19.01% | 15.49% | 15.49% | 19.01% | 19.01% | 19.01% | 15.49% | 15.49% | 19.01% | 19.01% | 19.01% |
| dp03 | 0.367 | 0.82% | 0.82% | 4.63% | 0.82% | 3.54% | 0.82% | 0.82% | 4.63% | 0.82% | 3.54% | 0.82% | 0.82% | 4.63% | 0.82% | 3.54% |
| dp04 | 0.505 | 14.85% | 14.85% | 20.79% | 16.83% | 16.83% | 14.85% | 14.85% | 20.79% | 16.83% | 16.83% | 14.85% | 14.85% | 20.79% | 16.83% | 16.83% |
| dp05 | 0.531 | 15.25% | 15.25% | 19.02% | 15.25% | 15.25% | 15.25% | 15.25% | 19.02% | 15.25% | 15.25% | 15.25% | 15.25% | 19.02% | 15.25% | 15.25% |
| dp06 | 0.570 | 12.28% | 12.28% | 15.79% | 14.04% | 14.04% | 12.28% | 12.28% | 15.79% | 14.04% | 14.04% | 10.53% | 12.28% | 15.79% | 12.28% | 12.28% |
| dp07 | 1.780 | 6.74% | 6.74% | 8.43% | 7.30% | 7.30% | 6.74% | 6.74% | 8.43% | 7.30% | 7.30% | 5.06% | 5.62% | 6.74% | 5.62% | 6.18% |
| dp08 | 0.798 | 0.25% | 0.25% | 0.25% | 0.25% | 0.25% | 0.25% | 0.25% | 0.25% | 0.25% | 0.25% | 0.25% | 0.25% | 0.25% | 0.25% | 0.25% |
| dp09 | 3.974 | 6.61% | 6.57% | 9.08% | 7.04% | 6.91% | 6.59% | 6.57% | 9.08% | 7.03% | 6.89% | 5.99% | 6.04% | 8.41% | 6.47% | 6.30% |
| Average | | 10.23% | 10.22% | 12.97% | 11.15% | 11.43% | 10.23% | 10.22% | 12.97% | 11.14% | 11.43% | 9.78% | 10.04% | 12.71% | 10.70% | 11.05% |

**Armand Two-Phase Friction Multiplier Suite**

| Pressure Tap | Measured | 31 | 32 | 33 | 34 | 35 | 36 | 37 | 38 | 39 | 40 | 41 | 42 | 43 | 44 | 45 |
|---|---|---|---|---|---|---|---|---|---|---|---|---|---|---|---|---|
| dp01 | 0.167 | 19.76% | 19.76% | 19.76% | 19.76% | 19.76% | 19.76% | 19.76% | 19.76% | 19.76% | 19.76% | 19.76% | 19.76% | 19.76% | 19.76% | 19.76% |
| dp02 | 0.284 | 15.49% | 15.49% | 15.49% | 15.49% | 15.49% | 15.49% | 15.49% | 15.49% | 15.49% | 15.49% | 15.49% | 15.49% | 15.49% | 15.49% | 15.49% |
| dp03 | 0.367 | 3.54% | 3.54% | 0.82% | 3.54% | 3.54% | 3.54% | 3.54% | 0.82% | 3.54% | 3.54% | 3.54% | 3.54% | 0.82% | 3.54% | 3.54% |
| dp04 | 0.505 | 14.85% | 14.85% | 18.81% | 14.85% | 14.85% | 14.85% | 14.85% | 18.81% | 14.85% | 14.85% | 14.85% | 14.85% | 18.81% | 14.85% | 14.85% |
| dp05 | 0.531 | 11.49% | 13.37% | 17.14% | 15.25% | 13.37% | 13.37% | 13.37% | 17.14% | 15.25% | 13.37% | 11.49% | 13.37% | 17.14% | 15.25% | 13.37% |
| dp06 | 0.570 | 12.28% | 10.53% | 14.04% | 12.28% | 12.28% | 10.53% | 12.28% | 14.04% | 12.28% | 12.28% | 12.28% | 10.53% | 14.04% | 10.53% | 12.28% |
| dp07 | 1.780 | 6.74% | 6.18% | 7.30% | 6.74% | 6.74% | 6.18% | 6.18% | 7.30% | 6.74% | 6.74% | 5.62% | 5.06% | 6.18% | 5.06% | 5.62% |
| dp08 | 0.798 | 0.25% | 0.25% | 0.25% | 0.25% | 0.25% | 0.25% | 0.25% | 0.25% | 0.25% | 0.25% | 0.25% | 0.25% | 0.25% | 0.25% | 0.25% |
| dp09 | 3.974 | 5.94% | 5.89% | 7.77% | 6.29% | 6.23% | 5.92% | 5.89% | 7.76% | 6.28% | 6.21% | 5.33% | 5.37% | 7.12% | 5.74% | 5.64% |
| Average | | 10.04% | 9.99% | 11.26% | 10.50% | 10.28% | 9.99% | 10.18% | 11.26% | 10.50% | 10.28% | 9.85% | 9.80% | 11.07% | 10.05% | 10.09% |

**4.10.4 P60007 and P60015, Total Pressure Drop**

These two test cases reflect the same trends and are therefore presented together. The darker
blue cells are where the absolute relative differences are less than 3% and less than 8% for the
P60007 and P60015 test cases respectively. As expected, both test cases strongly indicate the
selection of a two-phase multiplier and void/quality relationship are the most significant
contributor to differences between computed and measured pressure drops. The subcooled
boiling model choice appears to be a weak contributor as expected for higher powers and mass
flow rates seen in these test cases. The EPRI two-phase friction multiplier suite result in the
smallest absolute relative difference for both P60007 and P60015 test cases. All three two-
phase multiplier suites reflect that the homogenous bulk void/quality relationship provides the
better results regardless of the subcooled boiling model selected.

**Table 4.10: P60007 Evaluation for Total Pressure Drop of Measured Value 8.396 psi**

| EPRI Two-Phase Friction Multiplier Suite | | | | | | | | | | | | | | |
|---|---|---|---|---|---|---|---|---|---|---|---|---|---|---|
| 1 | 2 | 3 | 4 | 5 | 6 | 7 | 8 | 9 | 10 | 11 | 12 | 13 | 14 | 15 |
| Total Pressure Drop (psi) | | | | | | | | | | | | | | |
| 7.945 | 7.918 | 8.164 | 7.894 | 7.847 | 7.959 | 7.931 | 8.178 | 7.907 | 7.860 | 7.929 | 7.898 | 8.145 | 7.873 | 7.828 |
| Absoulte Relative Difference | | | | | | | | | | | | | | |
| 5.37% | 5.69% | 2.76% | 5.98% | 6.54% | 5.20% | 5.53% | 2.59% | 5.82% | 6.39% | 5.56% | 5.94% | 2.99% | 6.22% | 6.77% |
| Difference | | | | | | | | | | | | | | |
| -0.4508 | -0.4778 | -0.2318 | -0.5020 | -0.5495 | -0.4369 | -0.4646 | -0.2178 | -0.4888 | -0.5363 | -0.4666 | -0.4983 | -0.2508 | -0.5226 | -0.5684 |
| **Homogenous Two-Phase Friction Multiplier Suite** | | | | | | | | | | | | | | |
| 16 | 17 | 18 | 19 | 20 | 21 | 22 | 23 | 24 | 25 | 26 | 27 | 28 | 29 | 30 |
| Total Pressure Drop (psi) | | | | | | | | | | | | | | |
| 7.4703 | 7.4222 | 7.8080 | 7.3834 | 7.3163 | 7.4748 | 7.4258 | 7.8152 | 7.3867 | 7.3192 | 7.4756 | 7.4251 | 7.8087 | 7.3865 | 7.3203 |
| Absoulte Relative Difference | | | | | | | | | | | | | | |
| 11.03% | 11.60% | 7.00% | 12.06% | 12.86% | 10.97% | 11.56% | 6.92% | 12.02% | 12.82% | 10.96% | 11.56% | 7.00% | 12.02% | 12.81% |
| Difference | | | | | | | | | | | | | | |
| -0.9257 | -0.9738 | -0.5880 | -1.0126 | -1.0797 | -0.9212 | -0.9702 | -0.5808 | -1.0093 | -1.0768 | -0.9204 | -0.9709 | -0.5873 | -1.0095 | -1.0757 |
| **Armand Two-Phase Friction Multiplier Suite** | | | | | | | | | | | | | | |
| 31 | 32 | 33 | 34 | 35 | 36 | 37 | 38 | 39 | 40 | 41 | 42 | 43 | 44 | 45 |
| Total Pressure Drop (psi) | | | | | | | | | | | | | | |
| 7.690 | 7.625 | 8.140 | 7.573 | 7.488 | 7.699 | 7.632 | 8.153 | 7.580 | 7.495 | 7.688 | 7.621 | 8.131 | 7.570 | 7.486 |
| Absoulte Relative Difference | | | | | | | | | | | | | | |
| 8.40% | 9.19% | 3.05% | 9.80% | 10.81% | 8.30% | 9.10% | 2.89% | 9.72% | 10.73% | 8.44% | 9.23% | 3.16% | 9.84% | 10.84% |
| Difference | | | | | | | | | | | | | | |
| -0.706 | -0.771 | -0.256 | -0.823 | -0.908 | -0.697 | -0.764 | -0.243 | -0.816 | -0.901 | -0.708 | -0.775 | -0.265 | -0.826 | -0.910 |

| Table 4.11: P60015 Evaluation for Total Pressure Drop of Measured Value 16.530 psi | | | | | | | | | | | | | | |
|---|---|---|---|---|---|---|---|---|---|---|---|---|---|---|
| **EPRI Two-Phase Friction Multiplier Suite** | | | | | | | | | | | | | | |
| 1 | 2 | 3 | 4 | 5 | 6 | 7 | 8 | 9 | 10 | 11 | 12 | 13 | 14 | 15 |
| **Total Pressure Drop (psi)** | | | | | | | | | | | | | | |
| 14.093 | 13.824 | 15.432 | 13.686 | 13.457 | 14.164 | 13.893 | 15.515 | 13.754 | 13.522 | 14.012 | 13.737 | 15.335 | 13.600 | 13.375 |
| **Absoulte Relative Difference** | | | | | | | | | | | | | | |
| 14.74% | 16.37% | 6.64% | 17.21% | 18.59% | 14.31% | 15.95% | 6.14% | 16.79% | 18.20% | 15.23% | 16.90% | 7.23% | 17.72% | 19.09% |
| **Difference** | | | | | | | | | | | | | | |
| -2.437 | -2.706 | -1.098 | -2.844 | -3.073 | -2.366 | -2.637 | -1.015 | -2.776 | -3.008 | -2.518 | -2.793 | -1.195 | -2.930 | -3.155 |
| **Homogenous Two-Phase Friction Multiplier Suite** | | | | | | | | | | | | | | |
| 16 | 17 | 18 | 19 | 20 | 21 | 22 | 23 | 24 | 25 | 26 | 27 | 28 | 29 | 30 |
| **Total Pressure Drop (psi)** | | | | | | | | | | | | | | |
| 12.952 | 12.559 | 14.843 | 12.344 | 11.989 | 13.002 | 12.606 | 14.916 | 12.388 | 12.027 | 12.910 | 12.516 | 14.777 | 12.303 | 11.953 |
| **Absoulte Relative Difference** | | | | | | | | | | | | | | |
| 21.65% | 24.02% | 10.20% | 25.32% | 27.47% | 21.34% | 23.74% | 9.77% | 25.06% | 27.24% | 21.90% | 24.29% | 10.60% | 25.57% | 27.69% |
| **Difference** | | | | | | | | | | | | | | |
| -3.5781 | -3.9707 | -1.6866 | -4.1857 | -4.5410 | -3.5280 | -3.9241 | -1.6143 | -4.1421 | -4.5028 | -3.6205 | -4.0144 | -1.7526 | -4.2266 | -4.5774 |
| **Armand Two-Phase Friction Multiplier Suite** | | | | | | | | | | | | | | |
| 31 | 32 | 33 | 34 | 35 | 36 | 37 | 38 | 39 | 40 | 41 | 42 | 43 | 44 | 45 |
| **Total Pressure Drop (psi)** | | | | | | | | | | | | | | |
| 14.144 | 13.466 | 17.797 | 13.102 | 12.533 | 14.212 | 13.526 | 17.911 | 13.159 | 12.582 | 14.079 | 13.404 | 17.697 | 13.043 | 12.480 |
| **Absoulte Relative Difference** | | | | | | | | | | | | | | |
| 14.44% | 18.54% | 7.67% | 20.74% | 24.18% | 14.02% | 18.17% | 8.35% | 20.39% | 23.89% | 14.83% | 18.91% | 7.06% | 21.09% | 24.50% |
| **Difference** | | | | | | | | | | | | | | |
| -2.386 | -3.064 | 1.267 | -3.428 | -3.997 | -2.318 | -3.004 | 1.381 | -3.371 | -3.948 | -2.451 | -3.126 | 1.167 | -3.487 | -4.050 |

## 4.10.5 P60007 and P60015, Pressure Drop for the Pressure Drop Identifiers

The darker blue cells specify where absolute relative differences are less than 3% and less than 8% for the P60007 and P60015 test cases respectively. Everything previously mentioned for total pressure drop for test cases P60007 and P60015 are observed in the evaluation of pressure drop for individual pressure drop identifiers. The EPRI two-phase friction multiplier suite indicates a reduction in absolute relative difference in the predicted values compared to the measured data for a majority of the pressure drop identifiers. The column averages reveal the EPRI two-phase friction multiplier match the measured data better on average. The subcooled boiling models exhibit a minor contribution, and the EPRI two-phase friction multiplier in combination with the homogenous bulk void/quality relationship will yield better results for pressure drop for operating conditions seen in test cases P60007 and P60015.

## Table 4.12: P60007, Absolute Relative Difference for Pressure Drop at Pressure Drop Identifiers

### EPRI Two-Phase Friction Multiplier Suite

| Pressure Tap | Measured | 1 | 2 | 3 | 4 | 5 | 6 | 7 | 8 | 9 | 10 | 11 | 12 | 13 | 14 | 15 |
|---|---|---|---|---|---|---|---|---|---|---|---|---|---|---|---|---|
| dp01 | 0.811 | 2.561% | 3.794% | 4.840% | 5.028% | 6.261% | 2.561% | 3.794% | 4.840% | 5.028% | 6.261% | 2.561% | 3.794% | 4.840% | 5.028% | 6.261% |
| dp02 | 0.972 | 14.587% | 14.587% | 8.413% | 16.646% | 16.646% | 14.587% | 14.587% | 9.442% | 16.646% | 16.646% | 14.587% | 14.587% | 8.413% | 16.646% | 16.646% |
| dp03 | 1.176 | 0.318% | 0.532% | 5.419% | 0.532% | 2.232% | 0.318% | 0.532% | 5.419% | 0.532% | 2.232% | 0.318% | 0.532% | 5.419% | 0.532% | 2.232% |
| dp04 | 1.385 | 10.477% | 11.199% | 6.867% | 11.921% | 12.643% | 11.199% | 11.199% | 6.867% | 12.643% | 12.643% | 10.477% | 11.199% | 6.867% | 11.921% | 12.643% |
| dp05 | 1.314 | 7.918% | 8.679% | 4.113% | 9.440% | 10.201% | 7.918% | 8.679% | 4.874% | 8.679% | 10.201% | 7.918% | 7.918% | 3.352% | 8.679% | 10.201% |
| dp06 | 1.218 | 7.249% | 7.249% | 3.966% | 7.249% | 8.070% | 7.249% | 7.249% | 3.966% | 7.249% | 8.891% | 5.608% | 6.428% | 3.145% | 6.428% | 7.249% |
| dp07 | 3.313 | 5.212% | 5.212% | 3.401% | 5.212% | 5.514% | 4.609% | 4.910% | 2.797% | 4.910% | 5.212% | 5.816% | 6.118% | 4.307% | 6.118% | 6.118% |
| dp08 | 1.197 | 1.384% | 1.384% | 2.220% | 2.220% | 1.384% | 1.384% | 1.384% | 1.384% | 1.384% | 1.384% | 1.384% | 1.384% | 1.384% | 2.220% | 1.384% |
| dp09 | 8.396 | 5.372% | 5.693% | 2.764% | 5.981% | 6.547% | 5.206% | 5.537% | 2.597% | 5.825% | 6.390% | 5.561% | 5.938% | 2.989% | 6.227% | 6.773% |
| Average | | 6.120% | 6.481% | 4.667% | 7.137% | 7.722% | 6.115% | 6.430% | 4.687% | 6.988% | 7.762% | 6.026% | 6.433% | 4.524% | 7.089% | 7.723% |

### Homogenous Two-Phase Friction Multiplier Suite

| Pressure Tap | Measured | 16 | 17 | 18 | 19 | 20 | 21 | 22 | 23 | 24 | 25 | 26 | 27 | 28 | 29 | 30 |
|---|---|---|---|---|---|---|---|---|---|---|---|---|---|---|---|---|
| dp01 | 0.811 | 9.961% | 12.428% | 0.094% | 13.662% | 14.895% | 9.961% | 12.428% | 0.094% | 13.662% | 14.895% | 9.961% | 12.428% | 0.094% | 13.662% | 14.895% |
| dp02 | 0.972 | 20.762% | 21.791% | 13.558% | 22.820% | 24.878% | 21.791% | 21.791% | 13.558% | 22.820% | 24.878% | 20.762% | 21.791% | 13.558% | 22.820% | 24.878% |
| dp03 | 1.176 | 10.734% | 12.434% | 2.232% | 13.284% | 14.985% | 10.734% | 12.434% | 2.232% | 13.284% | 14.985% | 10.734% | 12.434% | 2.232% | 13.284% | 14.985% |
| dp04 | 1.385 | 20.584% | 21.306% | 14.086% | 22.028% | 23.472% | 20.584% | 21.306% | 14.086% | 22.028% | 23.472% | 20.584% | 20.584% | 13.364% | 22.028% | 23.472% |
| dp05 | 1.314 | 15.528% | 16.289% | 9.440% | 17.050% | 19.333% | 16.289% | 17.050% | 10.201% | 17.811% | 19.333% | 14.767% | 17.050% | 10.201% | 17.050% | 18.572% |
| dp06 | 1.218 | 12.995% | 12.995% | 8.891% | 13.816% | 13.816% | 12.995% | 12.995% | 8.891% | 12.174% | 14.636% | 12.174% | 11.353% | 7.249% | 12.174% | 12.995% |
| dp07 | 3.313 | 8.533% | 8.835% | 6.420% | 8.835% | 8.835% | 7.929% | 8.231% | 5.816% | 8.533% | 8.835% | 8.533% | 8.533% | 6.420% | 8.835% | 9.137% |
| dp08 | 1.197 | 1.384% | 1.384% | 1.384% | 2.220% | 1.384% | 2.220% | 1.384% | 1.384% | 1.384% | 1.384% | 1.384% | 1.384% | 1.384% | 1.384% | 1.384% |
| dp09 | 8.396 | 11.028% | 11.601% | 7.006% | 12.063% | 12.863% | 10.975% | 11.558% | 6.920% | 12.023% | 12.827% | 10.966% | 11.567% | 6.998% | 12.026% | 12.814% |
| Average | | 12.390% | 13.229% | 7.012% | 13.975% | 14.940% | 12.609% | 13.242% | 7.020% | 13.929% | 15.027% | 12.207% | 13.014% | 6.834% | 13.696% | 14.792% |

### Armand Two-Phase Friction Multiplier Suite

| Pressure Tap | Measured | 31 | 32 | 33 | 34 | 35 | 36 | 37 | 38 | 39 | 40 | 41 | 42 | 43 | 44 | 45 |
|---|---|---|---|---|---|---|---|---|---|---|---|---|---|---|---|---|
| dp01 | 0.811 | 6.26% | 8.73% | 6.07% | 9.96% | 12.43% | 6.26% | 8.73% | 6.07% | 9.96% | 12.43% | 6.26% | 8.73% | 6.07% | 9.96% | 12.43% |
| dp02 | 0.972 | 17.67% | 19.73% | 8.41% | 19.73% | 22.82% | 17.67% | 19.73% | 8.41% | 19.73% | 22.82% | 17.67% | 19.73% | 8.41% | 19.73% | 22.82% |
| dp03 | 1.176 | 4.78% | 6.48% | 7.12% | 8.18% | 10.73% | 4.78% | 6.48% | 7.12% | 8.18% | 10.73% | 4.78% | 6.48% | 7.12% | 8.18% | 10.73% |
| dp04 | 1.385 | 15.53% | 16.97% | 6.14% | 17.70% | 19.86% | 15.53% | 16.97% | 6.87% | 18.42% | 20.58% | 15.53% | 16.97% | 6.14% | 17.70% | 19.86% |
| dp05 | 1.314 | 12.48% | 13.24% | 4.87% | 14.77% | 16.29% | 12.48% | 14.01% | 4.87% | 14.01% | 16.29% | 11.72% | 13.24% | 4.11% | 14.01% | 16.29% |
| dp06 | 1.218 | 10.53% | 11.35% | 5.61% | 11.35% | 12.17% | 11.35% | 11.35% | 5.61% | 12.17% | 12.17% | 9.71% | 9.71% | 4.79% | 10.53% | 10.53% |
| dp07 | 3.313 | 7.33% | 7.63% | 4.91% | 7.93% | 7.93% | 7.02% | 7.33% | 4.31% | 7.63% | 7.33% | 7.63% | 7.93% | 5.51% | 8.23% | 7.93% |
| dp08 | 1.197 | 1.38% | 2.22% | 1.38% | 1.38% | 1.38% | 1.38% | 1.38% | 1.38% | 1.38% | 1.38% | 2.22% | 1.38% | 1.38% | 1.38% | 1.38% |
| dp09 | 8.396 | 8.41% | 9.19% | 3.06% | 9.80% | 10.81% | 8.31% | 9.10% | 2.89% | 9.72% | 10.74% | 8.44% | 9.23% | 3.16% | 9.84% | 10.85% |
| Average | | 9.38% | 10.62% | 5.29% | 11.20% | 12.72% | 9.42% | 10.57% | 5.28% | 11.25% | 12.81% | 9.24% | 10.38% | 5.19% | 11.06% | 12.54% |

## Table 4.13: P60015, Absolute Relative Difference for Pressure Drop at Pressure Drop Identifiers

### EPRI Two-Phase Friction Multiplier Suite

| Pressure Tap | Measured | 1 | 2 | 3 | 4 | 5 | 6 | 7 | 8 | 9 | 10 | 11 | 12 | 13 | 14 | 15 |
|---|---|---|---|---|---|---|---|---|---|---|---|---|---|---|---|---|
| dp01 | 2.165 | 20.55% | 23.79% | 7.16% | 25.17% | 27.02% | 20.55% | 23.79% | 7.16% | 25.17% | 27.02% | 20.55% | 23.79% | 7.16% | 25.17% | 27.02% |
| dp02 | 2.466 | 28.22% | 31.06% | 17.27% | 31.87% | 33.50% | 28.22% | 31.06% | 17.27% | 31.87% | 33.50% | 28.22% | 31.06% | 17.27% | 31.87% | 33.50% |
| dp03 | 2.804 | 14.41% | 16.90% | 3.00% | 17.97% | 19.40% | 14.41% | 16.90% | 3.00% | 17.97% | 19.40% | 14.41% | 16.90% | 3.00% | 17.97% | 19.40% |
| dp04 | 3.040 | 19.08% | 21.71% | 8.55% | 22.04% | 23.68% | 19.08% | 21.71% | 8.88% | 22.37% | 23.68% | 19.08% | 21.71% | 8.55% | 22.04% | 23.68% |
| dp05 | 2.949 | 20.31% | 22.35% | 10.14% | 23.70% | 25.40% | 20.65% | 22.69% | 10.14% | 23.70% | 25.74% | 19.97% | 22.01% | 9.80% | 23.36% | 25.06% |
| dp06 | 2.524 | 17.19% | 18.78% | 8.48% | 19.97% | 21.95% | 17.19% | 18.38% | 8.48% | 19.57% | 21.95% | 16.80% | 18.38% | 8.08% | 19.57% | 21.95% |
| dp07 | 5.978 | 9.67% | 10.51% | 2.98% | 11.51% | 13.01% | 8.67% | 9.50% | 1.64% | 10.34% | 12.01% | 10.51% | 11.68% | 4.15% | 12.51% | 14.02% |
| dp08 | 1.520 | 2.63% | 3.29% | 2.63% | 2.63% | 2.63% | 1.32% | 1.97% | 1.32% | 2.63% | 1.97% | 5.26% | 4.61% | 4.61% | 5.26% | 4.61% |
| dp09 | 16.530 | 14.74% | 16.37% | 6.64% | 17.21% | 18.59% | 14.31% | 15.95% | 6.14% | 16.79% | 18.20% | 15.23% | 16.90% | 7.23% | 17.72% | 19.09% |
| Average | | 16.31% | 18.31% | 7.43% | 19.12% | 20.58% | 16.04% | 18.00% | 7.11% | 18.94% | 20.39% | 16.67% | 18.56% | 7.76% | 19.50% | 20.92% |

### Homogenous Two-Phase Friction Multiplier Suite

| Pressure Tap | Measured | 16 | 17 | 18 | 19 | 20 | 21 | 22 | 23 | 24 | 25 | 26 | 27 | 28 | 29 | 30 |
|---|---|---|---|---|---|---|---|---|---|---|---|---|---|---|---|---|
| dp01 | 2.165 | 26.56% | 30.72% | 9.47% | 32.10% | 34.87% | 26.56% | 30.72% | 9.47% | 32.10% | 34.87% | 26.56% | 30.72% | 9.47% | 32.10% | 34.87% |
| dp02 | 2.466 | 33.90% | 37.55% | 19.71% | 38.77% | 41.61% | 33.90% | 37.55% | 19.71% | 38.77% | 41.61% | 33.90% | 37.55% | 19.71% | 38.77% | 41.61% |
| dp03 | 2.804 | 24.39% | 28.32% | 6.92% | 30.10% | 32.60% | 24.39% | 28.32% | 6.92% | 30.10% | 32.60% | 24.39% | 28.32% | 6.92% | 30.10% | 32.60% |
| dp04 | 3.040 | 27.96% | 31.91% | 12.50% | 33.22% | 36.18% | 28.29% | 31.91% | 12.83% | 33.22% | 36.18% | 27.96% | 31.91% | 12.50% | 33.22% | 36.18% |
| dp05 | 2.949 | 28.45% | 31.16% | 14.21% | 32.86% | 35.91% | 28.45% | 31.50% | 14.21% | 33.20% | 35.91% | 28.11% | 31.16% | 13.87% | 32.52% | 35.57% |
| dp06 | 2.524 | 24.33% | 26.31% | 12.84% | 27.89% | 30.67% | 24.33% | 26.70% | 12.84% | 27.89% | 31.46% | 23.93% | 25.52% | 12.04% | 27.50% | 30.67% |
| dp07 | 5.978 | 15.52% | 16.69% | 6.83% | 18.03% | 19.87% | 14.85% | 16.03% | 5.65% | 17.20% | 19.37% | 15.86% | 17.03% | 7.66% | 18.37% | 20.04% |
| dp08 | 1.520 | 2.63% | 3.29% | 3.29% | 3.29% | 2.63% | 1.32% | 1.97% | 1.97% | 2.63% | 1.97% | 4.61% | 4.61% | 4.61% | 5.26% | 5.26% |
| dp09 | 16.530 | 21.65% | 24.02% | 10.20% | 25.32% | 27.47% | 21.34% | 23.74% | 9.77% | 25.06% | 27.24% | 21.90% | 24.29% | 10.60% | 25.57% | 27.69% |
| Average | | 22.82% | 25.55% | 10.66% | 26.84% | 29.09% | 22.60% | 25.38% | 10.37% | 26.69% | 29.02% | 23.02% | 25.68% | 10.82% | 27.05% | 29.39% |

### Armand Two-Phase Friction Multiplier Suite

| Pressure Tap | Measured | 31 | 32 | 33 | 34 | 35 | 36 | 37 | 38 | 39 | 40 | 41 | 42 | 43 | 44 | 45 |
|---|---|---|---|---|---|---|---|---|---|---|---|---|---|---|---|---|
| dp01 | 2.165 | 17.32% | 24.25% | 16.86% | 27.02% | 31.64% | 17.32% | 24.25% | 16.86% | 27.02% | 31.64% | 17.32% | 24.25% | 16.86% | 27.02% | 31.64% |
| dp02 | 2.466 | 26.20% | 31.47% | 0.97% | 34.31% | 38.77% | 26.20% | 31.47% | 1.38% | 34.31% | 38.77% | 26.20% | 31.47% | 1.38% | 34.31% | 38.77% |
| dp03 | 2.804 | 9.06% | 17.97% | 35.16% | 21.18% | 27.25% | 9.06% | 17.97% | 34.81% | 21.18% | 27.25% | 9.06% | 17.97% | 35.16% | 21.18% | 27.25% |
| dp04 | 3.040 | 16.78% | 23.36% | 18.09% | 26.64% | 31.91% | 16.78% | 23.36% | 18.42% | 26.97% | 32.24% | 16.45% | 23.36% | 18.09% | 26.64% | 31.91% |
| dp05 | 2.949 | 21.33% | 25.74% | 4.10% | 28.45% | 32.18% | 21.33% | 26.08% | 3.76% | 28.45% | 32.18% | 21.33% | 25.40% | 4.10% | 28.11% | 32.18% |
| dp06 | 2.524 | 19.18% | 21.55% | 4.52% | 23.93% | 27.50% | 19.57% | 21.55% | 3.72% | 23.93% | 27.50% | 19.18% | 21.55% | 4.12% | 23.53% | 27.10% |
| dp07 | 5.978 | 12.01% | 13.35% | 1.64% | 15.02% | 17.20% | 11.17% | 12.51% | 0.20% | 14.02% | 16.53% | 12.68% | 14.19% | 2.98% | 15.69% | 17.53% |
| dp08 | 1.520 | 2.63% | 3.29% | 3.29% | 3.29% | 2.63% | 1.32% | 1.97% | 2.63% | 2.63% | 1.97% | 4.61% | 5.26% | 4.61% | 5.26% | 5.26% |
| dp09 | 16.530 | 14.44% | 18.54% | 7.67% | 20.74% | 24.18% | 14.02% | 18.17% | 8.35% | 20.39% | 23.89% | 14.83% | 18.91% | 7.06% | 21.09% | 24.50% |
| Average | | 15.44% | 19.95% | 10.26% | 22.29% | 25.99% | 15.20% | 19.70% | 10.02% | 22.10% | 25.77% | 15.74% | 20.26% | 10.48% | 22.54% | 26.24% |

### 4.10.6 Result of the Correlations Study for Pressure Drop

The EPRI two-phase friction multiplier correlation yields the better results for pressure drop. Also, all three test cases reveal that the subcooled boiling models weakly contribute to the results for these test conditions. P60001 does indicate a slight influence on the results considering the void/quality relationship, but this test case exhibits lower power and mass flow rates than nominal BWR operating conditions. Observations of the P60007 and P60015 test cases indicate that the homogenous model for void/quality relationship yield the better results for pressure drop with increases in power and mass flow. The P60015 test case is more representative of nominal BWR conditions with a slightly higher mass flow rate. The *set 8* of correlations yields the better results for pressure drop and will be compared to the COBRA-CTF results.

| Table 4.14: COBRA-EN Results for Suite of Correlations, Set 8 | | | | | | | |
|---|---|---|---|---|---|---|---|
| **Two Phase Friction Multiplier** | | | **Subcooled Boiling** | **Bulk Void/Quality Relationship** | | | |
| EPRI | | | Levy | Homogeneous | | | |
| **Total Pressure Drop (psi)** | | | | **Absolute Relative Difference in Pressure Drop for Individual Pressure Drop Identifiers** | | | |
| **Measured** | **P60001** | **P60007** | **P60015** | **Identifier** | **P60001** | **P60007** | **P60015** |
| | 3.753 | 8.396 | 16.530 | dp01 | 25.75% | 4.840% | 7.16% |
| **Calculated** | **P60001** | **P60007** | **P60015** | dp02 | 11.97% | 9.442% | 17.27% |
| | 3.974 | 8.178 | 15.515 | dp03 | 6.27% | 5.419% | 3.00% |
| | | | | dp04 | 12.87% | 6.867% | 8.88% |
| | | | | dp05 | 13.37% | 4.874% | 10.14% |
| | | | | dp06 | 12.28% | 3.966% | 8.48% |
| | | | | dp07 | 6.74% | 2.797% | 1.64% |
| | | | | dp08 | 0.25% | 1.384% | 1.32% |
| | | | | dp09 | 5.57% | 2.597% | 6.14% |
| | | | | Average | 10.56% | 4.687% | 7.11% |

**4.10.7  Further Evaluation of the Correlations Study**

The homogenous void/quality relationship is known to over predict the vapor fraction and is typically not recommended when evaluating realistic two-phase flow conditions similar to the conditions observed in BWRs. Also, as noted in, *Nuclear Systems I*, by Tordeas and Kazimi that calculated vapor fraction is higher for the same quality and slip ratio at lower pressures where the density ratio $\rho_v/\rho_l$ is decreased [8].

The goals of this extended correlation study are to choose another set of correlations that provide acceptable code predictions compared to measured data for pressure drop, and exhibit vapor fractions representative of realistic two-phase flow conditions. The original criteria for the correlation study will be observed. There are three observations from the previous correlation study:

1. The choice of two-phase multipliers contributes significantly to differences between predicted and measured data for a majority of the pressure drop identifiers and total pressure drop.

2. The homogenous two-phase friction multiplier suite consistently resulted in a less than desirable comparison of predicted to measured pressures.

3. Subcooled boiling models exhibit a minor contribution to differences in the predicted values.

As a result, different subcooled boiling models will not be considered, and the homogenous two-phase friction factor suite will be omitted. Since benchmark data was not available, the vapor fractions predicted by COBRA-CTF were chosen as the basis for comparison. Vapor fractions at axial positions along the heated assembly for both the EPRI and Armand two-phase friction factor suites for P60001, P60007, and P60015 have been collected. These vapor fractions are plotted with the 1X24 COBRA-CTF results for each test case to determine which set of correlations within COBRA-EN provides the best match. The plots containing the suite of correlations for both the EPRI and Armand two-phase friction factors are practically identical when the same combination of subcooled boiling model and void/quality relationships are applied. For this reason, plots for the equivalent test case Armand two-phase friction factor suite is omitted. *Figures 4.4*, *4.7*, and *4.10* are plots of the entire EPRI two-phase friction factor suite. *Figures 4.5*, *4.8*, and *4.11* are plots of both the EPRI and Armand two-phase friction factor set of correlations that best match the exit vapor fraction from COBRA-CTF. *Figures 4.6*, *4.9*, and *4.12* are plots of the selected set of correlations that best match the COBRA-CTF predicted values for vapor fraction along the entire heated length of the bundle. This last set of plots will be considered for a "best choice" to compare with the COBRA-CTF results.

## 4.10.8 P60001, Plots for the Extended Correlations Study
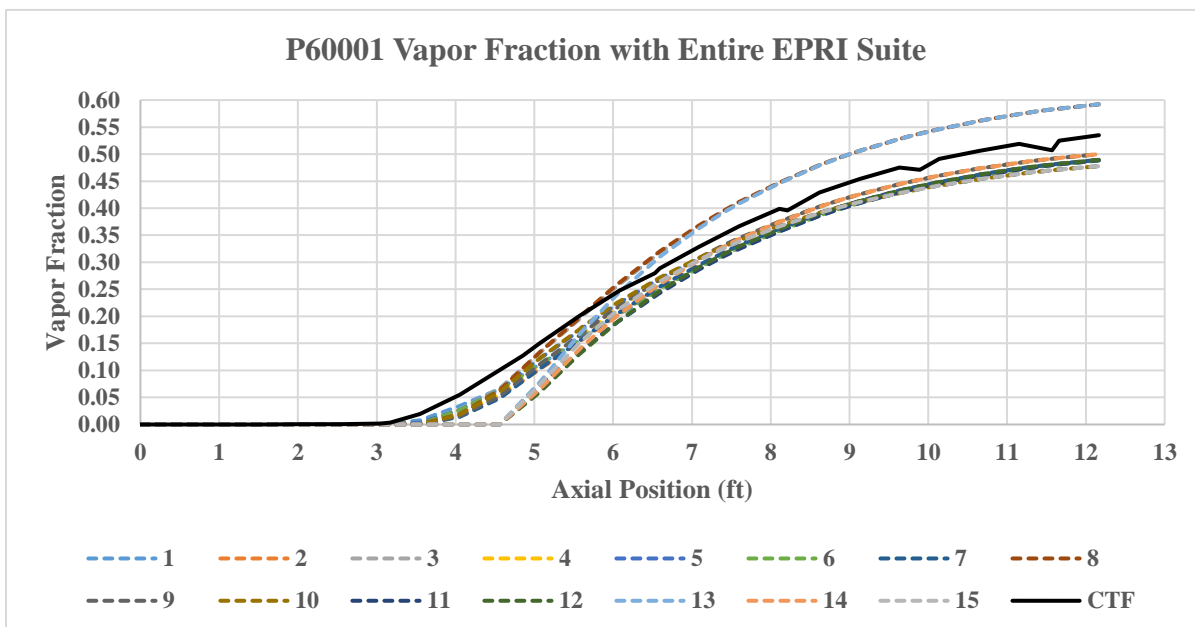


**Figure 4.4:** P60001, COBRA-EN EPRI suite's vapor fraction predictions compared to COBRA-CTF
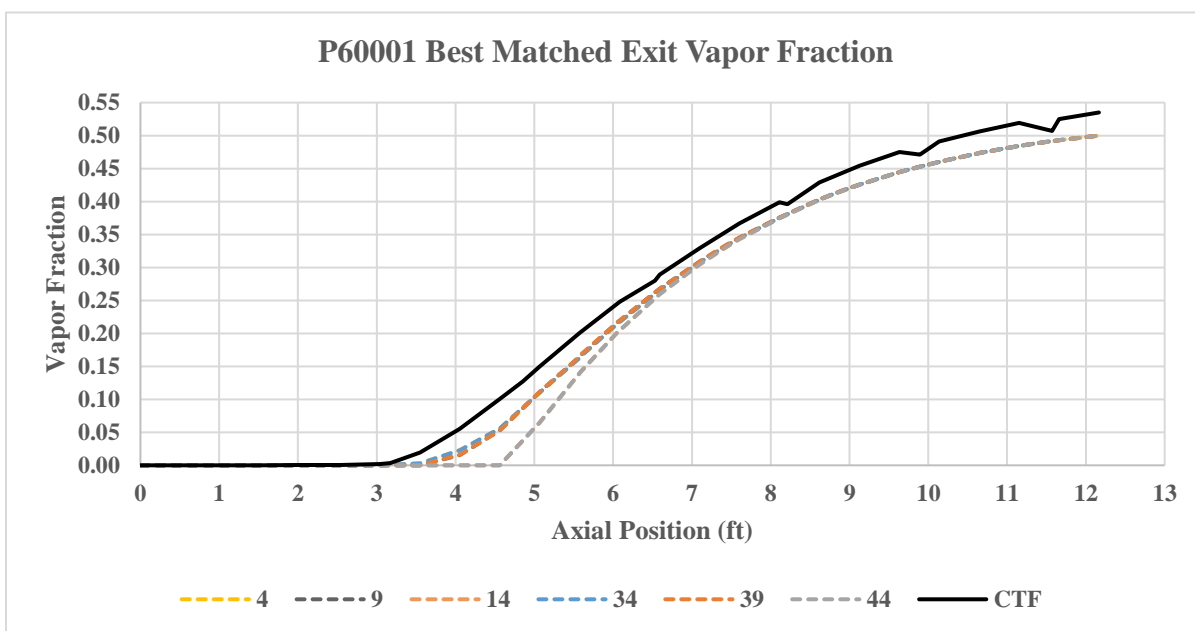


**Figure 4.5:** P60001, Matched COBRA-EN sets compared to COBRA-CTF exit vapor fraction predictions

**P60001 Best Choice Sets for Vapor Fraction**
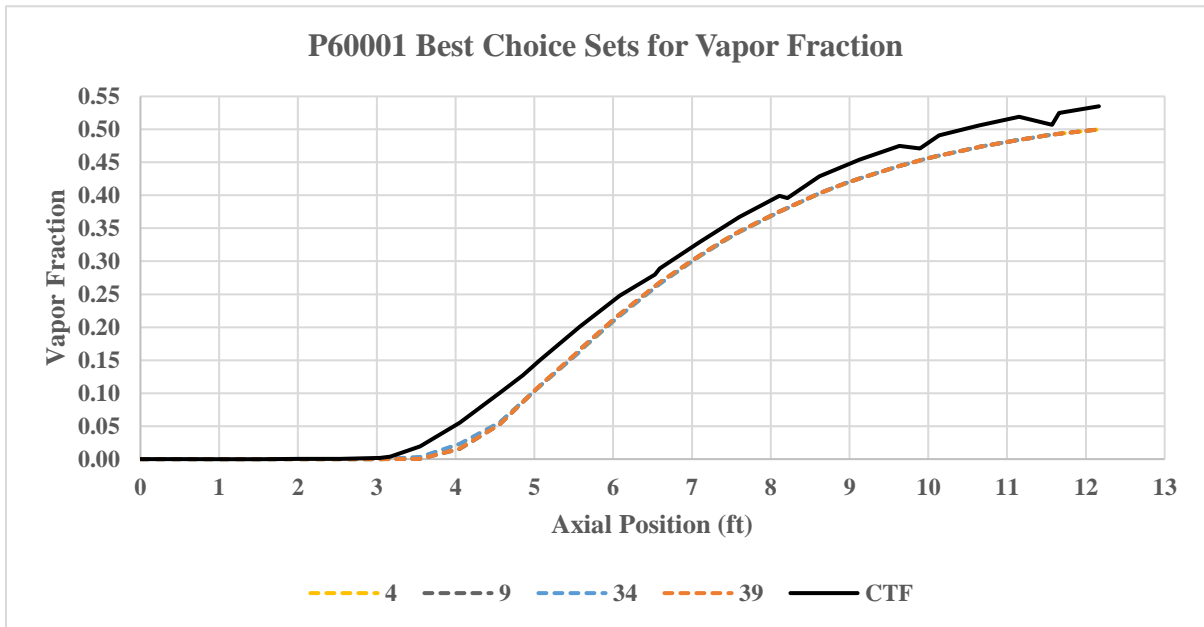


**Figure 4.6:   P60001, Selected COBRA-EN sets compared to COBRA-CTF vapor fraction trends**

Refer to *tables 4.8* and *4.9* for the sets' absolute relative difference in pressure drop for total

and pressure drop identifiers. *Table 4.7* is a legend of the set of correlations seen in *figure 4.5*.

As mentioned before, the plots with the same combination of subcooled boiling model and

void/quality relationships are practically identical, so those curves are on top of each other.

| Table 4.15: P60001, Extended Combinations of Correlations Study | | Subcooled Boiling | Void/Quality Relationship |
|---|---|---|---|
| Two Phase Friction Multiplier | | | |
| EPRI | Armand | | |
| Identifier | | | |
| 4 | 34 | EPRI | Armand-Messena |
| 9 | 39 | Levy | Armand-Messena |

**4.10.9  P60007, Plots for the Extended Correlations Study**
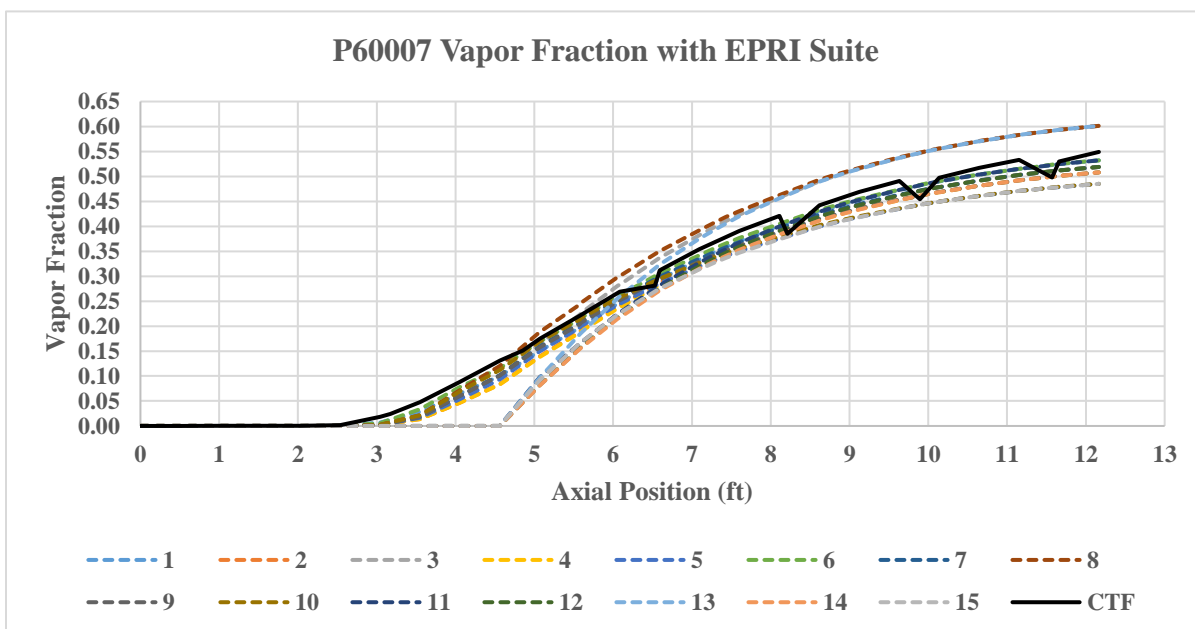


**Figure 4.7:   P60007, COBRA-EN EPRI suite's vapor fraction predictions compared to COBRA-CTF**
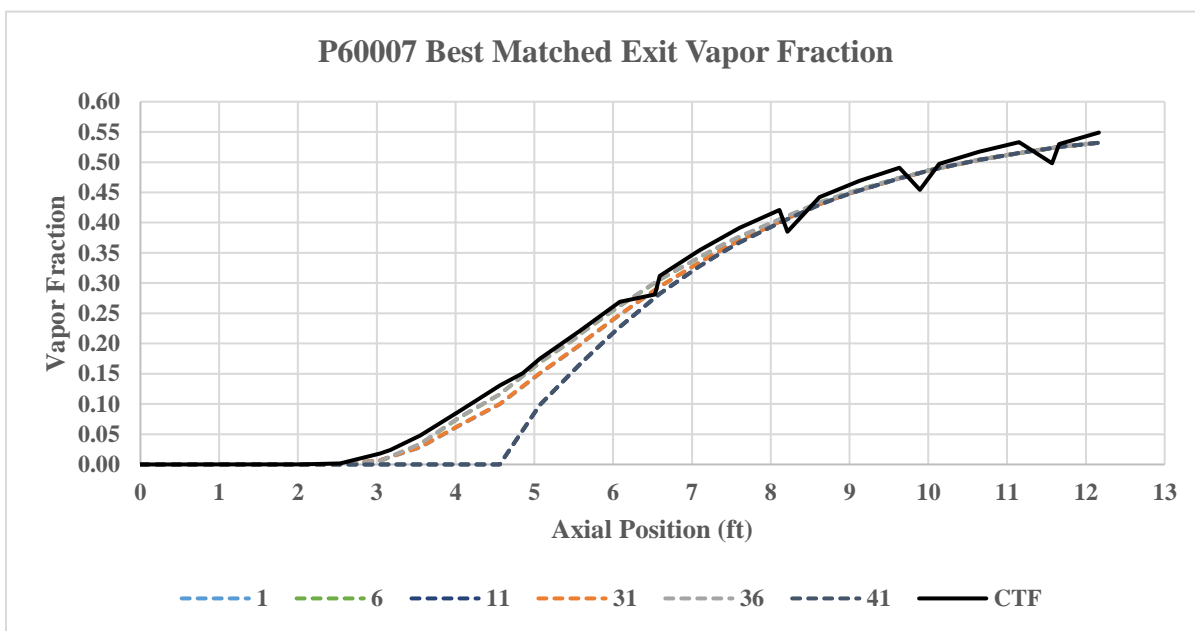


**Figure 4.8:   P60007, Matched COBRA-EN sets compared to COBRA-CTF exit vapor fraction predictions**

**P60007 Best Choice Sets for Vapor Fraction**
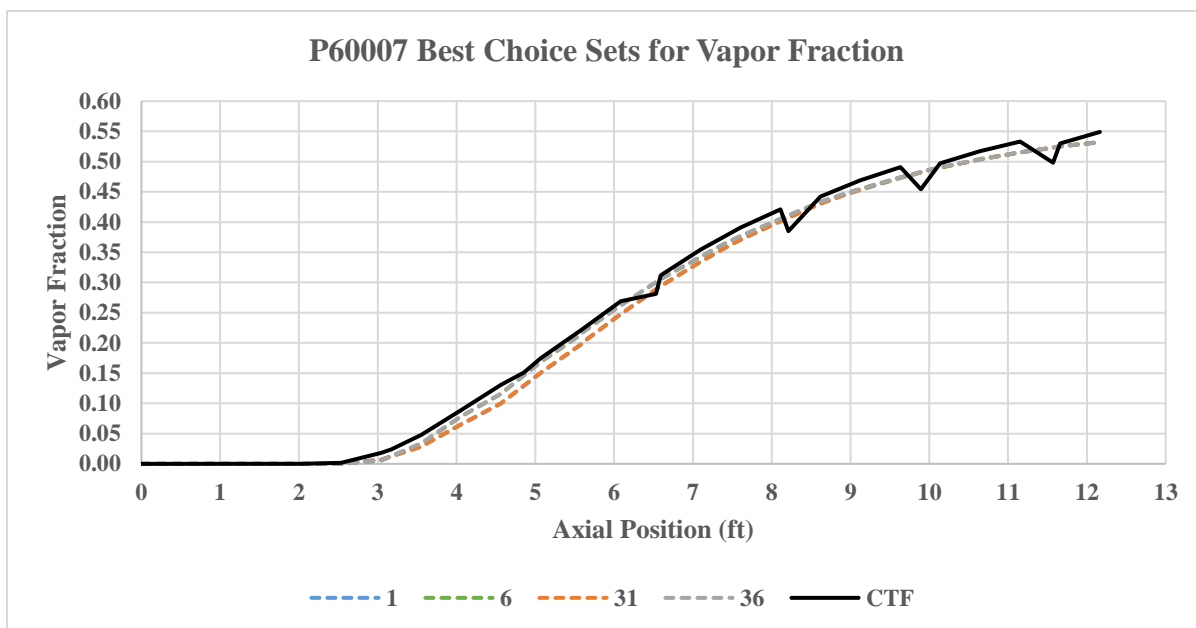


**Figure 4.9: P60007, Selected COBRA-EN sets compared to COBRA-CTF vapor fraction trends**

Refer to *table 4.10* and *4.12* for the sets' absolute relative difference in pressure drop for total

and pressure drop identifiers.

| Table 4.16: P60007, Extended Combinations of Correlations Study | | | |
|---|---|---|---|
| Two Phase Friction Multiplier | | Subcooled Boiling | Void/Quality Relationship |
| EPRI | Armand | | |
| Identifier | | | |
| 1 | 31 | EPRI | EPRI |
| 6 | 36 | Levy | EPRI |

**4.10.10  P60015, Plots for the Extended Correlations Study**
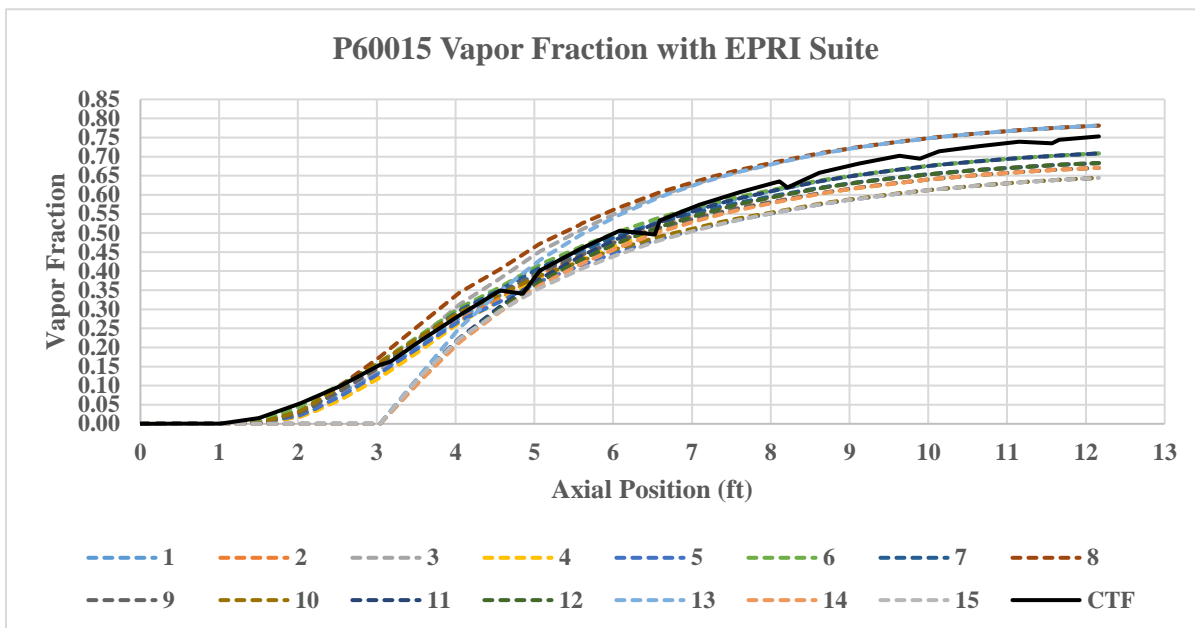


**Figure 4.10: P60015, COBRA-EN EPRI suite's vapor fraction predictions compared to COBRA-CTF**
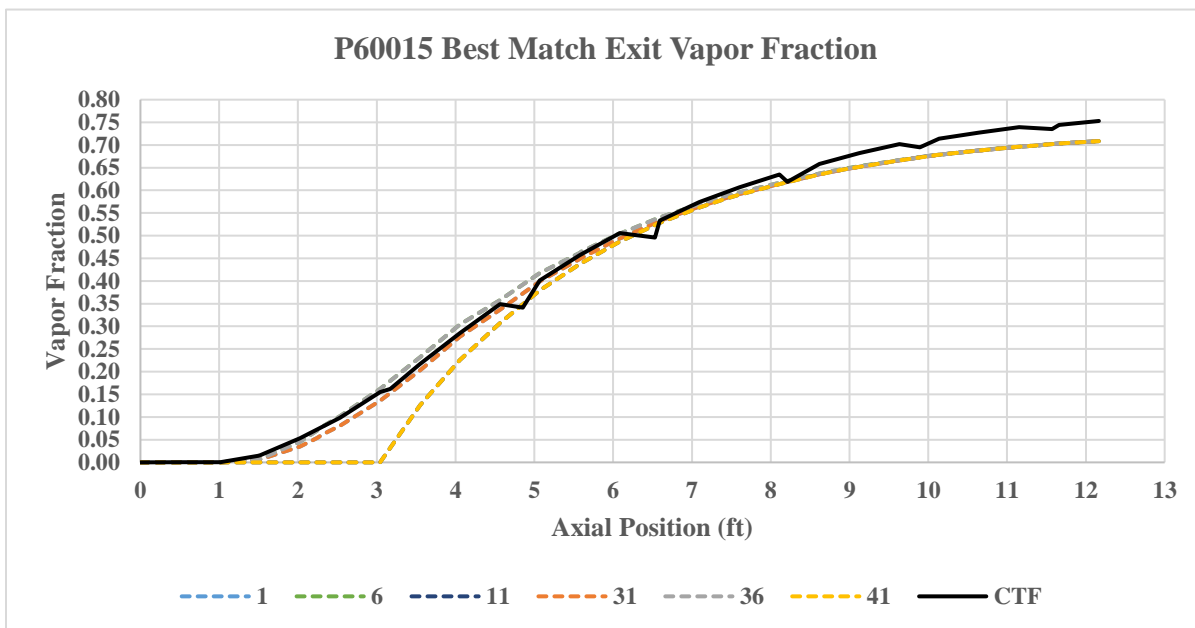


**Figure 4.11: P60015, Matched COBRA-EN sets compared to COBRA-CTF exit vapor fraction predictions**

**P60015 Best Choice Sets for Vapor Fraction**
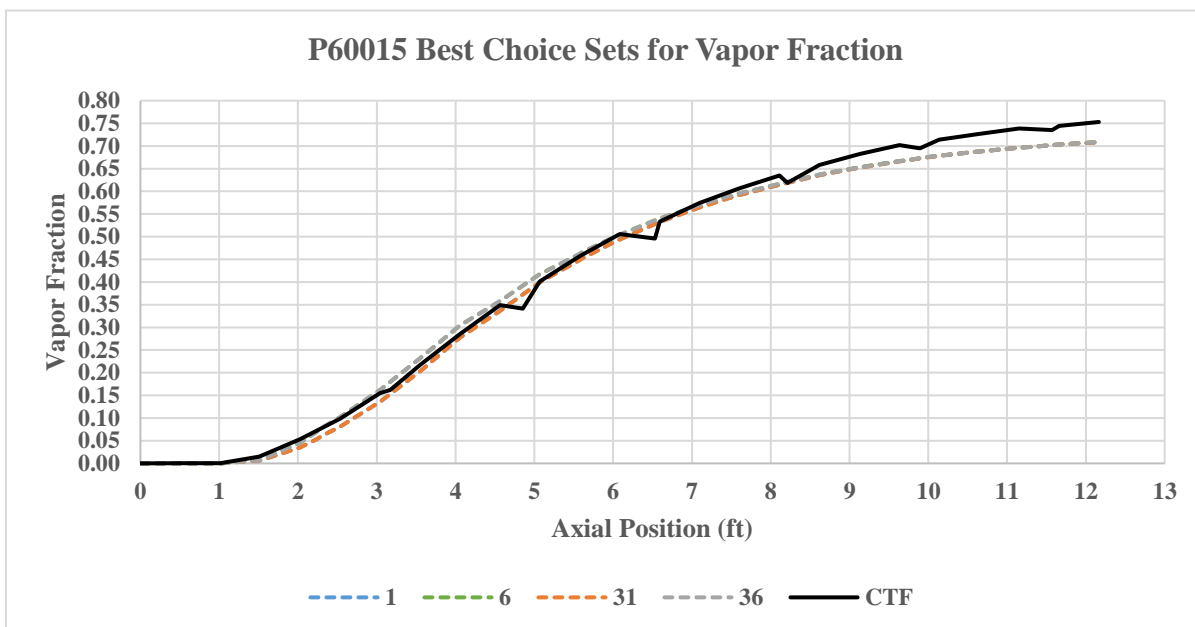


**Figure 4.12: P60015, Selected COBRA-EN sets compared to COBRA-CTF vapor fraction trends**

Refer to *table 4.11* and *4.13* for the sets' absolute relative difference in pressure drop in total

and pressure drop identifiers.

| Table 4.17: P60015, Extended Combinations of Correlations Study | | | |
|---|---|---|---|
| Two Phase Friction Multiplier | | Subcooled Boiling | Void/Quality Relationship |
| EPRI | Armand | | |
| Identifier | | | |
| 1 | 31 | EPRI | EPRI |
| 6 | 36 | Levy | EPRI |

### 4.10.11  Results of the Extended Correlations Study

*Figures 4.5*, *4.8*, and *4.11* illustrate the combination of COBRA-EN correlations that provide a best match to COBRA-CTF void fraction results. *Tables 4.18*, *4.19*, and *4.20* contain the absolute relative difference between the code predictions compared to measured data for pressure drop with the selected set of correlations that best match to COBRA-CTF vapor fraction results.

| Table 4.18: P60001, COBRA-EN Extended Correlation Study Sets | | | | | |
|---|---|---|---|---|---|
| Pressure Drop Identifier | Measured (psi) | 4 | 9 | 34 | 39 |
| dp01 | 0.167 | 31.74% | 31.74% | 19.76% | 19.76% |
| dp02 | 0.284 | 8.45% | 8.45% | 15.49% | 15.49% |
| dp03 | 0.367 | 14.44% | 14.44% | 3.54% | 3.54% |
| dp04 | 0.505 | 8.91% | 8.91% | 14.85% | 14.85% |
| dp05 | 0.531 | 7.72% | 7.72% | 15.25% | 15.25% |
| dp06 | 0.570 | 8.77% | 10.53% | 12.28% | 12.28% |
| dp07 | 1.780 | 5.06% | 5.06% | 6.74% | 6.74% |
| dp08 | 0.798 | 0.25% | 0.25% | 0.25% | 0.25% |
| dp09 | 3.974 | 2.94% | 2.93% | 6.29% | 6.28% |
| Average | | 9.81% | 10.00% | 10.50% | 10.50% |
| Range of Two-Phase Friction Multiplier Suite Column Averages | | EPRI | | Armand | |
| | | 9.10% | 10.56% | 9.80% | 11.26% |

*Table 4.18* indicates the EPRI two-phase friction multiplier, and the Armand-Messena void/quality relationship provides the better match to the measured data for P60001.

| Table 4.19: P60007, COBRA-EN Extended Correlation Study Sets | | | | | |
|---|---|---|---|---|---|
| **Pressure Drop Identifier** | **Measured (psi)** | **1** | **6** | **31** | **36** |
| **dp01** | **0.811** | 2.561% | 2.561% | 6.26% | 6.26% |
| **dp02** | **0.972** | 14.587% | 14.587% | 17.67% | 17.67% |
| **dp03** | **1.176** | 0.318% | 0.318% | 4.78% | 4.78% |
| **dp04** | **1.385** | 10.477% | 11.199% | 15.53% | 15.53% |
| **dp05** | **1.314** | 7.918% | 7.918% | 12.48% | 12.48% |
| **dp06** | **1.218** | 7.249% | 7.249% | 10.53% | 11.35% |
| **dp07** | **3.313** | 5.212% | 4.609% | 7.33% | 7.02% |
| **dp08** | **1.197** | 1.384% | 1.384% | 1.38% | 1.38% |
| **dp09** | **8.396** | 5.372% | 5.206% | 8.41% | 8.31% |
| **Average** | | 6.120% | 6.115% | 9.38% | 9.42% |
| **Range of Two-Phase Friction Multiplier Suite Column Averages** | | **EPRI** | | **Armand** | |
| | | 4.52% | 7.76% | 5.19% | 12.81% |

| Table 4.20: P60015, COBRA-EN Extended Correlation Study Sets | | | | | |
|---|---|---|---|---|---|
| **Pressure Drop Identifier** | **Measured (psi)** | **1** | **6** | **31** | **36** |
| **dp01** | **2.165** | 20.55% | 20.55% | 17.32% | 17.32% |
| **dp02** | **2.466** | 28.22% | 28.22% | 26.20% | 26.20% |
| **dp03** | **2.804** | 14.41% | 14.41% | 9.06% | 9.06% |
| **dp04** | **3.040** | 19.08% | 19.08% | 16.78% | 16.78% |
| **dp05** | **2.949** | 20.31% | 20.65% | 21.33% | 21.33% |
| **dp06** | **2.524** | 17.19% | 17.19% | 19.18% | 19.57% |
| **dp07** | **5.978** | 9.67% | 8.67% | 12.01% | 11.17% |
| **dp08** | **1.520** | 2.63% | 1.32% | 2.63% | 1.32% |
| **dp09** | **16.530** | 14.74% | 14.31% | 14.44% | 14.02% |
| **Average** | | 16.31% | 16.04% | 15.44% | 15.20% |
| **Range of Two-Phase Friction Multiplier Suite Column Averages** | | **EPRI** | | **Armand** | |
| | | 7.11% | 20.92% | 10.02 | 26.24% |

P60007 and P60015 use the EPRI void/quality relationship. *Table 4.19*, and *4.20* indicate the EPRI and Armand two-phase friction multipliers predict pressure comparable to the measured data. There is a marginal improvement with the Armand correlation observed in P60015.

**4.10.12  Conclusion of the Extended Correlations Study**

The EPRI two-phase friction multiplier exhibits a better match in predicted values to measured data for pressure drop as observed in the initial correlation study for pressure drop alone. There is a slight improvement observed in the test case with operating parameters closer to nominal BWR conditions, P60015, with the Armand two-phase friction multiplier. This slight improvement is not significant enough in comparison to the larger contribution of the EPRI correlation observed in P60001 and P60007 in the extended correlation study. The P60001 test case does designate that the Armand-Messena void/quality relationship should be considered, but P60001 operating parameters are lower than typical BWR conditions. The EPRI void/quality relationship is observed in all four sets in the final selection of the extended correlation study for both P60007 and P60015. *Set 1* is chosen based on the results of the extend correlation study, and on referral of the COBRA-EN manual to use all EPRI correlations.

| Table 4.21: COBRA-EN Results for Extended Set of Correlations, Set 1 | | | | | | |
|---|---|---|---|---|---|---|
| **Two Phase Friction Multiplier** | | | **Subcooled Boiling** | **Bulk Void/Quality Relationship** | | |
| EPRI | | | EPRI | EPRI | | |
| **Total Pressure Drop (psi)** | | | **Absolute Relative Difference in Pressure Drop for Individual Pressure Drop Identifiers** | | | |
| **Measured** | **P60001** | **P60007** | **P60015** | **Identifier** | **P60001** | **P60007** | **P60015** |
| | 3.974 | 8.396 | 16.53 | dp01 | 31.74% | 2.56% | 20.55% |
| **Calculated** | **P60001** | **P60007** | **P60015** | dp02 | 8.45% | 14.59% | 28.22% |
| | 3.877 | 7.945 | 14.093 | dp03 | 14.44% | 0.32% | 14.41% |
| | | | | dp04 | 6.93% | 10.48% | 19.08% |
| | | | | dp05 | 7.72% | 7.92% | 20.31% |
| | | | | dp06 | 7.02% | 7.25% | 17.19% |
| | | | | dp07 | 4.49% | 5.21% | 9.67% |
| | | | | dp08 | 0.25% | 1.38% | 2.63% |
| | | | | dp09 | 2.43% | 5.37% | 14.74% |
| | | | | Average | 9.27% | 6.12% | 16.31% |

**4.11   Convergence Study with COBRA-EN**

The convergence study for COBRA-EN is not as extensive as the one performed in COBRA-CTF. COBRA-EN does not exhibit the same issues with the vapor fraction seen in the COBRA-CTF convergence study. In addition, there is a limitation in COBRA-EN on how many axial nodes can be allocated with all the other given geometric information such as number of subchannels, number of fuel and water rods, and lateral gaps between fuel rods and/or structural (BWR can) surfaces. This is explained in more detail in the COBRA-EN user manual on pages 72 and 73 pertaining to the *Storage Requirements*. The limit for this comparative study was discovered to be when attempting to subdivide the uniform mesh size beyond a factor of five while including the designated pressure tap positions. The mesh refinement cases are categorized by the number of times the original node size seen in *figure 2.5* is subdivided.

$$Uniform\ Node\ Length = \frac{H_{fuel}}{DN}$$

| Table 4.22: COBRA-EN Convergence Study Uniform Node Lengths | | |
|:---:|:---:|:---:|
| **Mesh Refinement Case** | | |
| 1X24 | 3X24 | 5X24 |
| **Uniform Node Length** | | |
| **Metric (m)** | | |
| 0.1545 | 0.0515 | 0.0309 |
| **Standard (ft)** | | |
| 0.5069 | 0.1690 | 0.1014 |

## 4.12 Results of Convergence Study with COBRA-EN

*Table 4.23* list the $L_{\infty Norm}$ and the $L_{2 Norm}$ for the comparison between the mesh refinement cases 1X24 to 3X24, and 3X24 to 5X24. The results for pressure along the axial length of the heated channel in the output file are provided with a precision to the second decimal. The largest absolute relative difference observed in *table 4.23* is $10^{-4}$ for both $L_{\infty Norm}$ and $L_{2 Norm}$ is beyond the resolution of the compared values for pressure by two orders of magnitude. This indicates that there is little gain in determining pressure drop by reducing the uniform node size.

| Table 4.23: Results of COBRA-EN Convergence Study for Pressure (psi) | | | | | | |
|---|---|---|---|---|---|---|
| Error | P60001 | | P60007 | | P60015 | |
| | 1 to 3 | 3 to 5 | 1 to 3 | 3 to 5 | 1 to 3 | 3 to 5 |
| $L_{\infty Norm}$ | 1.92E-05 | 9.61E-06 | 3.82E-05 | 9.60E-06 | 1.52E-04 | 1.90E-05 |
| $L_{2 Norm}$ | 6.29E-05 | 3.18E-05 | 1.34E-04 | 3.17E-05 | 5.50E-04 | 7.24E-05 |

**CHAPTER 5: Comparison of COBRA-EN and COBRA-CTF**

The primary focus for this study is to evaluate both COBRA-EN and COBRA-CTF where the validation metric is the NUPEC BFBT steady-state, two-phase pressure drop benchmark database. Both codes have undergone a convergence study to determine the sensitivity of simulation results to changes in node length. It was determined that for both codes, the 1X24 mesh refinement case with a uniform node length of 0.1545m (0.50689ft) yielded negligible change in pressure drop associated with further reduction in node length. This was deemed valid considering changes in vapor volume fraction near spacer grids was not an issue for COBRA-EN, nor was vapor volume fraction a measured value provided in the NUPEC BFBT benchmark database. COBRA-CTF requires additional work to resolve the vapor volume fraction anomalies at the grid spacers. The COBRA-EN section includes an additional study that results in a best choice suite of correlations for typical BWR conditions with the least amount of absolute relative difference in predicted values compared to measured data in the NUPEC BFBT benchmark database. The initial study resulted in a set of correlations listed in *table 4.14* that provides the better match of predicted to measured data considering pressure drop alone. The extended study results in a set of correlations listed in *table 4.21* including vapor fraction as a metric. The preliminary correlation set will be labeled *EN8* while the extended correlation study will be labeled *EN1*.

## 5.1    Comparison for Test Case P60001

Test case P60001 maintains lower than normal BWR operating conditions and may be representative of conditions during a reactor start-up. Both codes slightly under predicted the total pressure drop compared to the benchmark data. The range in absolute relative differences for the total pressure drop is between 2.43% and 5.57%. However, COBRA-EN matches the benchmark data better for each individual pressure drop identifier seen along the column of differences and absolute relative differences, except at the top of the assembly indicated by values seen for *dp01*. The absolute relative difference column averages suggest a slight advantage for COBRA-EN compared COBRA-CTF for pressure drop predictions compared to measured data in the NUPEC BFBT benchmark database.

| Table 5.1:   P60001 COBRA-EN and COBRA-CTF Pressure Drop Comparison | | | | | | | | | |
|---|---|---|---|---|---|---|---|---|---|
| Measured and Calculated Pressure Drop at Individual Pressure Drop Identifiers (psi) | | | | Difference Between Measured and Calculated Total Pressure Drop (psi) | | | Absolute Relative Difference Between Measured and Calculated Total Pressure Drop | | |
| Identifier | Measured | EN1 | EN8 | CTF | EN1 | EN8 | CTF | EN1 | EN8 | CTF |
| dp01 | 0.167 | 0.220 | 0.210 | 0.195 | 0.053 | 0.043 | 0.028 | 31.74% | 25.75% | 16.72% |
| dp02 | 0.284 | 0.260 | 0.250 | 0.215 | -0.024 | -0.034 | -0.069 | 8.45% | 11.97% | 24.37% |
| dp03 | 0.367 | 0.420 | 0.390 | 0.412 | 0.053 | 0.023 | 0.045 | 14.44% | 6.27% | 12.35% |
| dp04 | 0.505 | 0.470 | 0.440 | 0.439 | -0.035 | -0.065 | -0.066 | 6.93% | 12.87% | 12.98% |
| dp05 | 0.531 | 0.490 | 0.460 | 0.455 | -0.041 | -0.071 | -0.076 | 7.72% | 13.37% | 14.32% |
| dp06 | 0.570 | 0.530 | 0.500 | 0.484 | -0.040 | -0.070 | -0.086 | 7.02% | 12.28% | 15.11% |
| dp07 | 1.780 | 1.700 | 1.660 | 1.668 | -0.080 | -0.120 | -0.112 | 4.49% | 6.74% | 6.27% |
| dp08 | 0.798 | 0.800 | 0.800 | 0.852 | 0.002 | 0.002 | 0.054 | 0.25% | 0.25% | 6.72% |
| dp09 | 3.974 | 3.877 | 3.753 | 3.827 | -0.097 | -0.221 | -0.147 | 2.43% | 5.57% | 3.70% |
| | | | | | Average | | | 9.27% | 10.56% | 12.51% |

Both codes over predict the pressure drop near the top of the assembly seen at *dp01*. Also, there is a slight over prediction seen in both codes for *dp03*. There is a small over prediction at *dp08* for COBRA-CTF. Otherwise, both codes' predictions match the measured data closely with a slight trend to under predict pressure drop.



**Figure 5.1: P60001, Pressure drop values at pressure tap identifiers**



**Figure 5.2: P60001, Percent difference in predicted to measured pressure drop**

**Figure 5.3:  P60001, Pressure predictions of COBRA-CTF compared to COBRA-EN**



**Figure 5.4:  P60001, Vapor fraction predictions of COBRA-CTF compared to COBRA-EN**

## 5.2    Comparison for Test Case P60007

Test case P60007 maintains slightly lower than normal BWR operating conditions. Both codes slightly under predicted the total pressure drop compared to the benchmark data. COBRA-CTF does exhibit an advantage for total pressure drop with an absolute relative difference of 0.92% compared to 2.6% and 5.37% for COBRA-EN. COBRA-EN matches the benchmark data better for individual pressure drop identifiers near the top of the assembly. Otherwise, both codes perform similarly, with the exception that COBRA-CTF displays a distinct advantage for the total pressure drop at *dp09.* The absolute relative difference column averages suggest a slight advantage for COBRA-EN compared COBRA-CTF for pressure drop predictions compared to measured data in the NUPEC BFBT benchmark database.

| Table 5.2:   P60007 COBRA-EN and COBRA-CTF Pressure Drop Comparison ||||||||||
|---|---|---|---|---|---|---|---|---|---|
| Measured and Calculated Pressure Drop at Individual Pressure Drop Identifiers (psi) ||||  Difference Between Measured and Calculated Total Pressure Drop (psi) ||| Absolute Relative Difference Between Measured and Calculated Total Pressure Drop |||
| Identifier | Measured | EN1 | EN8 | CTF | EN1 | EN8 | CTF | EN1 | EN8 | CTF |
| dp01 | 0.811 | 0.790 | 0.850 | 0.727 | -0.021 | 0.039 | -0.084 | 2.56% | 4.84% | 10.38% |
| dp02 | 0.972 | 0.830 | 0.880 | 0.768 | -0.142 | -0.092 | -0.204 | 14.59% | 9.44% | 21.02% |
| dp03 | 1.176 | 1.180 | 1.240 | 1.316 | 0.004 | 0.064 | 0.140 | 0.32% | 5.42% | 11.86% |
| dp04 | 1.385 | 1.240 | 1.290 | 1.323 | -0.145 | -0.095 | -0.062 | 10.48% | 6.87% | 4.47% |
| dp05 | 1.314 | 1.210 | 1.250 | 1.229 | -0.104 | -0.064 | -0.085 | 7.92% | 4.87% | 6.50% |
| dp06 | 1.218 | 1.130 | 1.170 | 1.132 | -0.088 | -0.048 | -0.087 | 7.25% | 3.97% | 7.12% |
| dp07 | 3.313 | 3.140 | 3.220 | 3.192 | -0.173 | -0.093 | -0.120 | 5.21% | 2.80% | 3.63% |
| dp08 | 1.197 | 1.180 | 1.180 | 1.260 | -0.017 | -0.017 | 0.063 | 1.38% | 1.38% | 5.26% |
| dp09 | 8.396 | 7.945 | 8.178 | 8.319 | -0.451 | -0.218 | -0.077 | 5.37% | 2.60% | 0.92% |
| | | | | | Average ||| 6.12% | 4.69% | 7.91% |

Both codes over predict the pressure drop near the top of the assembly seen at *dp01,* except for the *EN1*. There is a small over prediction at *dp08* for COBRA-CTF. Otherwise, both codes' predictions match the measured data closely with the slight trend to under predict pressure drop.
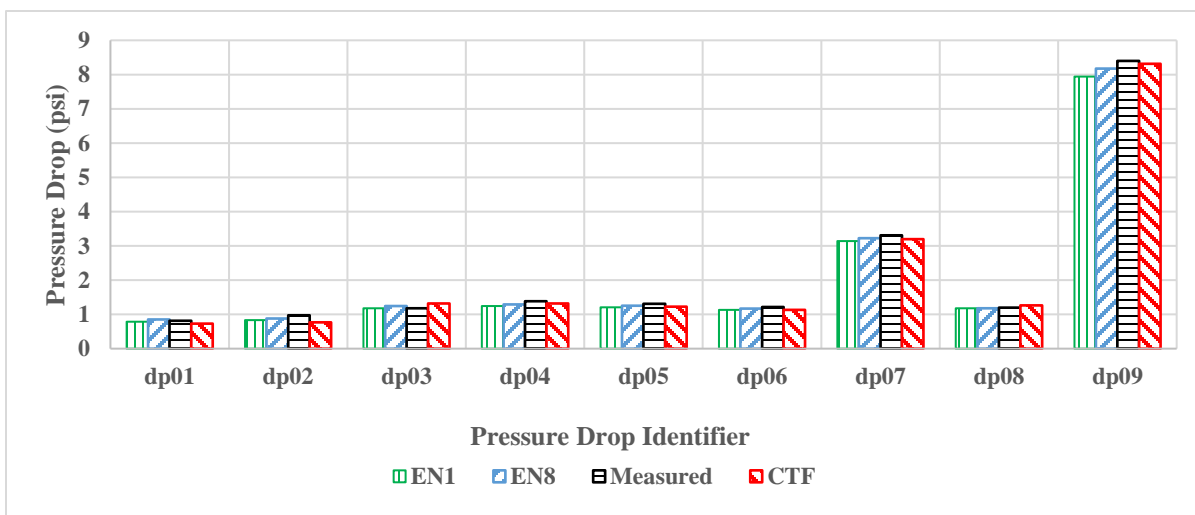


**Figure 5.5:   P60007, Pressure drop values at pressure drop identifiers**
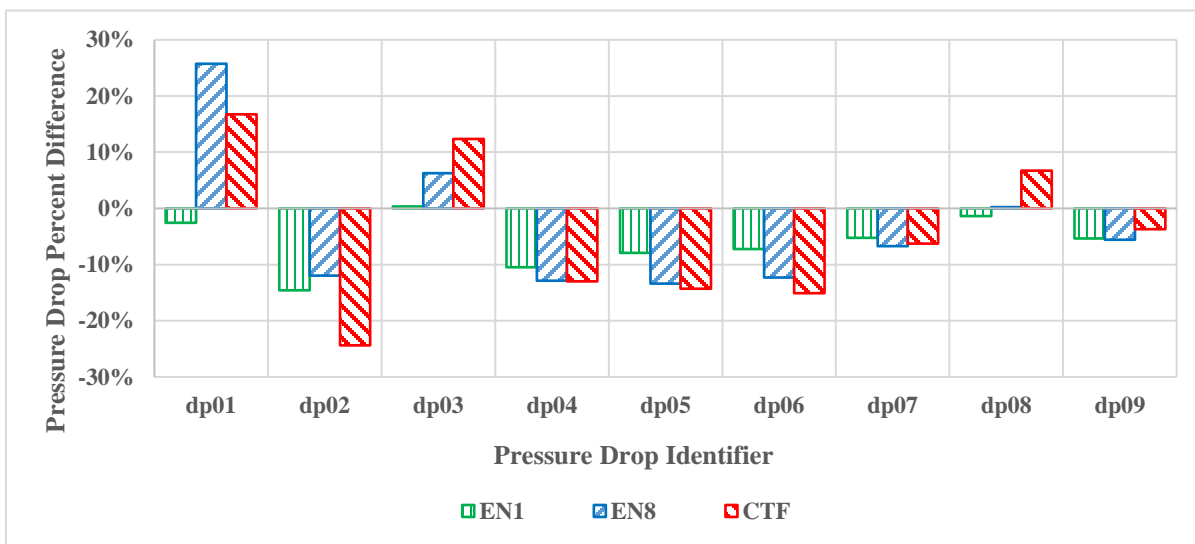


**Figure 5.6:   P60007, Percent difference in predicted to measured pressure drop**
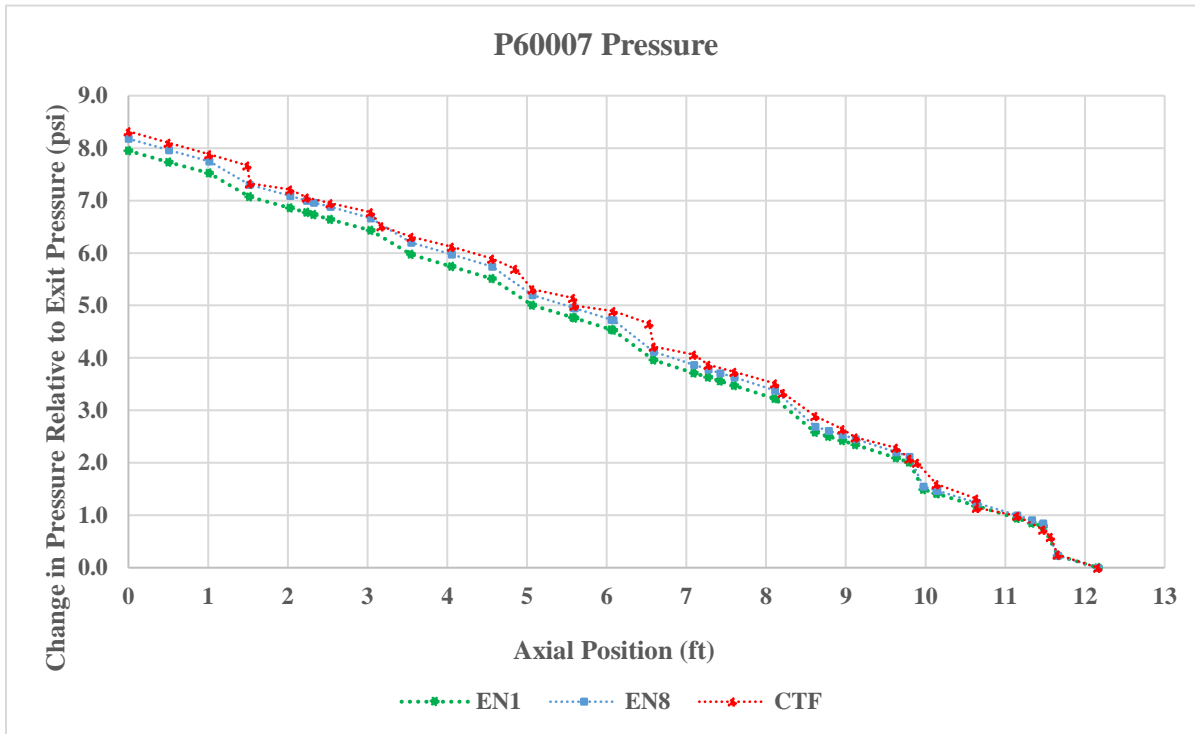
**Figure 5.7:   P60007, Pressure predictions of COBRA-CTF compared to COBRA-EN**
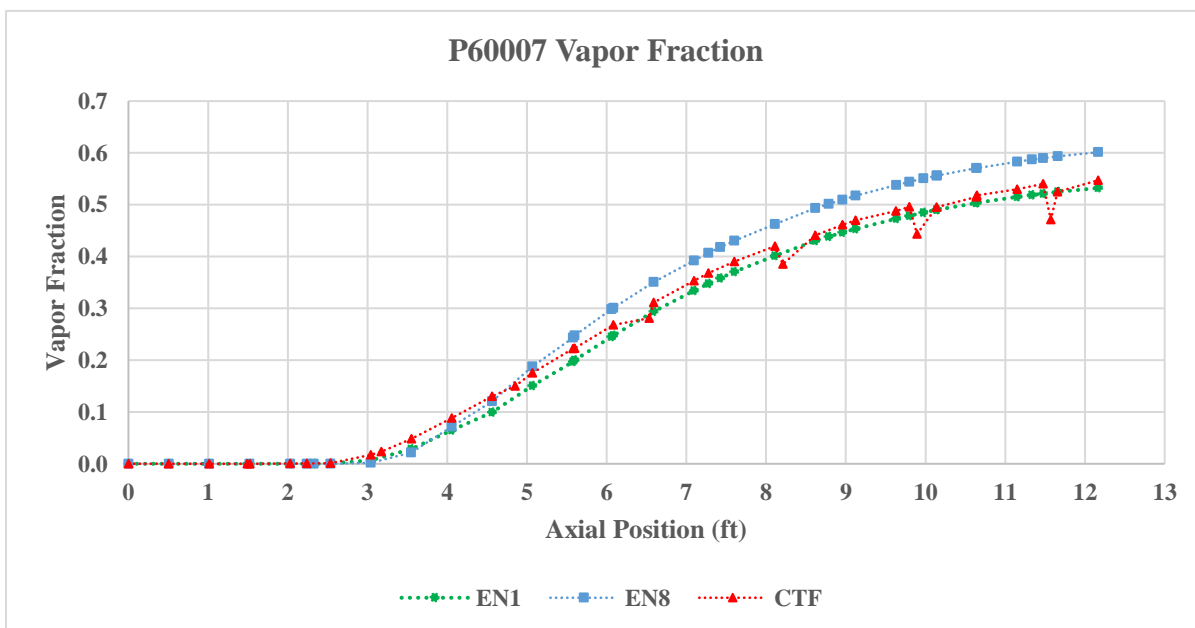


**Figure 5.8:   P60007, Vapor fraction predictions of COBRA-CTF compared to COBRA-EN**

### 5.3    Comparison for Test Case P60015

Test case P60015 better represents normal BWR operating conditions with only a slightly higher mass flow. Both codes under predicted the total pressure drop compared to the benchmark data. The *EN1* results exhibit a slight disadvantage for total pressure drop with an absolute relative difference of 14.74% compared to 6.14% and 6.34% for *EN8* and CTF respectively. The *EN8* results noticeably match the benchmark data better for a majority of the individual pressure drop identifiers, including the total pressure drop at *dp09*. Otherwise, *EN1* and COBRA-CTF perform similarly at most of the individual pressure drop identifiers. COBRA-CTF displays a distinct advantage for the total pressure drop at *dp09* compared to *EN1*. The absolute relative difference column averages suggest a distinct advantage for the *EN8* results for pressure drop predictions compared to measured data in the NUPEC BFBT benchmark database.

| Table 5.3:   P60015 COBRA-EN and COBRA-CTF Pressure Drop Comparison | | | | | | | | | |
|---|---|---|---|---|---|---|---|---|---|
| Measured and Calculated Pressure Drop at Individual Pressure Drop Identifiers (psi) | | | | Difference Between Measured and Calculated Total Pressure Drop (psi) | | | Absolute Relative Difference Between Measured and Calculated Total Pressure Drop | | |
| Identifier | Measured | EN1 | EN8 | CTF | EN1 | EN8 | CTF | EN1 | EN8 | CTF |
| dp01 | 2.165 | 1.720 | 2.010 | 1.340 | -0.445 | -0.155 | -0.825 | 20.55% | 7.16% | 38.09% |
| dp02 | 2.466 | 1.770 | 2.040 | 1.447 | -0.696 | -0.426 | -1.019 | 28.22% | 17.27% | 41.33% |
| dp03 | 2.804 | 2.400 | 2.720 | 2.743 | -0.404 | -0.084 | -0.061 | 14.41% | 3.00% | 2.17% |
| dp04 | 3.040 | 2.460 | 2.770 | 2.810 | -0.580 | -0.270 | -0.230 | 19.08% | 8.88% | 7.58% |
| dp05 | 2.949 | 2.350 | 2.650 | 2.604 | -0.599 | -0.299 | -0.345 | 20.31% | 10.14% | 11.70% |
| dp06 | 2.524 | 2.090 | 2.310 | 2.333 | -0.434 | -0.214 | -0.191 | 17.19% | 8.48% | 7.56% |
| dp07 | 5.978 | 5.400 | 5.880 | 5.735 | -0.578 | -0.098 | -0.243 | 9.67% | 1.64% | 4.06% |
| dp08 | 1.520 | 1.480 | 1.500 | 1.590 | -0.040 | -0.020 | 0.070 | 2.63% | 1.32% | 4.61% |
| dp09 | 16.530 | 14.093 | 15.515 | 15.482 | -2.437 | -1.015 | -1.048 | 14.74% | 6.14% | 6.34% |
| | | | | | | Average | | 16.31% | 7.11% | 13.71% |

Both codes exhibit a consistent trend to under predict the pressure drop at all pressure drop identifiers compared to the measured data for the P60015 operating conditions. The *EN8* predictions match the measured data better for pressure drop.
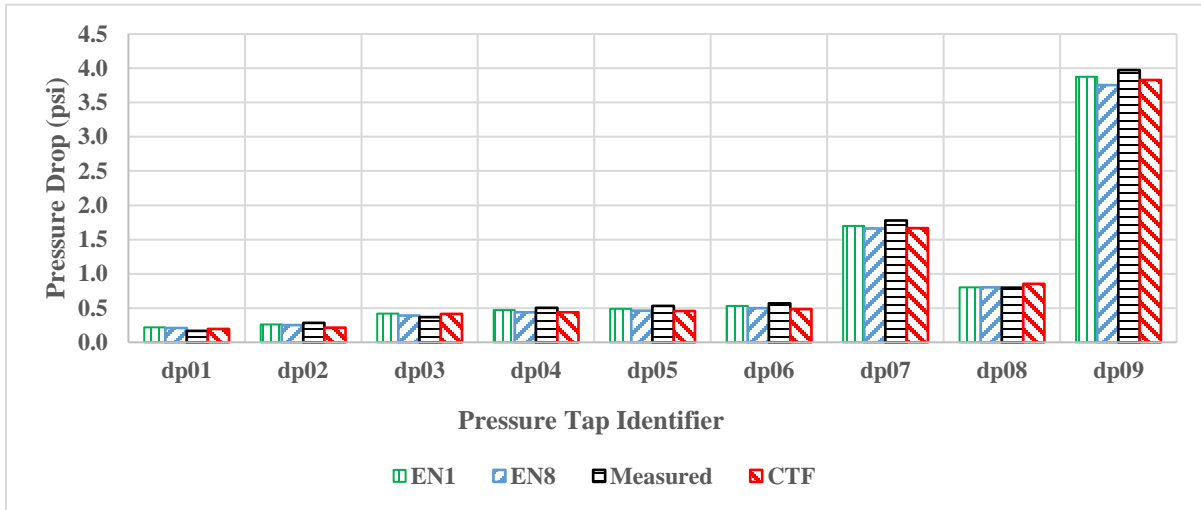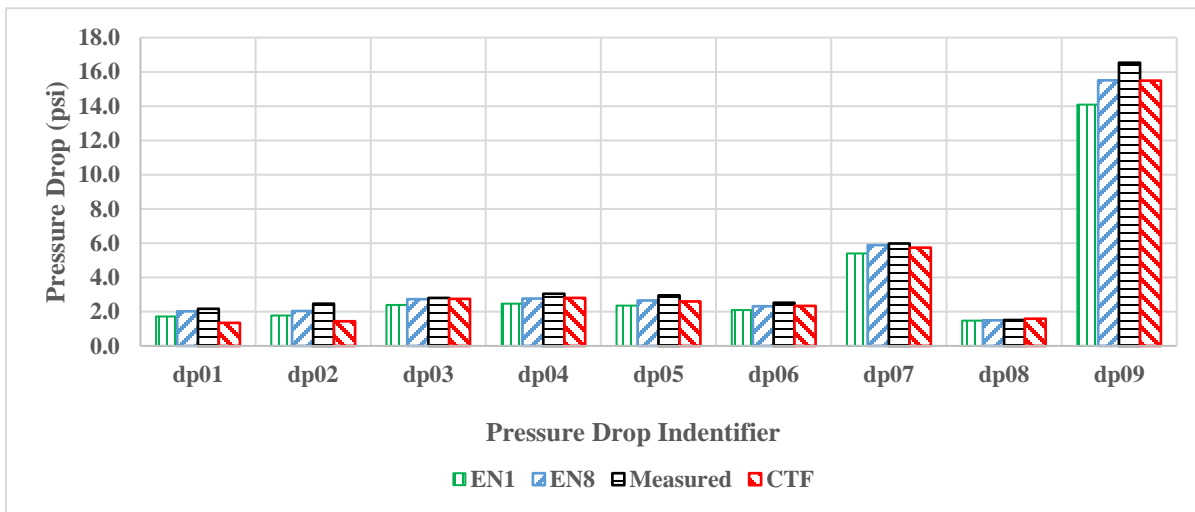


**Figure 5.9:   P60015, Pressure drop values at pressure drop identifiers**
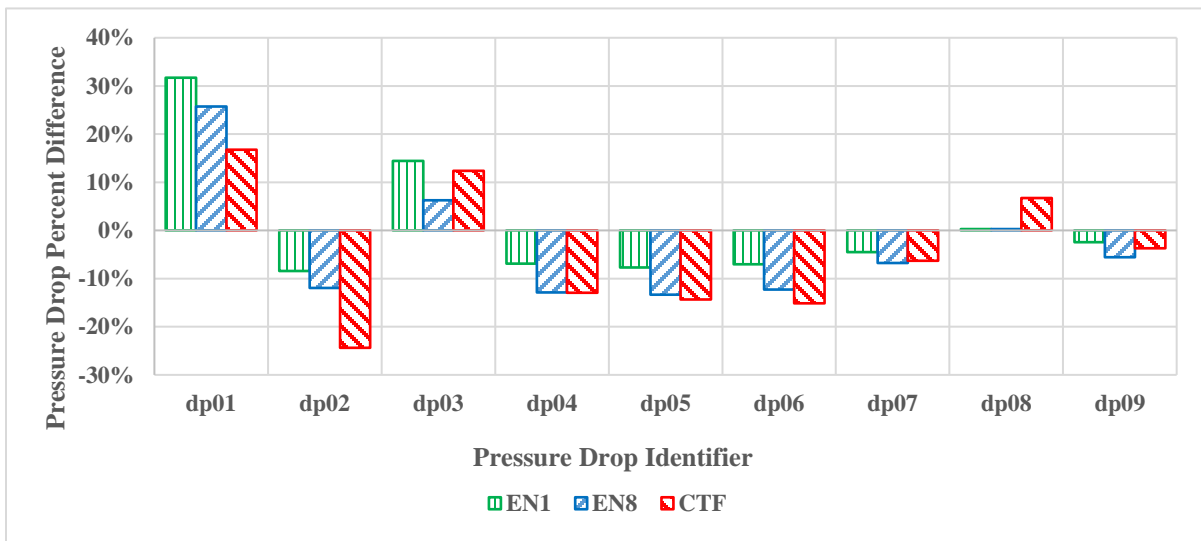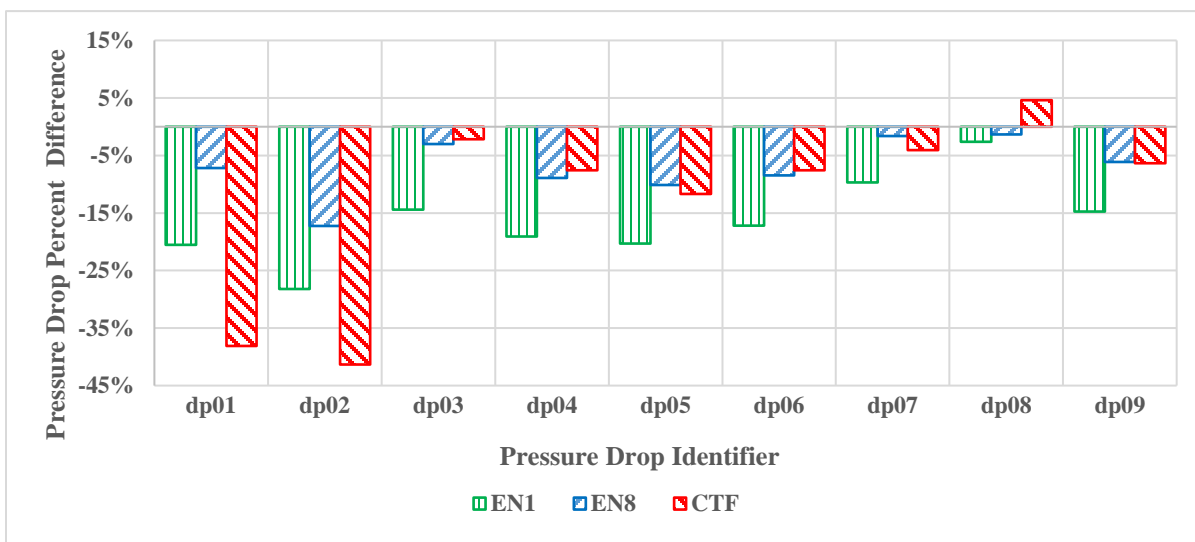


**Figure 5.10: P60015, Percent difference in predicted to measured pressure drop**
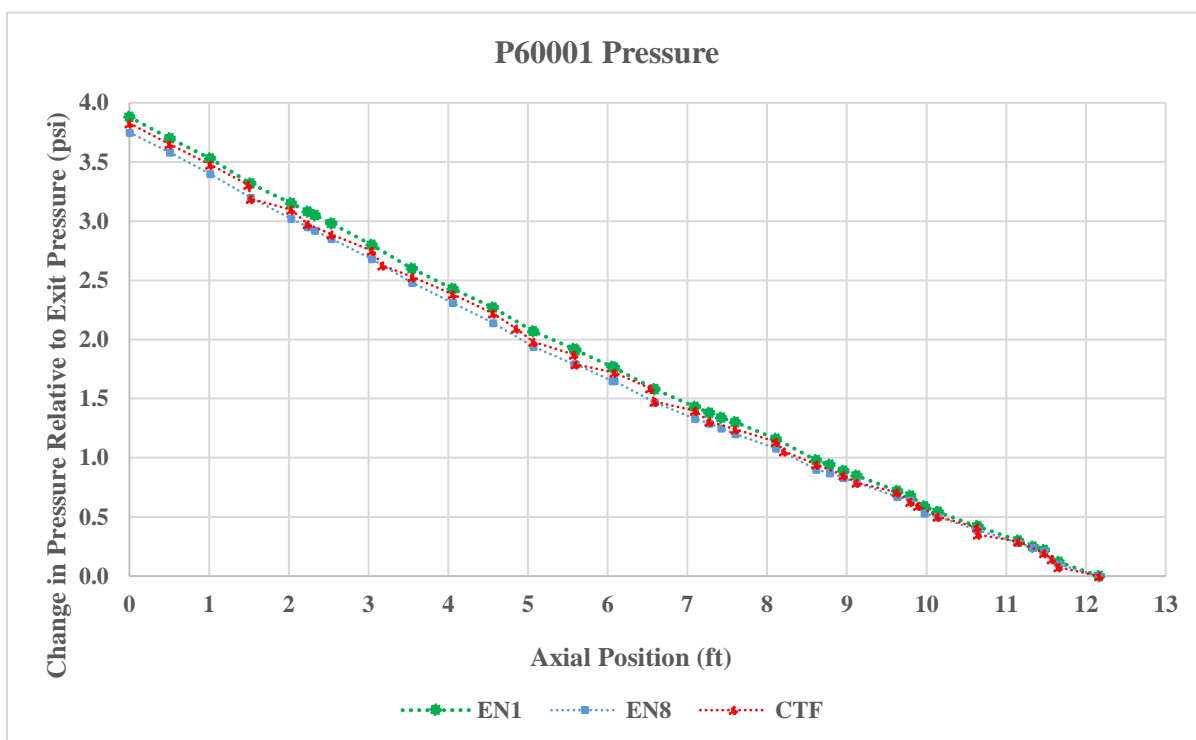
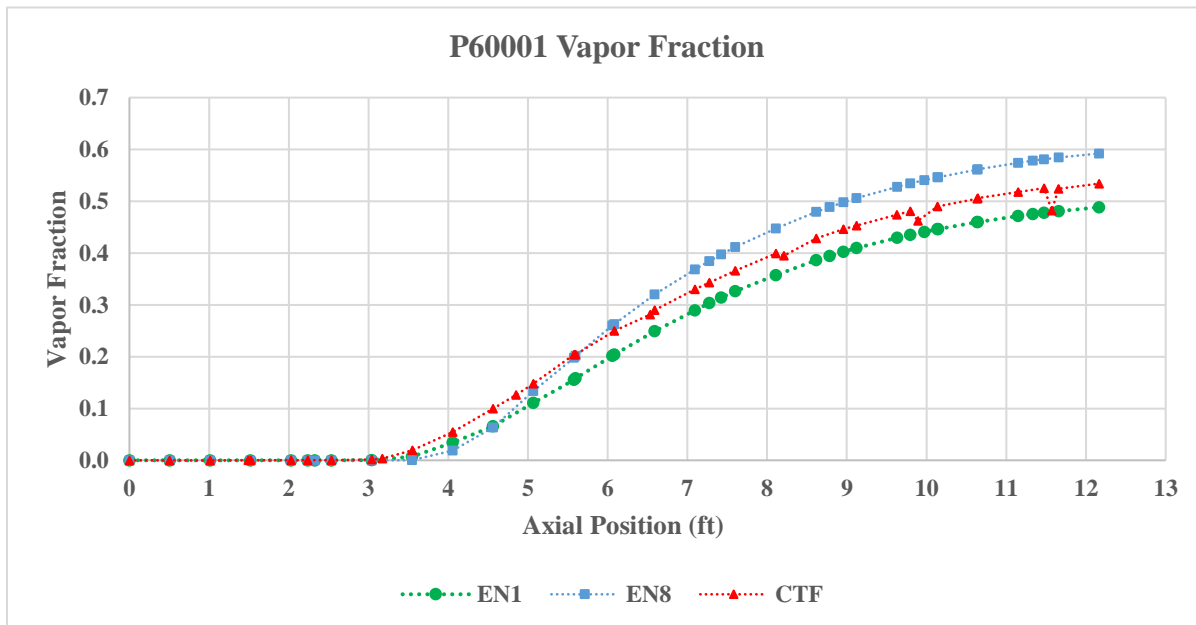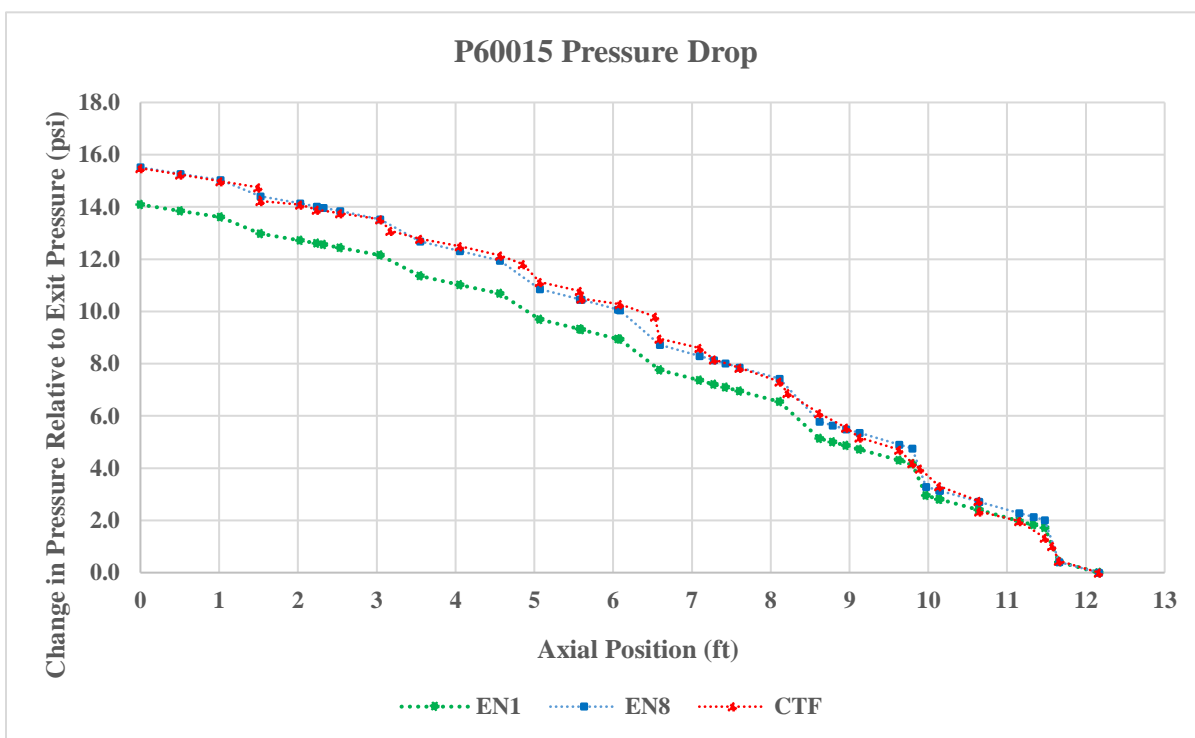Figure 5.11: P60015, Pressure predictions of COBRA-CTF compared to COBRA-EN
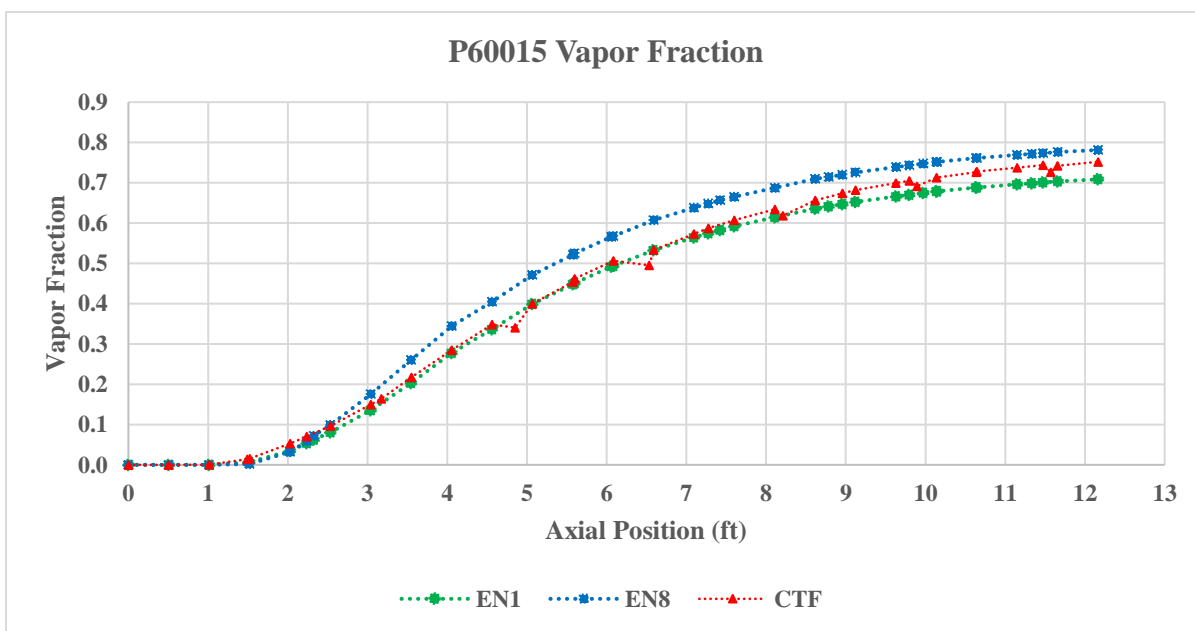


Figure 5.12: P60015, Vapor fraction predictions of COBRA-CTF compared to COBRA-EN

**Conclusion and Future Work**

This study has achieved its primary goal to compare predictions of two subchannel thermal-hydraulic codes, COBRA-EN and COBRA-CTF, under representative BWR operating conditions with the NUPEC BFBT benchmark database. There were two additional studies performed prior to the comparison with benchmark data. A mesh convergence study was conducted with both codes. A study to determine the optimum combination of correlations was also performed in COBRA-EN.

The convergence study revealed that pressure predictions in both thermal hydraulic codes were insensitive to the axial node length for node lengths consistent with the given power profile. A uniform node length of 0.1545m (0.50689ft) was sufficient to evaluate pressure drop. The range in absolute relative difference for pressure was approximately between the fourth and fifth decimal place. This margin of error is beyond the two-decimal precision of the COBRA-EN results for pressure and is negligible compared to the 1% uncertainty associated with the instrumentation to measure the pressure during the data collection process. COBRA-CTF displayed anomalies in vapor fraction near the grid spacer positions that will require further investigation into the code's management of local losses due to obstructions. Two unique issues were addressed in the COBRA-CTF convergence study. The convergence on a solution, and the results along the axial length of the assembly appear to be sensitive to nodes near the grid spacers. It was not definitively resolved if this issue was directly related to the axial position or the node length which results in the node edge, axial position, before the grid spacer location. This issue was not exhaustively explored because the most important criteria described in the mesh convergence study was to, "achieve a converged solution with COBRA-CTF." The U/V technique developed to achieve a converged solution suggest that

node sizes of approximately 0.02m (0.0656ft) are possible, but "padding" will be required at the grid spacer positions. This study was not able to define an appropriate repeating pattern to resolve solution convergence issues for runs with varying operating conditions. It was discovered that ignoring the data in the proximity of the grid spacers implied convergence between subsequent mesh refinements cases, and an acceptable absolute relative difference for vapor fraction. Suggestions for future work pertaining to the convergence study include:

1. Explore the sensitivity of the code generated values with a coarser axial mesh than the default from the NUPEC BFBT database axial power peaking factors.

2. Further investigation of the management of local losses due to obstructions in COBRA-CTF to resolve the nonphysical dips observed at the grid spacers locations with measured vapor fraction data along the length of the bundle.

An initial correlation study with COBRA-EN suggests the EPRI correlation for two-phase friction multiplier, Levy subcooled boiling correlation, and the homogenous model for the void/quality relationship provides the best match to the benchmark data when only considering pressure drop as a metric. The extended correlation study suggests the EPRI correlation for two-phase friction multiplier, subcooled boiling, and void/quality relationship when void fraction is also considered. In addition, the correlation study confirmed the sensitivity of the two-phase pressure drop to the choice of two-phase friction multiplier for BWR flow conditions. A suggestion for future work would be to acquire measured vapor fraction and pressure drop data from the same experiment to definitively select which combination of correlation best predicts typical BWR flow conditions.

It was observed that both thermal hydraulic codes slightly under predict the total pressure drop compared to the benchmark data for the selected test cases. The COBRA-EN *set 8* of correlations which includes the homogenous void/quality relationship does provide pressure drop predictions that better match the NUPEC BFBT benchmark data for more individual pressure drop identifiers for all three test cases. The *set 1* of correlations for COBRA-EN which includes all EPRI correlations does provide a possible avenue to further explore pressure drop under realistic two-phase flow conditions with other test cases. However, there was no uncertainty analysis performed during this study. The differences in the COBRA-EN and COBRA-CTF results may fall within the margin of uncertainty associated with the correlations used in these simulations. These conclusions are based on the data from the three cases selected from the NUPEC BFBT two-phase pressure drop, P6 series, experiments located in the Phase II, "*Critical Power Benchmark"*, Exercise 0, "*Steady State Pressure Drop Benchmark.*" The primary focus of this study was to evaluate pressure drop. The supplementary observations of the vapor fraction were due to the nonphysical dips in vapor fraction at the grid spacers observed in COBRA-CTF. There are other exercises within the NUPEC BFBT benchmark database pertaining to void distributions where vapor fraction has been measured. The Phase I, "*Void Distribution Benchmark*" contains exercises that have measured vapor fraction at the bundle exit. This data can be acquired by sending a request to Nuclear Energy Agency (NEA) within the Organization for Economic Co-operation and Development (OCED).

# REFERENCES

[1] Avramova, Maria N. and Robert K. Salko. *CTF Theory Manual*. Technical Report. PSU: RDFMGroup, 2015.

[2] Avramova, Maria N., Scott Palmtag and Robert K. Salko. *CTF Validation and Verification*. CASL-U-2016-1113-000. Oak Ridge: Consortium for Advanced Simulation of Light Water Reactors, 2016.

[3] Avramova, Maria N., Taylor S. Blyth and Robert K. Salko. *CTF User's Manual*. Technical Report CASL-U-2015-0238-000. PSU: RDFM Group, 2015.

[4] Basile, D., et al. *COBRA-EN, An Upgraded Version of the COBRA-3C/MIT Code for Thermal-Hydraulic Transient Analysis of Light Water Reactor Fuel Assemblies and Cores*. Report 1010/1. Oak Ridge National Laboratory: Radiation Safety Information Computational Center, 1991.

[5] Doster, J. M. "www4.ncsu.edu/~doster/NE402/Text/SinglePhaseFlow/ SubchannelAnalysis.pdf." n.d. *www4.ncsu.edu/~doster/NE402/NE402.htm.* 5 July 2018.

[6] *IAEA | ARIS Advanced Reactor Information System*. May 2013. https://aris.iaea.org/sites/core.html. 12 May 2018.

[7] Ivanov, K., et al. *NUPEC BWR Full-size Fine-mesh Bundle Test (BFBT) Benchmark,Volume I: Specifications*. Technical Report NEA No. 6212. Paris: OECD Nuclear Energy Agency, 2006. ISBN 92-64-01088-2.

[8] Kazimi, Mujid S. and Tordreas, Neil E. *Nuclear Systems Volume I Thermal Hydraulic Fundamentals*. Boca Raton: CRC Press Taylor & Francis Group, 2012. Book.

[9] Lyon, R. B. *Boiling Water Reactor Simulator with Passive Safety Systems*. User Manual. Vienna: INTERNATIONAL ATOMIC ENERGY AGENCY, 2009.

[10] Nero, Anthony V. *A guidebook to nuclear reactors*. Berkeley: University of California Press, 1979. Book ISBN 0-520-03661-1.

[11] *The ABWR Plant General Description*. Technical Report. Wilmington: GE Hitachi Nuclear Energy, 2007.

**APPENDICES**

**Appendix A**

Figure 3.3.1. Cross-sectional view of heater rod
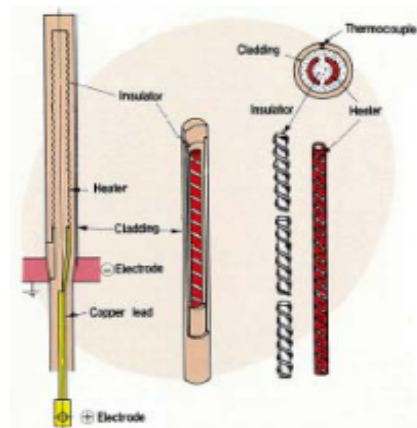


Table 3.3.1. Heater rod structure

| Item | | Data |
|---|---|---|
| Heater | Outer diameter (mm) | 7.3 |
| | Material | Nichrome |
| Insulator | Outer diameter (mm) | 9.7 |
| | Material | Boron nitride |
| Cladding | Thickness (mm) | 1.3 |
| | Material | Inconel 600/berylium |

## 3.4 Thermo-mechanical properties

The thermo-mechanical properties listed below are based on the MATPRO model used in TRAC code [8]. Updated values of the coil properties will be provided as they become available.

### 3.4.1 Properties of nichrome

It is assumed that nichrome coils have similar properties as those of constantan.

- *Density*
  A constant value of 8 393.4 kg/m$^3$ is used.

- *Specific heat*
  The specific heat is $c_p = 110 T_f^{0.2075}$, where $c_p$ is the specific heat (J/kg.K) and $T_f$ is the temperature (F).

- *Thermal conductivity*
  The thermal conductivity is $k = 29.18 + 2.683 \times 10^{-3}(T_f - 100)$, where $k$ is the thermal conductivity (W/m.K) and $T_f$ is the temperature (F).

34

### 3.4.2 Properties of boron nitride

- **Density**

  A constant value of 2 002 kg/m$^3$ is used.

- **Specific heat**

  The specific heat is $c_p = 760.59 + 1.7955T_f - 8.6704 \times 10^{-4}T_f^2 + 1.5896 \times 10^{-7}T_f^3$, where $c_p$ is the specific heat (J/kg.K) and $T_f$ is the temperature (F).

- **Thermal conductivity**

  The boron-nitride thermal-conductivity calculation, based on a conversion to SI units of a curve fit is $k = 25.27 - 1.365 \times 10^{-3}T_f$, where $k$ is the thermal conductivity (W/m.K) and $T_f$ is the temperature (F).

### 3.4.3 Properties of Inconel 600

- **Density**

  The density is $\rho = 16.01846 \times (5.261008 \times 10^2 - 1.345453 \times 10^{-2}T_f - 1.194357 \times 10^{-7}T_f^2)$, where $\rho$ is the density (kg/m$^3$) and $T_f$ is the temperature (F).

- **Specific heat**

  The specific heat is $c_p = 4186.8 \times (0.1014 + 4.378952 \times 10^{-5}T_f - 2.046138 \times 10^{-8}T_f^2 + 3.418111 \times 10^{-11}T_f^3 - 2.060318 \times 10^{-13}T_f^4 + 3.682836 \times 10^{-16}T_f^5 - 2.458648 \times 10^{-19}T_f^6 + 5.597571 \times 10^{-23}T_f^7)$, where $c_p$ is the specific heat (J/kg.K) and $T_f$ is the temperature (F).

- **Thermal conductivity**

  The thermal conductivity is $k = 1.729577 \times (8.011332 + 4.643719 \times 10^{-3}T_f + 1.872857 \times 10^{-6}T_f^2 - 3.914512 \times 10^{-9}T_f^3 + 3.475513 \times 10^{-12}T_f^4 - 9.936696 \times 10^{-16}T_f^5$, where $k$ is the thermal conductivity (W/m.K) and $T_f$ is the temperature (F).

Since no information on the heat loss is available in the NUPEC BFBT database, an adiabatic condition is suggested for the benchmark.

**Appendix B**

| Test number | Outlet pressure (MPa) | Inlet temperature (°C) | Inlet sub-cooling (kJ/kg) | Flow rate (t/h) | Power (MW) | Outlet quality (%) | dp301 (kPa) | dp302 (kPa) | dp303 (kPa) | dp304 (kPa) | dp305 (kPa) | dp306 (kPa) | dp307 (kPa) | dp308 (kPa) | dp309 (kPa) |
|---|---|---|---|---|---|---|---|---|---|---|---|---|---|---|---|
| P60001 | 7.16 | 277.3 | 53.3 | 20.2 | 0.863 | 6.7 | 1.15 | 1.96 | 2.53 | 3.48 | 3.66 | 3.93 | 12.27 | 5.50 | 27.40 |
| P60003 | 7.16 | 277.8 | 50.8 | 20.1 | 1.521 | 14.8 | 1.54 | 2.22 | 2.81 | 3.61 | 3.63 | 3.69 | 11.72 | 5.50 | 27.22 |
| P60005 | 7.16 | 277.7 | 51.1 | 20.0 | 2.357 | 24.9 | 2.10 | 2.81 | 3.43 | 4.26 | 4.11 | 3.97 | 11.84 | 5.47 | 29.16 |
| P60007 | 7.17 | 277.8 | 51.1 | 55.0 | 2.375 | 7.0 | 5.59 | 6.70 | 8.11 | 9.55 | 9.06 | 8.40 | 22.84 | 8.25 | 57.89 |
| P60009 | 7.17 | 277.8 | 51.1 | 55.0 | 4.197 | 15.0 | 9.24 | 10.91 | 12.39 | 14.26 | 13.54 | 11.83 | 29.30 | 8.48 | 78.59 |
| P60011 | 7.17 | 278.0 | 50.6 | 54.9 | 6.478 | 25.1 | 13.56 | 16.05 | 17.81 | 20.04 | 19.39 | 16.73 | 39.14 | 8.93 | 106.72 |
| P60013 | 7.16 | 278.4 | 47.2 | 69.9 | 3.022 | 7.3 | 8.92 | 10.24 | 12.15 | 13.58 | 12.98 | 11.65 | 30.31 | 10.07 | 79.71 |
| P60015 | 7.17 | 278.2 | 49.5 | 70.0 | 5.340 | 15.1 | 14.93 | 17.00 | 19.33 | 20.96 | 20.33 | 17.40 | 41.22 | 10.48 | 113.97 |
| P60017 | 7.16 | 277.8 | 51.0 | 45.1 | 1.919 | 6.8 | 3.93 | 4.91 | 6.08 | 7.23 | 7.03 | 6.73 | 18.92 | 7.24 | 46.54 |
| P60019 | 7.17 | 278.2 | 49.4 | 45.0 | 3.437 | 15.1 | 6.43 | 7.73 | 8.94 | 10.54 | 9.98 | 8.90 | 22.97 | 7.44 | 60.11 |
| P60021 | 7.16 | 277.8 | 50.8 | 45.1 | 5.312 | 25.0 | 9.30 | 11.24 | 12.51 | 14.42 | 13.98 | 12.17 | 29.32 | 7.72 | 78.76 |
| P60022 | 8.64 | 291.3 | 50.7 | 20.2 | 0.837 | 7.0 | 1.11 | 1.94 | 2.49 | 3.44 | 3.48 | 3.88 | 11.99 | 5.36 | 26.83 |
| P60023 | 8.63 | 291.0 | 52.3 | 20.2 | 1.464 | 14.8 | 1.39 | 2.08 | 2.62 | 3.44 | 3.49 | 3.63 | 11.54 | 5.36 | 26.38 |
| P60024 | 8.63 | 290.9 | 52.9 | 20.2 | 2.252 | 24.9 | 1.82 | 2.49 | 3.03 | 3.88 | 3.55 | 3.75 | 11.47 | 5.33 | 27.55 |
| P60025 | 8.64 | 291.3 | 51.3 | 55.0 | 2.271 | 6.9 | 4.96 | 6.08 | 7.29 | 8.74 | 8.15 | 7.96 | 22.05 | 8.17 | 54.66 |
| P60026 | 8.64 | 291.0 | 53.0 | 55.1 | 3.975 | 14.7 | 7.75 | 9.23 | 10.47 | 12.61 | 11.43 | 10.50 | 26.89 | 8.36 | 70.06 |
| P60027 | 8.64 | 291.2 | 51.5 | 55.1 | 6.137 | 24.9 | 11.18 | 13.30 | 14.69 | 17.40 | 16.10 | 14.40 | 34.79 | 8.79 | 92.41 |
| P60029 | 8.64 | 291.3 | 51.5 | 70.1 | 2.888 | 6.9 | 7.60 | 8.96 | 10.54 | 12.32 | 11.43 | 10.70 | 28.79 | 10.08 | 73.55 |
| P60030 | 8.64 | 291.2 | 51.4 | 70.2 | 5.076 | 14.9 | 12.39 | 14.28 | 16.19 | 18.14 | 17.16 | 15.33 | 37.62 | 10.40 | 100.77 |
| P60031 | 8.64 | 290.9 | 53.0 | 45.1 | 1.869 | 6.9 | 3.49 | 4.50 | 5.50 | 6.78 | 6.36 | 6.42 | 18.29 | 7.09 | 44.32 |
| P60032 | 8.63 | 291.2 | 51.3 | 45.2 | 3.262 | 14.9 | 5.42 | 6.62 | 7.63 | 9.34 | 8.47 | 8.02 | 21.35 | 7.28 | 54.32 |
| P60033 | 8.63 | 291.2 | 51.6 | 45.1 | 5.021 | 24.9 | 7.61 | 9.31 | 10.28 | 12.62 | 11.50 | 10.49 | 26.21 | 7.54 | 68.44 |

## Appendix C

## Generalized Phasic Mass Conservation Equation

$L_k$ = mass transfer into or out of phase $k$

Inter-phase mass transfer can occur by either evaporation/condensation or by entrainment/ de-entrainment.

$$L_v = \Gamma'''$$

$$L_l = -(1 - \eta)\Gamma''' - S'''$$

$$L_e = -\eta\Gamma''' + S'''$$

$\Gamma'''$ = volumetric mass transfer due to phase change.

$\eta$ = fraction of phase change occurring between vapor and entrained droplets.

The definition of $\eta_{evp}$ for the case of evaporation and $\eta_{cond}$ for the case of condensation:

$$\eta_{evp} = min \begin{cases} 1 - \dfrac{Q'''_{wl}}{\Gamma''' H_{fg}} \\ \dfrac{\alpha_e}{1 - \alpha_v} \end{cases}$$

$$\eta_{cond} = \frac{\alpha_e}{1 - \alpha_v}$$

$Q'''_{wl}$ = volumetric heat transfer from the wall to liquid phase

$H_{fg}$ = latent heat of vaporization.

**Generalized Phasic Momentum Conservation Equation**

$$\frac{\partial}{\partial t}\left(\alpha_k\rho_k\vec{V}_k\right) + \frac{\partial}{\partial x}\left(\alpha_k\rho_k u_k\vec{V}_k\right) + \frac{\partial}{\partial y}\left(\alpha_k\rho_k v_k\vec{V}_k\right) + \frac{\partial}{\partial z}\left(\alpha_k\rho_k w_k\vec{V}_k\right) =$$

$$\alpha_k\rho_k\vec{g} - \alpha_k\nabla P + \nabla\cdot\left[\alpha_k\left(\tau_k^{ij} + T_k^{ij}\right) + \vec{M}_k^L + \vec{M}_k^d + \vec{M}_k^T\right]$$

The turbulent shear stress term is not modeled, and turbulent mixing is captured using a simple turbulent diffusion approximation in COBRA-CTF. The liquid-liquid viscous shear stresses are not modeled by CTF. However, the viscous stress term can be expanded into wall shear and a fluid-fluid shear component, as follows:

$$\nabla\cdot\left(\alpha_e\tau_e^{ij}\right) = \vec{\tau}_{we}'''$$

$$\nabla\cdot\left(\alpha_v\tau_v^{ij}\right) = \vec{\tau}_{wv}''' + \nabla\cdot\left(\alpha_v\sigma_v^{ij}\right)$$

$$\nabla\cdot\left(\alpha_l\tau_l^{ij}\right) = \vec{\tau}_{wl}''' + \nabla\cdot\left(\alpha_l\sigma_l^{ij}\right)$$

$\vec{\tau}_{wk}'''$ =volumetric wall drag and form losses of phase $k$

$\vec{M}_k^L$ = momentum source/sink due to phase change and entrainment/de-entrainment.

$$\vec{M}_v^L = \Gamma'''\vec{V}$$

$$\vec{M}_l^L = -\Gamma'''(1-\eta)\vec{V} - S'''\vec{V}$$

$$\vec{M}_e^L = -\Gamma'''\eta\vec{V} + S'''\vec{V}$$

$\vec{V}$ = velocity of the phase that mass is coming from.

$\vec{M}_k^d$ = interfacial drag term for flow field, $k$

$$\vec{M}_v^d = -\vec{\tau}_{i,vl}''' - \vec{\tau}_{i,ve}'''$$

$$\vec{M}_l^d = \vec{\tau}_{i,vl}'''$$

$$\vec{M}_e^d = \vec{\tau}_{i,ve}'''$$

The $\vec{\tau}_{i,vl}^{\prime\prime\prime}$ and $\vec{\tau}_{i,ve}^{\prime\prime\prime}$ terms are the volumetric inter-phase drag forces for the vapor-liquid and vapor-droplet interfaces, respectively. Note that the drag terms are subtractive for the vapor field and additive for the droplet and liquid fields. *This is because the CTF convention is for the vapor phase to move faster than liquid and droplet phases, which means that interfacial friction would act against the vapor phase, but with the liquid and droplet phases.* If the opposite were true, and the vapor phase were somehow moving slower than the liquid and droplet phases, the signs of the terms would simply be reversed in CTF.

**Generalized Phasic Energy Conservation Equation**

The generalized energy equation is presented in Equation 2.11.

$$\frac{\partial}{\partial t}(\alpha_k \rho_k h_k) + \nabla \cdot (\alpha_k \rho_k h_k \vec{V}_k) = -\nabla \cdot \left[\alpha_k\left(\vec{Q}_k + \vec{q}_k^T\right)\right] + \Gamma_k h_k^i + q_{wk}^{\prime\prime\prime} + \alpha_k \frac{\partial P}{\partial t}$$

It is assumed that there is no volumetric heat generation occurring in the fluid, radiative heat transfer only occurs between solid surfaces and the vapor/droplet fields, internal dissipation is negligible allowing pressure to be considered uniform throughout the phases. There is no modeling of heat conduction in the fluids and so $\vec{Q}$ is zero in CTF.

**Appendix D**

## 1X24

| NONO | DXS | IVAR | MSIM |
|------|-----|------|------|
| 31 | 0.119612903226 | 22 | 2480 |

| JLEV | VARDX | JLEV | VARDX | JLEV | VARDX | JLEV | VARDX | JLEV | VARDX |
|------|-------|------|-------|------|-------|------|-------|------|-------|
| 3 | 0.15450 | 4 | 0.14600 | 5 | 0.00850 | 8 | 0.15450 | 9 | 0.04000 |
| 10 | 0.11450 | 12 | 0.15450 | 13 | 0.08850 | 14 | 0.06600 | 16 | 0.15450 |
| 17 | 0.13700 | 18 | 0.01750 | 21 | 0.15450 | 22 | 0.03100 | 23 | 0.12350 |
| 25 | 0.15450 | 26 | 0.07950 | 27 | 0.07500 | 29 | 0.15450 | 30 | 0.12800 |
| 31 | 0.02650 | 32 | 0.15450 | | | | | | |

| Grid Spacer Identifiers, JLEV | | | | | | |
|---|---|---|---|---|---|---|
| 4 | 9 | 13 | 17 | 22 | 26 | 30 |

---------------------------------------------------------------------------------------------------------------------

## 3X24

| NONO | DXS | IVAR | MSIM |
|------|-----|------|------|
| 79 | 0.046936708861 | 22 | 6320 |

| JLEV | VARDX | JLEV | VARDX | JLEV | VARDX | JLEV | VARDX | JLEV | VARDX |
|------|-------|------|-------|------|-------|------|-------|------|-------|
| 9 | 0.05150 | 10 | 0.04300 | 11 | 0.00850 | 20 | 0.05150 | 21 | 0.04000 |
| 22 | 0.01150 | 31 | 0.05150 | 32 | 0.03700 | 33 | 0.01450 | 42 | 0.05150 |
| 43 | 0.03400 | 44 | 0.01750 | 53 | 0.05150 | 54 | 0.03100 | 55 | 0.02050 |
| 64 | 0.05150 | 65 | 0.02800 | 66 | 0.02350 | 75 | 0.05150 | 76 | 0.02500 |
| 77 | 0.02650 | 80 | 0.05150 | | | | | | |

| Grid Spacer Identifiers, JLEV | | | | | | |
|---|---|---|---|---|---|---|
| 10 | 21 | 32 | 43 | 54 | 65 | 76 |

**4X24**

| NONO | DXS | IVAR | MSIM |
|------|-----|------|------|
| 103 | 0.036 | 22 | 8240 |

| JLEV | VARDX | JLEV | VARDX | JLEV | VARDX | JLEV | VARDX | JLEV | VARDX |
|------|-------|------|-------|------|-------|------|-------|------|-------|
| 12 | 0.038625 | 13 | 0.030125 | 14 | 0.008500 | 27 | 0.038625 | 12 | 0.038625 |
| 28 | 0.001375 | 29 | 0.037250 | 41 | 0.038625 | 42 | 0.011250 | 28 | 0.001375 |
| 43 | 0.027375 | 55 | 0.038625 | 56 | 0.021125 | 57 | 0.017500 | 43 | 0.027375 |
| 69 | 0.038625 | 70 | 0.031000 | 71 | 0.007625 | 84 | 0.038625 | 69 | 0.038625 |
| 85 | 0.002250 | 86 | 0.036375 | 98 | 0.038625 | 99 | 0.012125 | 85 | 0.002250 |

| Grid Spacer Identifiers, JLEV | | | | | | |
|----|----|----|----|----|----|----|
| 13 | 28 | 42 | 56 | 70 | 85 | 99 |

-----------------------------------------------------------------------------------------------------------------

**5X24**

| NONO | DXS | IVAR | MSIM |
|------|-----|------|------|
| 126 | 0.029428571 | 22 | 10080 |

| JLEV | VARDX | JLEV | VARDX | JLEV | VARDX | JLEV | VARDX | JLEV | VARDX |
|------|-------|------|-------|------|-------|------|-------|------|-------|
| 15 | 0.03090 | 16 | 0.02240 | 17 | 0.00850 | 33 | 0.03090 | 34 | 0.00911 |
| 35 | 0.02180 | 50 | 0.03090 | 51 | 0.02670 | 52 | 0.00420 | 68 | 0.03090 |
| 69 | 0.01340 | 70 | 0.01750 | 85 | 0.03090 | 86 | 0.03100 | 87 | 0.03080 |
| 102 | 0.03090 | 103 | 0.01770 | 104 | 0.01320 | 120 | 0.03090 | 121 | 0.00440 |
| 122 | 0.02650 | 127 | 0.03090 | | | | | | |

| Grid Spacer Identifiers, JLEV | | | | | | |
|----|----|----|----|----|-----|-----|
| 16 | 34 | 51 | 69 | 86 | 103 | 121 |

**6X24**

| NONO | DXS | IVAR | MSIM |
|---|---|---|---|
| 150 | 0.02472 | 22 | 12000 |

| JLEV | VARDX | JLEV | VARDX | JLEV | VARDX | JLEV | VARDX |
|---|---|---|---|---|---|---|---|
| 18 | 0.02575 | 19 | 0.01725 | 20 | 0.00850 | 39 | 0.02575 |
| 40 | 0.01425 | 41 | 0.01150 | 60 | 0.02575 | 61 | 0.01125 |
| 62 | 0.01450 | 81 | 0.02575 | 82 | 0.00825 | 83 | 0.01750 |
| 102 | 0.02575 | 103 | 0.00525 | 104 | 0.02050 | 123 | 0.02575 |
| 124 | 0.00225 | 125 | 0.02350 | 143 | 0.02575 | 144 | 0.02500 |
| 145 | 0.02650 | 151 | 0.02575 | | | | |

| Grid Spacer Identifiers, JLEV | | | | | | |
|---|---|---|---|---|---|---|
| 19 | 40 | 61 | 82 | 103 | 124 | 144 |

**7X24**

| With 0.214mm | | Without 0.214mm | |
|---|---|---|---|
| **JLEV** | **VARDX** | **JLEV** | **VARDX** |
| 21 | 0.022071428571 | 21 | 0.022071428571 |
| 22 | 0.013571428571 | 22 | 0.013571428571 |
| 23 | 0.008500000000 | 23 | 0.008500000000 |
| 45 | 0.022071428571 | 45 | 0.022071428571 |
| 46 | 0.017928571429 | 46 | 0.017928571429 |
| 47 | 0.004142857143 | 47 | 0.004142857143 |
| 70 | 0.022071428571 | 69 | 0.022071428571 |
| **71** | **0.000214285714** | **70** | **0.022285714286** |
| 72 | 0.021857142857 | 71 | 0.021857142857 |
| 94 | 0.022071428571 | 93 | 0.022071428571 |
| 95 | 0.004571428571 | 94 | 0.004571428571 |
| 96 | 0.017500000000 | 95 | 0.017500000000 |
| 118 | 0.022071428571 | 117 | 0.022071428571 |
| 119 | 0.008928571429 | 118 | 0.008928571429 |
| 120 | 0.013142857143 | 119 | 0.013142857143 |
| 142 | 0.022071428571 | 141 | 0.022071428571 |
| 143 | 0.013285714286 | 142 | 0.013285714286 |
| 144 | 0.008785714286 | 143 | 0.008785714286 |
| 166 | 0.022071428571 | 165 | 0.022071428571 |
| 167 | 0.017642857143 | 166 | 0.017642857143 |
| 168 | 0.004428571429 | 167 | 0.004428571429 |
| 176 | 0.022071428571 | 175 | 0.022071428571 |

| Test 1 | | Test 2 | | Test 3 | |
|---|---|---|---|---|---|
| **JLEV** | **VARDX** | **JLEV** | **VARDX** | **JLEV** | **VARDX** |
| 21 | 0.022071428571 | 21 | 0.022071428571 | 21 | 0.013571428571 |
| 22 | 0.013571428571 | 22 | 0.013571428571 | 22 | 0.008500000000 |
| 23 | 0.008500000000 | 23 | 0.008500000000 | 23 | 0.022071428571 |
| 45 | 0.022071428571 | 45 | 0.022071428571 | 45 | 0.017928571429 |
| 46 | 0.017928571429 | 46 | 0.017928571429 | 46 | 0.026214285714 |
| 47 | 0.026214285714 | 47 | 0.026214285714 | 47 | 0.022071428571 |
| 68 | 0.022071428571 | 68 | 0.022071428571 | 68 | 0.022285714286 |
| 69 | 0.022285714286 | 69 | 0.022285714286 | 69 | 0.021857142857 |
| 70 | 0.021857142857 | 70 | 0.021857142857 | 70 | 0.022071428571 |
| 92 | 0.022071428571 | 92 | 0.022071428571 | 92 | 0.004571428571 |
| 93 | 0.004571428571 | 93 | 0.004571428571 | 93 | 0.017500000000 |
| 94 | 0.017500000000 | 94 | 0.017500000000 | 94 | 0.022071428571 |
| 116 | 0.022071428571 | 115 | 0.022071428571 | 115 | 0.031000000000 |
| 117 | 0.008928571429 | 116 | 0.031000000000 | 116 | 0.013142857143 |
| 118 | 0.013142857143 | 117 | 0.013142857143 | 117 | 0.022071428571 |
| 140 | 0.022071428571 | 139 | 0.022071428571 | 139 | 0.013285714286 |
| 141 | 0.013285714286 | 140 | 0.013285714286 | 140 | 0.030857142857 |
| 142 | 0.008785714286 | 141 | 0.030857142857 | 141 | 0.022071428571 |
| 164 | 0.022071428571 | 162 | 0.022071428571 | 162 | 0.017642857143 |
| 165 | 0.017642857143 | 163 | 0.017642857143 | 163 | 0.048571428571 |
| 166 | 0.026500000000 | 164 | 0.026500000000 | 164 | 0.022071428571 |
| 174 | 0.022071428571 | 171 | 0.022071428571 | 170 | 0.013571428571 |

| Test 4 | | Test 6 | |
|---|---|---|---|
| JLEV | VARDX | JLEV | VARDX |
| 21 | 0.022071428571 | 15 | 0.022071428571 |
| 22 | 0.013571428571 | 22 | 0.020857142857 |
| 23 | 0.008500000000 | 23 | 0.008500000000 |
| 45 | 0.022071428571 | 44 | 0.022071428571 |
| 46 | 0.017928571429 | 46 | 0.020000000000 |
| 47 | 0.114500000000 | 51 | 0.022900000000 |
| 64 | 0.022071428571 | 68 | 0.022071428571 |
| 65 | 0.022285714286 | 69 | 0.022285714286 |
| 66 | 0.066000000000 | 72 | 0.022000000000 |
| 86 | 0.022071428571 | 86 | 0.022071428571 |
| 87 | 0.004571428571 | 92 | 0.022833333333 |
| 88 | 0.017500000000 | 93 | 0.017500000000 |
| 110 | 0.022071428571 | 114 | 0.022071428571 |
| 111 | 0.008928571429 | 116 | 0.015500000000 |
| 112 | 0.123500000000 | 122 | 0.020583333333 |
| 129 | 0.022071428571 | 136 | 0.022071428571 |
| 130 | 0.013285714286 | 140 | 0.019875000000 |
| 131 | 0.075000000000 | 144 | 0.018750000000 |
| 150 | 0.022071428571 | 158 | 0.022071428571 |
| 151 | 0.017642857143 | 164 | 0.021333333333 |
| 152 | 0.026500000000 | 165 | 0.026500000000 |
| 159 | 0.022071428571 | 172 | 0.022071428571 |

| Test 7 | | Test 8 | |
|---|---|---|---|
| **JLEV** | **VARDX** | **JLEV** | **VARDX** |
| 18 | 0.0220 | 15 | 0.022071428571 |
| 22 | 0.0205 | 22 | 0.020857142857 |
| 38 | 0.0220 | 23 | 0.008500000000 |
| 46 | 0.0200 | 44 | 0.022071428571 |
| 62 | 0.0220 | 46 | 0.020000000000 |
| 70 | 0.0200 | 51 | 0.022900000000 |
| 86 | 0.0220 | 68 | 0.022071428571 |
| 94 | 0.0200 | 69 | 0.022285714286 |
| 110 | 0.0220 | 72 | 0.022000000000 |
| 118 | 0.0200 | 86 | 0.022071428571 |
| 134 | 0.0220 | 92 | 0.022833333333 |
| 142 | 0.0200 | 98 | 0.028666666667 |
| 158 | 0.0220 | 112 | 0.022071428571 |
| 166 | 0.0200 | **113** | **0.031000000000** |
| 173 | 0.0220 | 119 | 0.020583333333 |
| 174 | 0.0270 | 133 | 0.022071428571 |
| | | 137 | 0.019875000000 |
| | | 141 | 0.018750000000 |
| | | 158 | 0.022071428571 |
| | | 161 | 0.020595238095 |
| | | 162 | 0.026500000000 |
| | | 169 | 0.022071428571 |

| Test | Grid Spacer Identifiers, JLEV | | | | | | |
|---|---|---|---|---|---|---|---|
| With 0.214mm | 22 | 46 | 71 | 95 | 120 | 143 | 167 |
| With Out 0.214mm | 19 | 46 | 70 | 94 | 118 | 142 | 166 |
| **Test 1** | **22** | **46** | **69** | **93** | **117** | **141** | **165** |
| Test 2 | 22 | 46 | 69 | 93 | 116 | 140 | 163 |
| Test 3 | 22 | 46 | 69 | 93 | 116 | 140 | 163 |
| Test 4 | 22 | 46 | 65 | 67 | 111 | 130 | 151 |
| **Test 5** | **22** | **46** | **69** | **93** | **117** | **141** | **165** |
| Test 6 | 22 | 46 | 69 | 92 | 116 | 140 | 164 |
| Test 7 | 22 | 46 | 70 | 94 | 118 | 142 | 166 |
| Test 8 | 22 | 46 | 69 | 92 | 113 | 137 | 161 |

| Test | DXS (m) | MSIM | NONO | IVAR |
|---|---|---|---|---|
| With 0.214mm | 0.021188571429 | 14000 | 175 | 22 |
| With Out 0.214mm | 0.021310344828 | 13920 | 174 | 22 |
| **Test 1** | **0.021558139535** | **13760** | **172** | **22** |
| Test 2 | 0.021811764706 | 13600 | 170 | 22 |
| Test 3 | 0.021940828402 | 13520 | 169 | 22 |
| Test 4 | 0.023468354430 | 12640 | 158 | 22 |
| **Test 5** | **0.021558139535** | **13760** | **172** | **22** |
| Test 6 | 0.021684210526 | 13680 | 171 | 22 |
| Test 7 | 0.021433526012 | 13840 | 173 | 16 |
| Test 8 | 0.022071428571 | 13440 | 168 | 22 |

**8X24**

| Original | | Test 1 | | Test 2 | |
|---|---|---|---|---|---|
| **JLEV** | **VARDX** | **JLEV** | **VARDX** | **JLEV** | **VARDX** |
| 24 | 0.0193125 | 10 | 0.019312500000 | 10 | 0.019312500000 |
| 25 | 0.0108125 | 25 | 0.018745833333 | 25 | 0.018745833333 |
| 26 | 0.0085000 | 34 | 0.019312500000 | 34 | 0.019312500000 |
| 52 | 0.0193125 | 51 | 0.019893382353 | 51 | 0.019893382353 |
| 53 | 0.0013750 | 62 | 0.019312500000 | 62 | 0.019312500000 |
| 54 | 0.0179375 | 78 | 0.018722656250 | 78 | 0.018722656250 |
| 79 | 0.0193125 | 86 | 0.019312500000 | 86 | 0.019312500000 |
| 80 | 0.0112500 | 104 | 0.019861111111 | 104 | 0.019861111111 |
| 81 | 0.0080625 | 114 | 0.019312500000 | 112 | 0.030000000000 |
| 107 | 0.0193125 | 131 | 0.018757352941 | 126 | 0.019428571429 |
| 108 | 0.0018125 | 148 | 0.019312500000 | 145 | 0.019312500000 |
| 109 | 0.0175000 | 158 | 0.018368750000 | 153 | 0.018132812500 |
| 134 | 0.0193125 | 161 | 0.032785714286 | 168 | 0.019312500000 |
| 135 | 0.0116875 | 168 | 0.018734693878 | 180 | 0.018526041667 |
| 136 | 0.0076250 | 180 | 0.019312500000 | 188 | 0.019312500000 |
| 162 | 0.0193125 | 183 | 0.016916666667 | 189 | 0.026500000000 |
| 163 | 0.0022500 | 191 | 0.019312500000 | | |
| 164 | 0.0170625 | 192 | 0.027000000000 | | |
| 189 | 0.0193125 | | | | |
| 190 | 0.0121250 | | | | |
| 191 | 0.0071875 | | | | |
| 200 | 0.0193125 | | | | |

| Test | Grid Spacer Identifiers, JLEV | | | | | | |
|---|---|---|---|---|---|---|---|
| Original | 25 | 53 | 80 | 108 | 135 | 163 | 190 |
| Test 1 | 25 | 51 | 78 | 104 | 131 | 158 | 183 |
| Test 2 | 25 | 51 | 78 | 104 | 126 | 153 | 180 |

| Test | DXS (m) | MSIM | NONO | IVAR |
|---|---|---|---|---|
| Original | 0.018633165829 | 15920 | 199 | 22 |
| Test 1 | 0.019413612565 | 15280 | 191 | 18 |
| Test 2 | 0.019723404255 | 15040 | 188 | 16 |

**Appendix E**



**P60007 Pressure Drop**
**Grid Spacer Position, 1.493ft**



**P60007 Pressure Drop**
**Grid Spacer Position, 3.173ft**

P60007 Vapor Fraction
Grid SpacerPosition, 4.852ft



P60007 Pressure Drop
Grid SpacerPosition, 4.852ft

**P60007 Vapor Fraction**
**Grid Spacer Position, 6.532ft**



**P60007 Pressure Drop**
**Grid Spacer Position, 6.532ft**

**P60007 Vapor Fraction**
**Grid Spacer Position, 8.212ft**

Legend: 1X24, 3X24, 4X24, 5X24, 6X24, 7X24, 8X24



**P60007 Pressure Drop**
**Grid Spacer Position, 8.212ft**

Legend: 1X24, 3X24, 4X24, 5X24, 6X24, 7X24, 8X24

P60007 Vapor Fraction
Grid Spacer Position, 9.892ft



P60007 Pressure Drop
Grid Spacer Position, 9.892ft

P60007 Vapor Fraction
Grid Spacer Position, 11.572ft



P60007 Pressure Drop
Grid Spacer Position, 11.572ft

# Appendix F

| Axial End of Node (ft) | 1X24 to 3X24 | | | 3X24 to 4X24 | | | 4X24 to 5X24 | | | 5X24 to 6X24 | | | 6X24 to 7X24 | | | 7X24 to 8X24 | | |
|---|---|---|---|---|---|---|---|---|---|---|---|---|---|---|---|---|---|---|
| | Pressure (bar) | Vapor | Flow Quality | Pressure (bar) | Vapor | Flow Quality | Pressure (bar) | Vapor | Flow Quality | Pressure (bar) | Vapor | Flow Quality | Pressure (bar) | Vapor | Flow Quality | Pressure (bar) | Vapor | Flow Quality |
| 0.000 | 0.008% | 0.000% | 0.000% | 0.001% | 0.000% | 0.000% | 0.001% | 0.000% | 0.000% | 0.001% | 0.000% | 0.000% | 0.000% | 0.000% | 0.000% | 0.000% | 0.000% | 0.000% |
| 0.154 | 0.008% | 0.000% | 0.200% | 0.001% | 0.000% | 0.000% | 0.001% | 0.000% | 0.000% | 0.001% | 0.000% | 0.000% | 0.000% | 0.000% | 0.000% | 0.000% | 0.000% | 0.000% |
| 0.309 | 0.008% | 70.470% | 68.901% | 0.001% | 2.362% | 2.381% | 0.001% | 1.613% | 1.626% | 0.001% | 0.820% | 0.826% | 0.000% | 0.826% | 0.833% | 0.000% | 0.833% | 0.840% |
| 0.455 | 0.008% | 15.209% | 14.902% | 0.001% | 2.466% | 2.765% | 0.001% | 1.609% | 1.422% | 0.001% | 1.168% | 0.962% | 0.001% | 0.946% | 0.971% | 0.000% | 0.477% | 0.490% |
| 0.464 | 0.003% | 13.669% | 13.929% | 0.001% | 2.405% | 2.075% | 0.000% | 1.457% | 1.695% | 0.000% | 1.042% | 0.862% | 0.000% | 0.632% | 0.435% | 0.000% | 0.656% | 0.873% |
| 0.618 | 0.008% | 10.744% | 11.017% | 0.001% | 1.389% | 1.905% | 0.001% | 0.939% | 0.971% | 0.001% | 0.948% | 0.971% | 0.000% | 0.478% | 0.478% | 0.000% | 0.000% | 0.000% |
| 0.773 | 0.008% | 9.015% | 9.122% | 0.001% | 1.284% | 1.115% | 0.001% | 0.743% | 1.128% | 0.001% | 0.562% | 0.380% | 0.000% | 0.377% | 0.382% | 0.000% | 0.189% | 0.383% |
| 0.927 | 0.008% | 7.568% | 6.995% | 0.001% | 4.678% | 4.700% | 0.001% | 3.067% | 3.083% | 0.001% | 1.899% | 2.163% | 0.000% | 1.935% | 1.691% | 0.001% | 1.316% | 1.685% |
| 0.967 | 0.003% | 4.202% | 3.429% | 0.003% | 2.632% | 2.367% | 0.000% | 4.805% | 4.848% | 0.000% | 2.208% | 1.911% | 0.000% | 0.968% | 1.299% | 0.000% | 0.977% | 0.658% |
| 1.082 | 0.006% | 8.808% | 9.406% | 0.001% | 1.705% | 2.077% | 0.001% | 1.734% | 2.232% | 0.000% | 1.176% | 1.142% | 0.001% | 0.595% | 0.693% | 0.000% | 0.599% | 0.581% |
| 1.236 | 0.009% | 7.428% | 7.932% | 0.001% | 1.174% | 1.231% | 0.001% | 0.792% | 0.935% | 0.001% | 0.599% | 0.629% | 0.000% | 0.201% | 0.316% | 0.000% | 0.402% | 0.317% |
| 1.391 | 0.009% | 4.851% | 4.878% | 0.001% | 0.520% | 0.603% | 0.001% | 0.418% | 0.303% | 0.001% | 0.210% | 0.304% | 0.001% | 0.105% | 0.153% | 0.000% | 0.105% | 0.153% |
| 1.479 | 0.006% | 4.724% | 2.275% | 0.002% | 1.653% | 0.000% | 0.001% | 0.840% | 0.554% | 0.001% | 0.847% | 0.000% | 0.000% | 0.858% | 0.446% | 0.001% | 0.862% | 0.666% |
| 1.545 | 0.004% | 0.667% | 0.917% | 0.001% | 0.662% | 0.909% | 0.001% | 0.667% | 0.000% | 0.001% | 0.662% | 0.000% | 0.000% | 0.000% | 0.000% | 0.000% | 0.000% | 0.000% |
| 1.700 | 0.009% | 0.000% | 0.000% | 0.001% | 0.000% | 0.637% | 0.001% | 0.000% | 0.641% | 0.001% | 0.000% | 0.657% | 0.000% | 0.000% | 0.000% | 0.000% | 0.000% | 0.000% |
| 1.854 | 0.009% | 0.000% | 0.481% | 0.001% | 0.000% | 0.000% | 0.001% | 0.000% | 0.000% | 0.001% | 0.000% | 0.000% | 0.000% | 0.000% | 0.000% | 0.000% | 0.000% | 0.000% |
| 1.991 | 0.009% | 3.214% | 3.394% | 0.001% | 1.476% | 0.000% | 0.001% | 1.124% | 0.000% | 0.001% | 1.515% | 0.000% | 0.000% | 1.538% | 0.000% | 0.001% | 1.172% | 0.000% |
| 2.009 | 0.004% | 0.346% | 0.385% | 0.001% | 0.000% | 0.000% | 0.001% | 0.345% | 0.000% | 0.000% | 0.000% | 0.000% | 0.000% | 0.346% | 0.000% | 0.000% | 0.347% | 0.000% |
| 2.163 | 0.009% | 0.304% | 0.321% | 0.001% | 0.000% | 0.000% | 0.001% | 0.000% | 0.000% | 0.001% | 0.000% | 0.000% | 0.000% | 0.000% | 0.000% | 0.000% | 0.000% | 0.000% |
| 2.317 | 0.009% | 0.272% | 0.000% | 0.001% | 0.000% | 0.274% | 0.001% | 0.000% | 0.000% | 0.001% | 0.000% | 0.000% | 0.000% | 0.273% | 0.000% | 0.000% | 0.000% | 0.000% |
| 2.472 | 0.009% | 0.000% | 0.241% | 0.001% | 0.251% | 0.000% | 0.001% | 0.250% | 0.000% | 0.001% | 0.000% | 0.000% | 0.000% | 0.000% | 0.000% | 0.000% | 0.000% | 0.000% |
| 2.503 | 0.004% | 5.051% | 5.235% | 0.001% | 2.128% | 3.533% | 0.001% | 3.533% | 6.562% | 0.001% | 6.562% | 0.000% | 0.000% | 1.404% | 0.000% | 0.000% | 1.140% | 0.000% |
| 2.627 | 0.007% | 0.000% | 0.216% | 0.001% | 0.000% | 0.000% | 0.001% | 0.000% | 0.000% | 0.001% | 0.233% | 0.000% | 0.000% | 0.000% | 0.000% | 0.000% | 0.000% | 0.000% |
| 2.781 | 0.008% | 0.000% | 0.000% | 0.001% | 0.000% | 0.197% | 0.001% | 0.000% | 0.000% | 0.001% | 0.000% | 0.000% | 0.000% | 0.000% | 0.000% | 0.000% | 0.000% | 0.000% |
| 2.936 | 0.008% | 0.211% | 0.182% | 0.001% | 0.000% | 0.000% | 0.001% | 0.000% | 0.000% | 0.000% | 0.000% | 0.000% | 0.000% | 0.000% | 0.000% | 0.000% | 0.000% | 0.000% |
| 3.015 | 0.006% | 5.945% | 0.000% | 0.002% | 1.806% | 1.177% | 0.001% | 1.379% | 0.000% | 0.001% | 1.166% | 0.000% | 0.000% | 1.179% | 0.000% | 0.001% | 0.955% | 0.000% |
| 3.090 | 0.005% | 0.204% | 0.000% | 0.001% | 0.203% | 0.000% | 0.000% | 0.204% | 0.000% | 0.000% | 0.000% | 0.000% | 0.000% | 0.000% | 0.000% | 0.000% | 0.000% | 0.000% |
| 3.245 | 0.008% | 0.000% | 0.163% | 0.001% | 0.000% | 0.000% | 0.001% | 0.000% | 0.000% | 0.000% | 0.000% | 0.000% | 0.000% | 0.000% | 0.000% | 0.000% | 0.000% | 0.000% |
| 3.399 | 0.008% | 0.193% | 0.156% | 0.001% | 0.000% | 0.000% | 0.001% | 0.000% | 0.000% | 0.000% | 0.000% | 0.000% | 0.000% | 0.000% | 0.000% | 0.000% | 0.000% | 0.000% |
| 3.527 | 0.008% | 5.128% | 0.000% | 0.001% | 1.663% | 0.000% | 0.001% | 1.268% | 0.152% | 0.001% | 2.998% | 0.000% | 0.001% | 4.782% | 0.000% | 0.000% | 0.655% | 0.000% |
| 3.554 | 0.003% | 0.762% | 0.151% | 0.000% | 0.384% | 0.000% | 0.000% | 0.578% | 0.000% | 0.001% | 0.581% | 0.000% | 0.000% | 0.578% | 0.000% | 0.000% | 0.192% | 0.000% |
| 3.708 | 0.008% | 0.000% | 0.147% | 0.001% | 0.000% | 0.000% | 0.000% | 0.000% | 0.000% | 0.000% | 0.000% | 0.000% | 0.000% | 0.000% | 0.147% | 0.000% | 0.000% | 0.000% |
| Max | 0.00009 | 0.70470 | 0.68901 | 0.00003 | 0.04678 | 0.04700 | 0.00001 | 0.04805 | 0.04848 | 0.00001 | 0.06562 | 0.02163 | 0.00001 | 0.04782 | 0.01691 | 0.00001 | 0.03081 | 0.01058 |
| L2 | 0.00042 | 0.77028 | 0.74905 | 0.00007 | 0.08399 | 0.07600 | 0.00003 | 0.07997 | 0.07132 | 0.00003 | 0.08476 | 0.03609 | 0.00002 | 0.06106 | 0.02881 | 0.00002 | 0.03081 | 0.02077 |

**Appendix G**

*Two Phase Friction Model:*

The homogeneous two-phase friction multiplier as a function of the flowing quality:

$x$ = flowing vapor quality,
$\alpha$ = vapor volume (void fraction),
$\rho_m = \alpha\rho_v + (1 - \alpha)\rho_l$ = two-phase mixture density (lb$_m$/ft$^3$),
$\rho_l$ = liquid density ($\rho_l = \rho_f$ for saturated liquid),
$\rho_v$ = vapor density ($\rho_v = \rho_g$ for saturated vapor),
$\mu_f$ = dynamic viscosity of saturated liquid (lb$_m$/ft/s),
$\mu_g$ = dynamic viscosity of saturated vapor (lb$_m$/ft/s),
$v_f$ = specific volume of saturated liquid (ft$^3$/lb$_m$),
$v_g$ = specific volume of saturated vapor (ft$^3$/lb$_m$),
$G$ = coolant mass flux (lb$_m$/ft$^2$/s),
$P$ = pressure (psi),
$P_c$ = critical pressure (3208 psi).

Pressure dependent parameter used in the EPRI correlation:

$$C_F = 1.02x^{-0.175}(0.0036\ G)^{-0.45} \qquad\qquad if\ P \geq 600psi$$

$$C_F = 0.357x^{-0.175}(0.0036\ G)^{-0.45}\left(1 + 10\frac{P}{P_c}\right) \qquad if\ P < 600psi$$

### *Subcooled Boiling Models*

$x_e$ = thermodynamic equilibrium quality,

$x_d$ = equilibrium quality at the bubble departure point, flowing (vapor) quality

$h$ = mixture enthalpy (Btu/lb),

$h_f$ = saturated liquid enthalpy,

$h_g$ = saturated vapor enthalpy,

$C_{pf}$ = specific heat of saturated liquid (Btu/lb$_m$/°F),

$\Delta T_d$ = coolant bulk subcooling at the bubble departure point (°F),

$h_{fg} = h_g - h_f$ latent heat of vaporization (Btu/lb$_m$),

$s$ = surface tension (lb$_f$/ft),

$D_h$ = hydraulic diameter (ft),

$v_f$ = saturated liquid specific volume (ft$^3$/lb$_m$),

$\mu_f$ = saturated liquid dynamic viscosity (lb$_m$/ft/s),

$q'$ = linear heat flux (Btu/ft/s),

$P_h$ = heated perimeter (ft),

$G$ = coolant mass flux (lb$_m$/ft$^2$/s),

$k_f$ = saturated liquid thermal conductivity (Btu/ft/s/°F),

$Pr$ = Prandtl number computed with saturated liquid properties,

$$Pr = \frac{C_{pf}\mu_f}{k_f}$$

$Re$ = Reynolds number computed with saturated liquid properties,

$$Re = \frac{GD_h}{\mu_f}$$

$H_f$ = Dittus-Boelter heat transfer coefficient, computed with saturated liquid properties,

$$H_f = \frac{0.023 Re_f^{0.8} Pr_f^{0.4} k_f}{D_h}$$

$\rho_f$ = saturated liquid density (lb$_m$/ft$^3$),

$\tau_w$ = wall shear stress (lb$_f$/ft$^2$),

$f$ = friction factor,

$g_c$ = conversion factor, lb$_m$ ft/s$^2$ to lb$_f$ unit (32.18 lb$_m$ ft/s$^2$/lb$_f$.

$Z$ = empirical function analogous to the coolant subcooling $\Delta T_d$ seen in the Levy correlation,

$q''$ = local heat flux (Btu/ft$^2$/s),

$P$ = pressure (psi),

$k_l$ = liquid thermal conductivity (Btu/ft/s/°F),

$\mu_l$ = liquid dynamic viscosity (lb$_m$/ft/s),

$C_{pl}$ = liquid specific heat (Btu/lb$_m$/°F),

$Y_B^+$ = Dimensionless distance from the wall to the bubble tip

### *Subcooled Boiling Models *Continued*

The Levy model defines the flow quality by the equation:

$$x = x_e - x_d \exp\left(\frac{x_e}{x_d} - 1\right) \qquad if \ x_e \geq x_d$$

$$x = 0 \qquad if \ x_e < x_d$$

$$x_d = -\frac{C_{pf}\Delta T_d}{h_{fg}}$$

Solve for coolant bulk sub-cooling

$$Y_B^+ = \frac{0.015}{\mu_f}\sqrt{\frac{\sigma g_c D_h}{v_f}}$$

$$\Delta T_d = \frac{q'}{P_h H_f} \qquad if \ Y_B^+ < 0$$

$$\Delta T_d = \frac{q'}{P_h H_f} - QPrY_B^+ \qquad if \ 0 \leq Y_B^+ < 5$$

$$\Delta T_d = \frac{q'}{P_h H_f} - 5Q\left\{Pr + \ln\left[1 + Pr\left(\frac{Y_B^+}{5} - 1\right)\right]\right\} \qquad if \ 5 \leq Y_B^+ < 30$$

$$\Delta T_d = \frac{q'}{P_h H_f} - 5Q\left\{Pr + \ln(1 + 5Pr) + 0.5\ln\left(\frac{Y_B^+}{30}\right)\right\} \qquad if \ Y_B^+ \geq 30$$

where:

$$Q = \frac{q'}{P_h C_{pf}\sqrt{\rho_f \tau_w g_c}}$$

and

$$\tau_w = 0.125\frac{f v_f G^2}{g_c}$$

### Subcooled Boiling Models *Continued

Flow quality for the EPRI model:

$$x = \frac{x_e - x_d \left[1 - \tanh\left(1 - \frac{x_e}{x_d}\right)\right]}{1 - x_d \left[1 - \tanh\left(1 - \frac{x_e}{x_d}\right)\right]} \qquad if \; x_e \geq x_d$$

$$x = 0 \qquad\qquad\qquad\qquad if \; x_e < x_d$$

Bubble departure quality:

$$x_d = -\frac{C_{pl}Z}{h_{fg}}$$

$$Z = \frac{B - \sqrt{B^2 - 4AC}}{2A}$$

$$A = 4C_B(H_{DB} + H_{HN})^2$$

$$B = 2H_{DB}^2\left(H_{HN} + \frac{1}{2}H_{DB}\right) + 8q''C_B(H_{HN} + H_{DB})$$

$$C = 4C_B(q'')^2 + q''H_{DB}^2$$

Liquid-phase forced-convection heat transfer coefficient (Btu/ft$^2$/s/°F), Dittus-Boelter correlation:

$$H_{DB} = \frac{0.023Re_l^{0.8}Pr_l^{0.4}k_l}{D_h}$$

Re-condensation heat transfer coefficient (Btu/ft$^2$/s/°F), Hancox-Nicoll correlation:

$$H_{HN} = \frac{0.2Re_l^{0.662}Pr_l k_l}{D_h}$$

Pressure dependent coefficient (Btu/ft$^2$/s/°F$^2$), Thom correlation for nucleate boiling heat flux:

$$C_B = 0.05358e^{P/630}$$

## Appendix H

## Pressure Drop

$P$ = pressure ($\text{lb}_\text{f}/\text{ft}^2$),

$X$ = axial coordinate (ft),

$v'$ = specific volume for momentum transport ($\text{ft}^3/\text{lb}_\text{m}$),

$G$ = two-phase coolant mass flux ($\text{lb}_\text{m}\,\text{ft}/\text{s}^2$),

$D_h$ = hydraulic diameter (ft),

$g_c$ = conversion factor from $\text{lb}_\text{f}$ to $\text{lb}_\text{m}\,\text{ft}/\text{s}^2$ (32.18 $\text{lb}_\text{m}\,\text{ft}/\text{s}^2/\text{lb}_\text{f}$),

$f$ = wall friction factor,

$K_D$ = form drag loss coefficient specified in input at axial positions for each channel type,

$K_G$ = loss coefficient supplied as a single input value (see card 26a),

$w$ = crossflow rate through a gap ($\text{lb}_\text{m}/\text{ft/s}$),

$s$ = gap width (ft)

## Appendix I

```
!Greg Maultsby
!07/25/2016

PROGRAM Linear_Heat
IMPLICIT NONE

REAL::ThrmOpt=0.0,Hfuel=0.0
REAL::GAMf=0.97,ConvA=0.0,LnrHR=0.0
REAL,DIMENSION(102)::AxlPwr
REAL,DIMENSION(60)::RadPwr
REAL,ALLOCATABLE::AxlPosIntv(:),AxlIntvSz(:),Axial(:),AxialSz(:)

INTEGER::iErr,n,AxlPosNum=0,FRNum=0,FRNumTot=0
INTEGER::ct=0,ct2=0,ct4=0,i=0,j=0,IVAR=17
INTEGER,ALLOCATABLE::Qty(:)

 CHARACTER(15)::fName

!---------------------------------------Variable Declaration Documentation----------------------------------------

!---------------------------------------End of Variable Documentation----------------------------------------

CALL SYSTEM("clear")

!WRITE(*,'(A)',ADVANCE="NO")"Enter the filename with ten characters or less: "
!READ(*,*) fName
!OPEN (UNIT=11, FILE=fName,STATUS="REPLACE", ACTION="WRITE", IOSTAT=iErr)
!WRITE(*,*)

!WRITE(*,'(A)',ADVANCE="NO")"Enter in the Thermal Output (MW): "
!READ(*,*)ThrmOpt
ThrmOpt=1.521
!WRITE(*,'(A,ES12.4,A)')"Thermal Output is : ",ThrmOpt," MW"
ConvA=ThrmOpt*3412141.63
!WRITE(*,'(A,ES12.4,A,/)')"Thermal Output is : ",ConvA," Btu/hr"

!WRITE(*,'(A)',ADVANCE="NO")"Enter the fraction of power in the fuel: "
!READ(*,*)GAMf
!WRITE(*,'(A,F6.4,/)')"The fraction of power in the fuel is ",GAMf
GAMf=1.0

!WRITE(*,'(A)',ADVANCE="NO")"Enter in the height of the fuel (ft): "
!READ(*,*)Hfuel
!WRITE(*,'(A,F6.3,A,/)')"The height of the fuel is ",Hfuel," ft"
Hfuel=12.165
```

```
!WRITE(*,'(A)',ADVANCE="NO")"Enter the total number of fuel loaded rods in the assembly: "
!READ(*,*)FRNumTot
!WRITE(*,'(A,I4,/)')"The total number of fuel rods in the assembly is ",FRNumTot
FRNumTot=60

!WRITE(*,'(A)',ADVANCE="NO")"Enter the number of fuel rods being evaluated: "
!READ(*,*)FRNum
!WRITE(*,'(A,I4,/)')"The number of fuel rods being evaluated is ",FRNum
FRNum=60

!WRITE(*,'(A)',ADVANCE="NO")"Enter the number of axial positions: "
!READ(*,*)AxlPosNum
AxlPosNum=102

ALLOCATE
(AxlPosIntv(AxlPosNum),AxlIntvSz(AxlPosNum),Qty(IVAR),Axial(IVAR),AxialSz(AxlPosNum))

!----------------------------------------------------Array Declarations--------------------------------------------------------
AxlPwr=(/0.460,0.463,0.517,0.580,0.616,0.648,0.681,0.711,0.740,0.770,0.800, &
     0.829,0.859,0.890,0.926,0.962,0.998,1.032,1.066,1.102,1.146,1.190, &
     1.219,1.220,1.220,1.234,1.273,1.312,1.339,1.340,1.340,1.345,1.364, &
     1.383,1.399,1.400,1.400,1.396,1.377,1.357,1.341,1.340,1.340,1.333, &
     1.297,1.257,1.224,1.220,1.220,1.212,1.176,1.142,1.107,1.076,1.049, &
     1.023,1.000,0.979,0.958,0.940,0.926,0.912,0.899,0.888,0.878,0.868, &
     0.859,0.850,0.840,0.827,0.815,0.802,0.789,0.776,0.762,0.748,0.734, &
     0.720,0.706,0.692,0.678,0.665,0.652,0.639,0.626,0.613,0.600,0.587, &
     0.574,0.559,0.545,0.531,0.517,0.503,0.488,0.471,0.460,0.460,0.460, &
     0.460,0.460,0.460/)

!AxlPwr=(/0.46 ,0.58 ,0.69 ,0.79 ,0.88 ,0.99 ,1.09 ,1.22 ,1.22 ,1.34 ,1.34 ,1.40 , &
!     1.40 ,1.34 ,1.34 ,1.22 ,1.22 ,1.09 ,0.99 ,0.88 ,0.79 ,0.69 ,0.58 ,0.46 ,0.46 /)

AxlPosIntv=(/0.0228,0.0683,0.1138,0.1593,0.2048,0.2503,0.2958,0.3413,0.3867, &
     0.4323,0.4803,0.5308,0.5813,0.6318,0.6823,0.7335,0.7855,0.8375, &
     0.8895,0.9415,0.9935,1.0455,1.0975,1.1495,1.2015,1.2535,1.3045, &
     1.3545,1.4045,1.4545,1.5047,1.5552,1.6057,1.6562,1.7067,1.7579, &
     1.8096,1.8614,1.9131,1.9649,2.0160,2.0665,2.1170,2.1675,2.2180, &
     2.2692,2.3212,2.3732,2.4252,2.4772,2.5239,2.5652,2.6065,2.6478, &
     2.6891,2.7304,2.7660,2.7960,2.8260,2.8510,2.8710,2.8910,2.9088, &
     2.9243,2.9398,2.9553,2.9708,2.9863,3.0045,3.0259,3.0474,3.0691, &
     3.0906,3.1122,3.1338,3.1555,3.1770,3.1986,3.2202,3.2418,3.2617, &
     3.2799,3.2982,3.3164,3.3346,3.3528,3.3710,3.3892,3.4074,3.4256, &
     3.4438,3.4620,3.4802,3.4984,3.5172,3.5399,3.5657,3.5916,3.6175, &
     3.6433,3.6692,3.6951/)
```

```
RadPwr=(/1.15,1.30,1.15,1.30,1.30,1.15,1.30,1.15, &
          1.30,0.45,0.89,0.89,0.89,0.45,1.15,1.30, &
          1.15,0.89,0.89,0.89,0.89,0.89,0.45,1.15, &
          1.30,0.89,0.89,0.89,0.89,1.15,1.30,0.89,0.89,0.89,0.89,1.15, &
          1.15,0.45,0.89,0.89,0.89,0.89,0.45,1.15, &
          1.30,1.15,0.45,0.89,0.89,0.45,1.15,1.30, &
          1.15,1.30,1.15,1.15,1.15,1.15,1.30,1.15/)

Axial=(/0.0455,0.0505,0.052,0.050,0.0505,0.05175,0.0505,0.052,0.0413, &
      0.030,0.020,0.0155,0.021,0.0216,0.0182,0.0195,0.02586428571/)

QTY=(/11,16,27,31,36,41,46,51,57,60,63,69,70,81,95,96,103/)
!-------------------------------------------------End Array Declarations-----------------------------------------------

!------------------------------------Axial Tube Size and Quantity of Tubes per Node Generated----------------------
!                          This would eliminate the need for the pre-set Axial and QTY arrays
!----------------------------------------------------------------------------------------------------------------------
!OPEN(UNIT=12,FILE='test.inp',ACTION="READ",IOSTAT=ierr)
!
!IVAR=0
!
!IF(iErr.NE.0) THEN
!  STOP "Error opening requested file"
!END IF
!
!DO
!  READ(12,*,IOSTAT=ierr)
!  IF(ierr.NE.0) EXIT
!  IVAR=IVAR+1
!END DO
!REWIND(12)
!
!DO i=1,IVAR
!  READ(12,'(I5,ES15.8)')QTY(i),Axial(i)
!  WRITE(*,'(I3,I5,ES15.7)')i,QTY(i),Axial(i)
!END DO
!
! CLOSE(UNIT=12, STATUS="KEEP")                                      ! Close output file
!----------------------------------End Axial Tube Size and Quantity of tubes per node Generated--------------------
```

```
!---------------------------------------------------Axial Positions Generated----------------------------------------------
!                         This would eliminate the need for the pre-set AxlPosIntv array
!----------------------------------------------------------------------------------------------------------------------------
! ct2=1
!DO i=1,IVAR
!  IF (i.EQ.1) THEN
!    DO j=1,Qty(i)-1
!      IF (j.EQ.1) THEN
!                 AxialSz(ct2)=0.50*Axial(i)
!                 ct2=ct2+1
!      ELSE
!                 AxialSz(ct2)=Axial(i)+AxialSz(ct2-1)
!                 ct2=ct2+1
!      END IF
!    END DO
!  ELSE IF (i.GT.1) THEN
!    DO j=1,Qty(i)-Qty(i-1)
!      IF (j.EQ.1) THEN
!                 AxialSz(ct2)=0.5*(Axial(i)+Axial(i-1))+AxialSz(ct2-1)
!                 ct2=ct2+1
!      ELSE
!                 AxialSz(ct2)=Axial(i)+AxialSz(ct2-1)
!                 ct2=ct2+1
!      END IF
!    END DO
!  END IF
!END DO

!DO i=1,AxlPosNum
!  IF (MOD(i,6).EQ.0) THEN
!    WRITE(*,'(F8.4)')AxialSz(i)
!!    WRITE(*,'(F9.6)')AxialSz(i)
!  ELSE
!    WRITE(*,'(F8.4)',ADVANCE='NO')AxialSz(i)
!!    WRITE(*,'(F9.6)')AxialSz(i)
!  END IF
!END DO
!---------------------------------------------------End Axial Positions Generated----------------------------------------

!---------------------------------------------------Linear Heat Rate array------------------------------------------------
! Populates the respective fuel rod with linear heat rates for each axial position
!----------------------------------------------------------------------------------------------------------------------------
LnrHR=(ConvA*GAMf)/(FRNumTot*Hfuel)

OPEN (UNIT=11, FILE="test",STATUS="REPLACE", ACTION="WRITE", IOSTAT=iErr)
```

```
DO ct=1,AxlPosNum
 IF(ct.EQ.1)THEN

   WRITE(11,'(A)')"$------------------------------------------------------------------------"
   WRITE(11,'(A)')"$ Card 3: General Thermal-Hydraulic Parameters"
   WRITE(11,'(A)')"$ IPLIE NCHANL NROD  NDX  NCTYP NGRID NGRIDT NODESF IGCON   IVEC2
NFUELT"
   WRITE(11,'(A,I6,I6,A)')"    1   80",FRNum,AxlPosNum,"  10   7   1   0   0   0   0   1"
   WRITE(11,'(A)')"$------------------------------------------------------------------------"
   WRITE(11,'(A)')"$ IPLIE - Channel connection indicator 1 = Open Channels"
   WRITE(11,'(A)')"$ NCHANL - Total number of coolant channels"
   WRITE(11,'(A)')"$ NROD - Number of fuel rods"
   WRITE(11,'(A)')"$ NDX - Number of axial intervals"
   WRITE(11,'(A)')"$ NCTYP - Number of channels to be read"
   WRITE(11,'(A)')"$ NGRID - Number of spacer grid positions"
   WRITE(11,'(A)')"$ NGRIDT - Number of grid types"
   WRITE(11,'(A)')"$ NODESF - Fuel pin model for fuel nodes and heating models"
   WRITE(11,'(A)')"$ IGCON - Number of radial nodes in the fuel pellet for fuel"
   WRITE(11,'(A)')"$         temperature calculations"
   WRITE(11,'(A)')"$ BLANK"
   WRITE(11,'(A)')"$ IVEC2 - 1 = Basic Version"
   WRITE(11,'(A)')"$ NFUELT - Number of fuel types for COBRA or TWIGL fuel pin model"
   WRITE(11,'(A)')"$------------------------------------------------------------------------"
   WRITE(11,'(A)')"$------------------------------------------------------------------------"
   WRITE(11,'(A)')"$ Card 4: Axial Intervals"
   WRITE(11,'(A)')"$   DX(J)"

   ct2=1
   DO i=1,IVAR
    IF (i.EQ.1) THEN
     DO j=1,Qty(i)-1
       AxialSz(ct2)=Axial(i)
       ct2=ct2+1
     END DO
    ELSE IF (i.GT.1) THEN
     DO j=1,Qty(i)-Qty(i-1)
       AxialSz(ct2)=Axial(i)
       ct2=ct2+1
     END DO
    END IF
   END DO
   DO i=1,AxlPosNum
    IF (MOD(i,6).EQ.0) THEN
     WRITE(11,'(F12.5)')AxialSz(i)*3.28084
    ELSE
     WRITE(11,'(F12.5)',ADVANCE='NO')AxialSz(i)*3.28084
    END IF
   END DO
```

```
                    WRITE(11,'(A)')"$------------------------------------------------------------------------"
                    WRITE(11,'(A)')"$ DX(J) - Length of the axial interval J"
                    WRITE(11,'(A)')"$       The negative indicates that all the intervals are the same"
                    WRITE(11,'(A)')"$------------------------------------------------------------------------"
                    WRITE(11,'(A)')"$------------------------------------------------------------------------"
                    WRITE(11,'(A)')"$ Card 5: Linear Rod Powers"
                    WRITE(11,'(A)')"$ Card 5a: Number of axial levels for power distribution"
                    WRITE(11,'(A)')"$ ******** DO NOT forget to change NDX in CARD 3 ********"
                    WRITE(11,'(A)')"$ ********          NDX = NAXP          ********"
                    WRITE(11,'(A)')"$  NAXP"
                    WRITE(11,'(I6)')AxlPosNum
                    WRITE(11,'(A)')"$------------------------------------------------------------------------"
                    WRITE(11,'(A)')"$ BELOW linear heat rates determined from the BFBT center water cooled"
                    WRITE(11,'(A)')"$   BWR-C2A data for experiment P60003"
                    WRITE(11,'(A)')"$------------------------------------------------------------------------"
                    WRITE(11,'(A)')"$ Card 5b: Coordinate of axial level J"
                    WRITE(11,'(A)')"$  XTAB(J)"
      WRITE(11,'(F8.4)')AxlPosIntv(ct)*3.28084
      WRITE(11,'(A)')"$ Card 5c: Linear fission power of rod N for axial level J"
      WRITE(11,'(A)')"$ QTAB(N,J))"
      DO ct4=1,FRNum
        IF (MOD(ct4,6).EQ.0) THEN
          WRITE(11,'(ES12.5)')LnrHR*AxlPwr(ct)*RadPwr(ct4)
        ELSE
          WRITE(11,'(ES12.5)',ADVANCE='NO')LnrHR*AxlPwr(ct)*RadPwr(ct4)
        END IF
      END DO
     ELSE
      WRITE(11,'(F9.4)')AxlPosIntv(ct)*3.28084
      DO ct4=1,FRNum
        IF (MOD(ct4,6).EQ.0) THEN
          WRITE(11,'(ES12.5)')LnrHR*AxlPwr(ct)*RadPwr(ct4)
        ELSE
          WRITE(11,'(ES12.5)',ADVANCE='NO')LnrHR*AxlPwr(ct)*RadPwr(ct4)
        END IF
      END DO
     END IF
! write(11,*)   Needed when not exactly six columns per row
END DO
!----------------------------------------Terminate memory allocations--------------------------------------------
DEALLOCATE (AxlPosIntv,AxlIntvSz,Qty,Axial,AxialSz)
! Deallocate arrays
!----------------------------------------End Terminate memory allocations----------------------------------------
 CLOSE(UNIT=11, STATUS="KEEP")
! Close output file
END PROGRAM Linear_Heat
```